2011

High Pressure and Micro-spectroscopic Studies of Single Living Erythrocytes and the Intraerythrocytic Multplication Cycle of Plasmodium Falciparum

Silki Arora
University of Central Florida

HIGH PRESSURE AND MICRO-SPECTROSCOPIC STUDIES OF SINGLE LIVING ERYTHROCYTES AND THE INTRAERYTHROCYTIC MULTPLICATION CYCLE OF *PLASMODIUM FALCIPARUM*

by

SILKI ARORA

B.S. Delhi University, 2002
M.Sc. Delhi University, 2005
M.S. Ohio University, 2007

A dissertation submitted in partial fulfillment of requirements
for the degree of Doctor of Philosophy in Physics
in the Department of Physics
in the College of Science
at the University of Central Florida
Orlando, Florida

Summer Term
2011

Major Professor: Alfons Schulte

ABSTRACT

A novel experimental approach for micro-absorption spectroscopy and high-pressure microscopy of single cells is developed and applied to the investigation of morphological, volume, and spectroscopic changes in healthy red blood cells (RBCs) and erythrocytes infected with the malaria parasite *Plasmodium falciparum*.

Through real-time optical imaging of individual erythrocytes (size ~ 7 μm) we determine the change in volume over the pressure range from 0.1 to 210 MPa. The lateral diameter of healthy RBCs decreases reversibly with pressure with an approximate slope of 0.015 μm / MPa. In infected cells, clear differences in the deformability and between the compression and decompression curves are observed. The results are discussed with respect to the elasticity of the phospholipid membrane and the spectrin molecular network.

Employing micro-absorption spectroscopy with spatial resolution of 1.4 μm in the lateral and 3.6 μm in the axial direction the visible absorption spectrum of hemoglobin in a single red blood cell is measured under physiological conditions. The spectra of cells infected with the malaria parasite show changes in peak positions and relative intensities in the Soret and α- and β- bands. These indicate hemoglobin degradation that can be correlated with the stages of the parasite multiplication cycle and can be used as a potential diagnostic marker.

The research is further extended towards the understanding of pressure effects on the ligand binding kinetics to heme proteins. For a well characterized reaction at ambient pressure, CO binding to myoglobin in solution, we investigate the transient absorption following laser flash photolysis over eight decades in time at variable pressure and temperature. The data demonstrate that pressure significantly affects the amplitudes (not just the rates) of the component processes. The amplitude of the geminate process increases with pressure corresponding to a smaller escape fraction of ligands into the solvent and a smaller inner barrier.

ACKNOWLEDGMENTS

I take this pleasant opportunity to convey my sincere gratitude to all who inspired me during my doctoral research.

First and foremost I offer my deep sense of gratitude to my advisor, Dr. Alfons Schulte, for his inspiring guidance and excellent supervision. I cannot thank him enough for rendering me the freedom of independent thinking which has given a significant boost in my career.

I am grateful to my committee members for their valuable advices during my proposal and thesis defense. I would also like to thank Dr. Debopam Chakrabarti for his biological insight and fruitful discussions. I also acknowledge him and his graduate student, Jennifer Mauser, for providing timely biological samples. I would like to thank Dr. Oleg Galkin for help with the binding kinetics measurements on myoglobin. I would also like to acknowledge Sang Hoon park for his help with the high pressure setup.

My deepest gratitude goes to my parents for their unconditional love and support. Without their motivation this dissertation was impossible. Thanks for being an inspiration in all my endeavors. I am indebted to my family who stood by me during all days of hardships and whom I miss every day. I convey my heartfelt gratitude to my in laws for their trust and support. My special thanks to my mother in law for her immense love and blessings. I would also like to thank all my friends and well wishers for their support.

My special thanks to my husband, Pranav Gupta, for his love, care, motivation and support. I just don’t have enough words to thank him. I would like to thank him for making all the sacrifices. I greatly acknowledge his patience and cheerfulness.

Finally, I would like acknowledge the Lord for the strength and the love. I thank my lord Krishna for always being there for me.

TABLE OF CONTENTS

LIST OF FIGURES

CHAPTER 1. INTRODUCTION

Physicists have always been intrigued by biological problems [1]. Bio-molecules are ideal systems to study complex phenomenon as they are reproducible and modifiable by genetic engineering, and thus offer many experimental advantages over non-biological complex systems such as disordered magnetic alloys [2]. The connection between physics and biology goes both ways. Many tools from physics have been adopted by researchers in biological fields and at the same time, the study of biological systems has led to interesting results in regards to physics of complexity and disordered systems. Despite tremendous progress in cellular biophysics, researchers are constantly looking for pathways to bridge the gap between understanding of individual molecules and how these molecules function collectively to form a living cell [3].

Biochemical reactions within the cells can differ from those in test tubes [4]. To understand the full functionality and mechanisms of proteins and other bio-molecules, they must be studied in living cell close to physiological conditions [5]. Single molecule experiments have enhanced our understanding of fundamental biological process like protein reactions, protein folding, ligand transport etc. [6-8]. These require in situ, non-destructive probes. Optical techniques can revolutionize the way in which biological questions can be answered directly in the living cell. Spectroscopic techniques such as Raman and fluorescence have been powerful tools to investigate small biological molecules with ease and precision using probe excitations. Spectral band parameters (frequencies, intensities, line shapes and widths) are sensitive to

dynamic and structural changes of biomolecules [9, 10] at the sub-Angstrom level, a length scale where small, yet significant conformational changes for enzyme activity occur. Fluorescence experiments have improved our understanding of various biological processes [11], however they require labeling of the target molecule. The label behaves as an amplifier for an otherwise undetectable target, however it restricts the experiments scope as there must be prior knowledge of the target's presence and the target molecule must be modified to incorporate label [12-14]. The intensity of fluorescence can be decreased by photobleaching and quenching [15]. Absorption spectroscopy, on the other hand provides a label free way to characterize materials and bio assemblies in close to natural conditions.

We developed a novel technique, Confocal Absorption Microscopy, to study biological assemblies on the micron scale and nano-liter volume solutions in a non invasive way. It is capable of collecting both spatial and physical information based on light absorption by microscopic structures. The attenuation of the light beam in the axial direction due to absorption provides a mechanism for contrast [16]. The method can be used to study cells in their native environment and other biological assemblies. Using this approach the absorption spectrum of single red blood cell (~ diameter 7 μm) with spatial resolution better than 1.4 microns and spectral resolution of 0.5 nm was measured

Biological systems are diverse and dynamic in nature. Static studies like X-ray crystallography thus are not able to provide a complete picture. To get a more comprehensive picture the studies have to be extended to elucidate the effect of environmental factors and thermodynamic variables on the structure, mechanical and biochemical functions. High pressure has significant effects on protein function and cell metabolism [2, 8, 17, 18]. Deep-sea life, for

instance, requires adaptation to pressures as high as 1200 atmospheres at the ocean floor. Pressure is an ideal perturbant as it yields crucial thermodynamic information without the need to alter the chemical composition. It introduces morphological and mechanical changes in cells and micro organisms [19]. Yet, as a fundamental thermodynamic variable, which determines both the thermodynamic equilibrium and the rate of a biochemical reaction, pressure has received comparatively little attention.

High pressure experiments, however, are challenging and often limited by the amount of available sample or the need for high optical resolution. We employ a new approach to study morphological and functional changes of individual cells as a function of pressure with a high pressure microscopy. High pressure experiments on the single cell level open up new avenues for studying intra-cellular bio-molecule dynamics. To start with, the deformability of cell as a function of pressure is investigated. We acquire optical microscopic images of erythrocytes at variable pressure and monitoring changes in shape and size of the cell. The experiments indicate that the average diameter of the cell decreases during compression. We record image sequences of the red blood cells, and observed a decrease of mobility with pressure. Membrane mechanical properties of living cells provide remarkable features to achieve crucial functions, such as adhesion, motility, and intra/extra-cellular communication. This versatility resides in the association of a fluid lipid bilayer with an elastic, and often dynamic, network of proteins: the cytoskeleton [20].

Pathological conditions lead to various complications in the biochemical and structural properties of the cells. Despite intensive efforts at eradication, malaria remains a major public

health problem. The World Health Organization (WHO) estimates that 300–500 million people are afflicted each year. It is caused by several species of parasites and has a complex life cycle.

Investigation of the homeostasis of red blood cell upon infection by the malaria parasite poses complex experimental challenges [21]. In the course of this dissertation, I discuss the two techniques we applied for quantitative measurements of critical homeostatic parameters in the malaria-infected cells. The combined application of these techniques shed new light on the detailed mechanism of malaria infection providing potential for new diagnostic and therapeutic approaches.

We investigated the elasticity of cell (pressure response) as affected by the malaria parasite *Plasmodium falciparum*. In parallel to that, the electronic spectral changes were probed in the single cell using micro-absorption spectroscopy as a marker for heme degradation. It has been reported that current methods to diagnose malaria through blood smears are in some instances unable to confirm and detect the disease at early stages. Our experiments suggest a new technique to measure the spectral changes in the host cell under pathogenesis that can be correlated to the parasite multiplication cycle and may be used as a potential diagnostic marker.

One of the key components in the living cell are proteins [22]. To understand the connection between protein structure and function we study the binding of ligands such as CO and O_2 to heme proteins. Transient absorption following flash photolysis is a dynamic technique to probe kinetic processes in proteins over a wide range of time scale. The ligand molecules entering the protein from the solvent encounter several potential barriers and low temperature kinetics is described by distribution of barrier heights [23]. Each protein is frozen into a particular conformational state [24] whereas at higher temperatures, each molecule can fluctuate

between different conformational states. If protein structures would be static, the ligands could not get to the binding site. The outer barrier depends on the bulk viscosity of the solvent [25, 26].

Though hemoglobin is the principle constituent of the red blood cell, it consist of four subunits (two α and two β) that are similar to a simple protein, myoglobin. Being one of the simplest heme proteins capable of reverse oxygenation, myoglobin serves as a prototype for more complex systems and has been widely used as a prime example in various experimental and theoretical studies of protein dynamics. Myoglobin is treated as the hydrogen atom of the protein periodic table [2]. Starting from a well characterized reaction at ambient pressure - ligand binding to myoglobin - the volume change of the component processes and the protein-solvent interface were investigated and activation volumes associated with the kinetic steps of the ligand binding reaction were determined. The research reported in the last part of this dissertation is directed towards the understanding of pressure effects on heme protein dynamics by using kinetic measurements over a wide time-range.

This dissertation is organized as follows. Chapter one discusses the central problem and the motivation of the studies and provides the reader with an overview of the scope and goals of the conducted research. The second chapter defines the conceptual framework as provided by the current literature. Chapter three presents the information regarding the experimental set up employed during the course of research. Chapter four introduces the novel approach, Confocal Absorption Microscopy, and provides results relative to the technique characterization. In chapter five, six and seven the observations and the results obtained for the three experiments were discussed and their biological significance is emphasized. Chapter eight provides an overview of the results obtained and their significance in terms of directing future studies.

CHAPTER 2. BACKGROUND INFORMATION

2.1 Red Blood Cells: A model system

Cells are basic functional units of life [27]. Some of them are organisms in themselves while some form a vital part of bigger organisms. Cells are required to withstand high mechanical stresses by elastic deformation to different extent without damaging the complex protein membrane network [28]. Biological physics is an enormously broad field in which, structural studies are very crucial as they lead to models and theories of the system [29].

Red Blood Cells are the predominant type of blood cell and the vertebrate organism's vital means of delivering oxygen to the body tissues via the blood. The main component of the cytoplasm of the erythrocyte is hemoglobin [30, 31], a globular protein which facilitates oxygen transport. Oxygen can easily diffuse through the erythrocyte's cell membrane. Effects of mild pressure of a few atmospheres on the function of red blood cells have been explored by examining the susceptibility of RBCs to hemolysis by snake venom phospholipase A2 (PLA2) [32]. In those experiments Halle and Yedgar subjected RBCs to pressure of several atmospheres. The cells were then returned to ambient pressure and interacted with PLA2 to induce hemolysis. The hemolysis of the cells, which were exposed to high pressure, was markedly decreased. In *Plasmodium* infected erythrocytes the mechanisms underlying parasite volume expansion are under discussion [33, 34].

Red blood cells are mechanically soft and flexible. They squeeze through narrow capillaries, arteries and veins nearly a million times during their 120-day life span. They are relatively simple biological structure as they are non-nucleated and lack intra-membrane organelles. It has been reported that the red blood cells are composed of water (721 ± 17mg ml $^{-1}$ of the red blood cells), proteins (371 mg ml $^{-1}$ of the red blood cells, out of which hemoglobin forms 335 mg ml $^{-1}$ of the red blood cells), lipids (5.1mg ml $^{-1}$ of the red blood cells) and carbohydrates (80mg ml $^{-1}$ of the red blood cells) [35]. The RBC skeleton provides peculiar mechanical properties. They are able to stand very high shear rates, up to 1000 s^{-1}, when traveling through capillaries thinner than their own size [20]. They are remarkably deformable due to dynamic coupling between the phospholipid bilayer and the spectrin network [36]. However, there have been several developments to bridge the gap between what is known about membrane biochemistry and the knowledge of in situ physical properties. We present results on the effect of pressure on the morphology of red blood cells in healthy and pathological conditions.

These cells have nuclei in their early stage that are extruded as they mature to make space for hemoglobin, a globular metalloprotein. A human erythrocyte has a 6-8 μm diameter and 2-3 μm thickness with a mean cell volume of 90 fl. The average surface area of the cell is 140 μm^2 which is greater than the area required to enclose the volume of 90 fl. This excess surface area is one of the major factors that allows the cell to undergo deformations while transit through narrow capillaries [37].

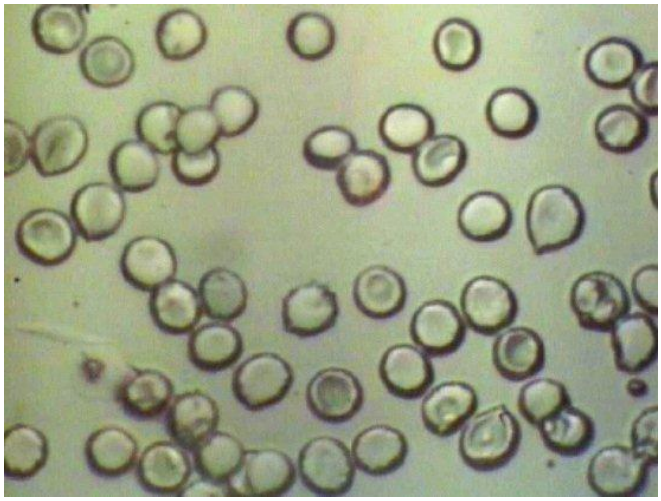

Figure 1 Red blood cells as seen under microscope with 50x microscope objective. Diameter of an individual cell is ~ 7 μm.

They are biconcave shaped disks which optimizes the flow properties in the vessels. In order to pass through the capillaries with the cross sectional area less than the cell's diameter the cell has to squeeze and compress against each other to move. The membrane of the cell is essential for regulating surface deformability and flexibility. The term deformability means the ability to alter the shape under external stress and to regain the original shape once normal conditions are retained [36]. Deformation characteristic of red blood cells have been a topic of research for decades.

Physical and rheological properties of red blood cells, as well as their shape, play a major role in blood flow and in their cellular-biochemical functions. Physiological levels of high pressure can change the cell morphology and membrane fluidity [38]. Reversible shape changes and stratification of red blood cells during centrifugation have been directly observed [39]. Gedde et al. have studied the shape response of human erythrocytes to altered cell pH [40]. They conclude that neither change in membrane lipid asymmetry nor normal levels of the pH-titrable inner monolayer lipids is necessary for cell pH-mediated shape change. These authors also

examined the effect of independent variation of membrane potential on red cell shape [41]. It was found that a broad variation in membrane potential does not perturb red cell shape [41, 42]. It follows that one or more of the other changing red cell properties mediates change in membrane curvature and shape in altered external pH. Rather a change in cytoplasmic pH can cause shape changes of human erythrocytes equilibrated in altered pH environments [43]. A recent development of a cytoskeletal dynamics simulation framework allows to model possible roles of external shear stress (related to deformability of healthy RBC at large strains), specific chemical energy, and protein association strength [44]. In a very recent report surface modifications in red blood cells were observed following high pressure treatment above 200 MPa [45]. These results offer a mechanistic rationale for the erythrocyte cytoskeleton mechanical function under loading. Shape changes may be related to molecular structure that affects mechanical properties. This provides a motivation for investigating morphological and volume changes of individual red blood cells over a wide range of pressure using optical and conformational sensitive probes.

2.1.1 Composition and structure of red blood cell membrane

Red blood cell membranes are composed of 19.5% water, 39.6% proteins, 35.1% lipids and 5.8% carbohydrates [35]. These structures along with performing the biological functions are collectively responsible for the cell deformability.

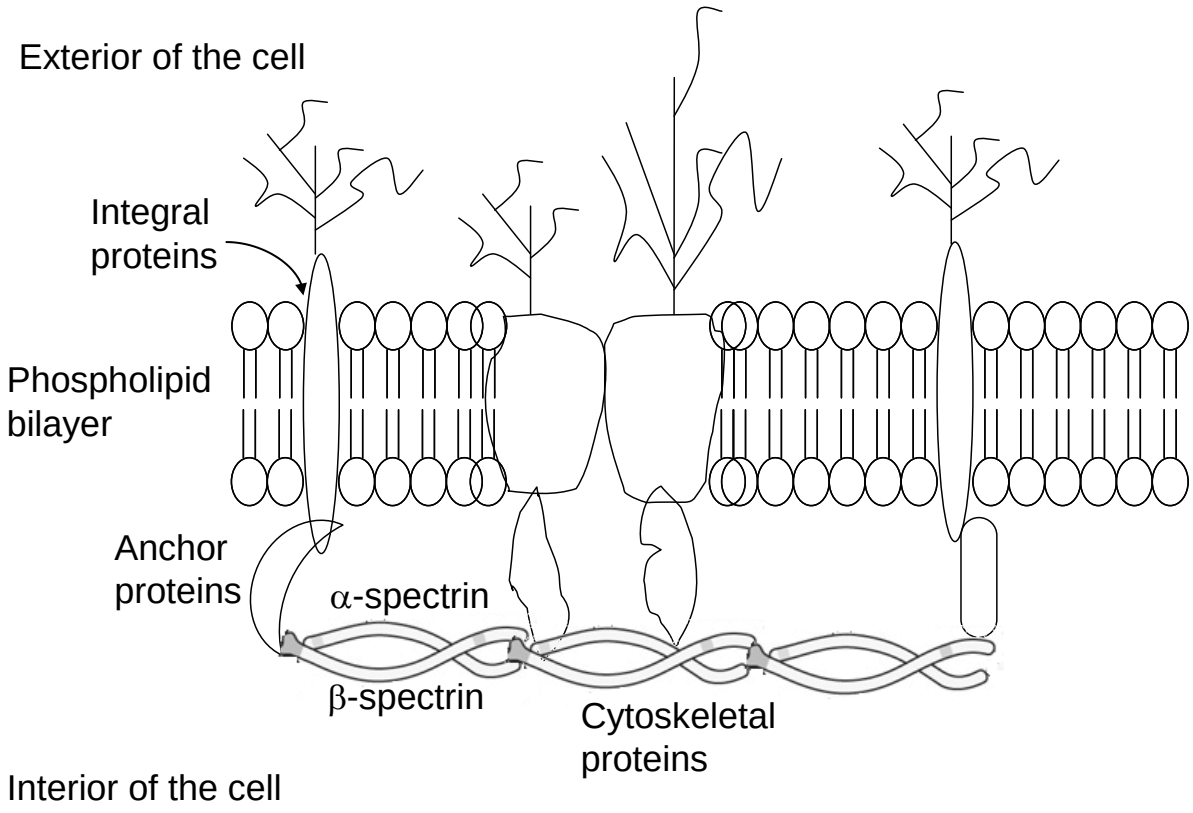

Figure 2 Schematics of Red blood cell membrane

The total lipid content can be further categorized into phospholipids 60%, neutral lipids 30% and glycolipids 10%. Most phospholipids are comprised of two fatty acids attached to the glycerol backbone. The degree of membrane fluidity is significantly affected by the state of saturation of these fatty acids and the length of these acyl chains. Membrane fluidity is enhanced as the degree of de-saturation increases as the packing of hydrophobic tails in the core of bilayer is disrupted. Short acyl chains are also reported to enhance membrane fluidity [35].

The lipids are arranged asymmetrically within a bilayer between the inner and the outer layer with more than 75% of choline-containing neutral phospholipids found in the outer layer

while 80% of the negatively charged phospholipids localized in the inner monolayer [36]. This membrane asymmetry plays a crucial role in the interaction of the cell with the outer environment [46, 47]. The lipid rich domains form the intrinsic feature of the membrane while positively charged amino acids are concentrated on the cytoplasmic side of glycophorins. A minimal change in inner and outer layer surface area can significantly affect the shape of red blood cell. Lipid composition of a healthy human red blood cell is tabulated below [48].

Table 1 Phospholipid composition of human Red Blood Cell membrane

Phospholipid	**Percentage by volume**
1-palmitoyl-2-linoleoyl-sn-glycero-3-phosphocholine	20%
1-palmitoyl-2-linoleoyl-sn-glycero-3-phosphoethanolamine	12%
1-stearoyl-2-linoleoyl-sn-glycero-3-phosphoethanolamine	8%
1-stearoyl-2-arachidonoyl-sn-glycero-3-phosphoethanolamine	4%
1-palmitoyl-2-linoleoyl-sn-glycero-3-phospho-L-serine	11%
L-α-phosphatidylinositol	3%
L-α-phosphatidylinositol-4-phosphate	0.5%
L-α-phosphatidylinositol-4,5-bisphosphate	0.5%
Sphingomyelin	22%
Cholestrol	19%

Membrane lipids interact with integral membrane proteins within the lipid bilayer. Membrane proteins are also an important determinant in the red blood cell shape and

deformability [49]. Based on the ease with which they can be removed, they can be categorized into two groups; *peripheral proteins* (spectrin) and *integral proteins* (band 3 and glycophorins). They are also classified into three categories based on the functionality in determining the membrane structure. *Cytoskeletal proteins*, namely, spectrin, 4.1 and actin. They form a cytoskeleton network located beneath the lipid bilayer. Band 3 and glycophorins forms the category of *integral proteins* which are tightly embedded into the lipid bilayer. *Anchoring proteins*, ankyrin and 4.1 connects the cytoskeletal network with the integral proteins. Advances in understanding the protein linkages shows actin filaments are associated in a ternary complex with spectrin and band 4.1 [50].

Through direct deformation measurements it has been established that the cell membrane behave like a semisolid with elastic properties [50]. Cell deformability has been studied experimentally through uniaxial perturbation [28, 51, 52] and mathematical simulations. Photomicrography of the cells has been used to accurately measure the diameter of the red blood cells suspended in plasma [53]. To evaluate mechanical properties of the membrane in terms of elasticity, compressibility and shear rigidity, a variety of techniques with different degree of perturbation are required [51]. Red cell filtration techniques have been used to measure the ability of the cells to enter and pass through narrow pores [54]. Though, this technique allows analyzing the elasticity of the membrane, information on individual cell compressibility is difficult to obtain [55]. The micropipette technique has also been widely used to study the shape change and recovery process by cell aspiration to pass through a small opening [56, 57]. Shape recovery is determined by membrane elasticity [58, 59].

It has been shown previously that stained and dry film measurements of the cell size are of limited accuracy as these techniques cause the shrinkage of the cells [53, 60]. Direct optical imaging

provides an excellent means to investigate interactions of molecules and membrane fluctuations in biological systems. To investigate the elastic properties of red blood cells we employ hydrostatic pressure and direct optical imaging to record the response in real time [61].

Pressure introduces morphological and volume changes in the cells. The novel use of capillaries to study the cell in vivo is one of the key elements of our study. Cells are viewed microscopically with an upright microscope that is equipped with a micro-positioning stage and a CCD camera. We have shown that RBCs can be enclosed in micro-capillaries and have obtained micro-images of individual living red blood cells. These investigations addressed two aspects. Firstly, measuring the mechanical properties of the cell and relating it to its structure and secondly, explaining the shape under physiological and pathological conditions. The dynamic mechanical properties were studied by measuring the size change over variable pressure range. These studies gave insight into the microscopic structure of the membranes, as they undergo deformations during circulation through vessels. They also provide a means to characterize the physiological state of the membrane and its changes caused by diseases, metabolic defects, or application of drugs in a quantitative way.

Rao et al. [62] have recently reported a transition between the oxygenation and deoxygenation states in an erythrocyte, which is induced by stretching the cell with optical tweezers. The transition is attributed to enhanced hemoglobin-membrane and hemoglobin neighbor-neighbor interactions. The micro-capillary technique used in our experiments lends itself to study the pressure dependence of such a transition under solution conditions. We compare shape changes observed at high pressure to those that might be induced through loss of hydration.

Bio-molecules and cells are dynamic systems which are very sensitive to their immediate environment. The ability to see and study a specimen optically is of great importance in the field of

biology, geology, chemistry and material science. Despite various techniques available to monitor samples at microscopic level, researchers are always hunting for methods that can be used without damaging the cells or using marker dyes. Absorption measurements provide a convenient way to characterize materials in laboratory without use of exogenous labels. It is a non invasive method that can allow the study of viable biological specimens without altering their behavior with marker dyes.

In Chapter 4, a novel approach is presented that couples well established confocal microscopy with absorption spectroscopy. This enables us to measure the absorption spectrum of single living erythrocytes in healthy and pathological condition with a spatial resolution of 1.4 μm and spectral resolution of 0.5 nm.

2.2 Intra-erythrocytic life cycle of the malaria parasite *Plasmodium falciparum*

Various studies reveal that the cells biochemical and structural composition changes upon pathogenesis. Red blood cell has been studied extensively under numerous hereditary diseases. We present the effect of malaria parasite *Plasmodium falciparum* on the host red blood cell.

Malaria is responsible for over million deaths every year mostly infants, pregnant women and young children in areas endemic for the parasites [63]. Close to half of the world's population still lives in areas with high risk of contracting malaria. According to world health Organization report a child dies of malaria every 30 seconds [64, 65]. According to the U.S. Center for Disease Control and Prevention, more than 1,400 new cases are reported annually in the United States in travelers returning from malaria-endemic areas.

The human malaria parasite has a complex life cycle that requires both a vector body (female anopheles mosquito) and a host body. The sexual reproduction of the parasite occurs in the mosquito

body and the resulting sporozoites are inoculated into the human host when bitten by the infection carrying mosquito. These sporozoites infect the liver cells and mature themselves into schizonts, each containing thousands of merozites, which are released into the blood stream through rupturing. These merozites invade erythrocytes and goes through another round of asexual reproduction in the 48- hour erythrocytic cycle [66].

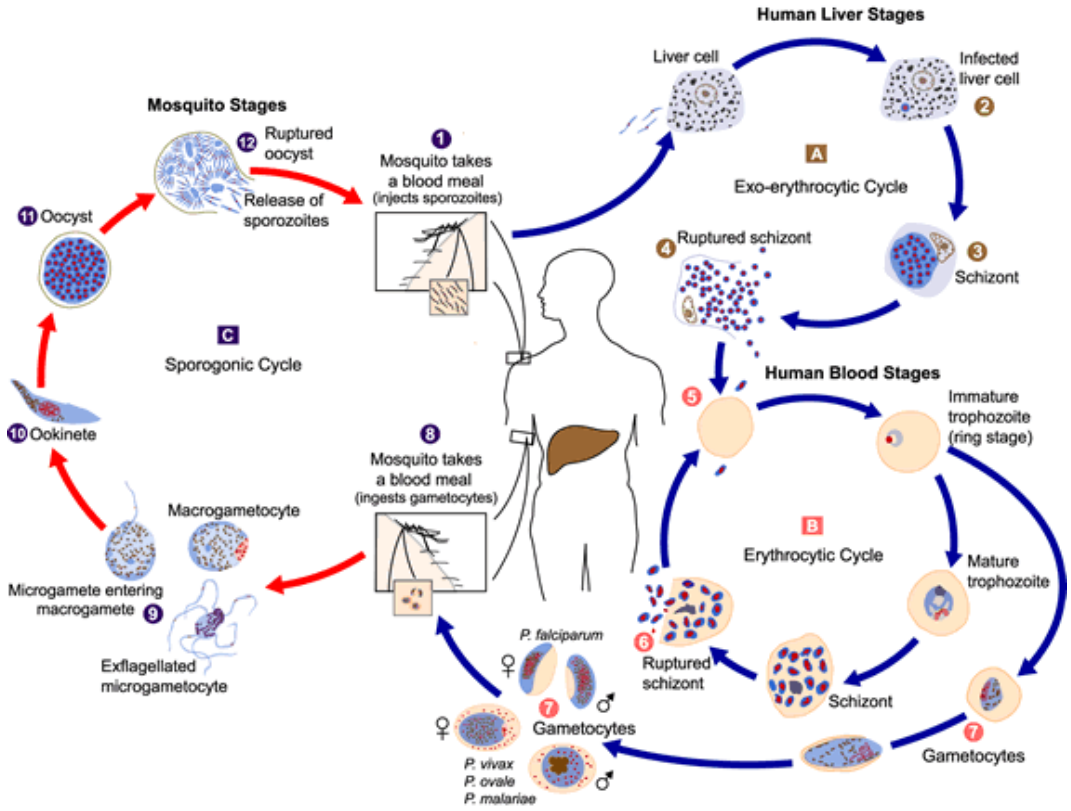

Figure 3 Life cycle of malaria parasite Plasmodium falciparum [223]

Intrusion of malaria-inducing *Plasmodium falciparum* leads to structural, biochemical, and mechanical modifications to the host red blood cells. The intra-erythrocytic multiplication cycle of the malaria parasite, *Plasmodium falciparum,* is divided into distinct stages and has a duration of 46-48 h [67, 68]. During the first half of the development inside erythrocytes, the

ring stage (1-18h after invasion), the parasite displays very little metabolic activity and contains no hemozoin pigment (a polymer of heme product of hemoglobin digestion). The ring stage matures into trophozoite stage (18-28 h post invasion). Extensive RNA and protein synthesis and accumulation of hemozoin characterize this stage. The volume of the parasite inside erythrocytes also increases significantly during this stage of growth. Ring and trophozoites are mono-nucleated cells, but in the subsequent schizont stage (28-38 h after invasion), the parasite undergoes multiple rounds of DNA replication and nuclear divisions, which result in a single syncytial cell containing 8-32 nuclei. The parasite now fills almost the entire cytoplasmic space of the erythrocyte. In the final segmenter stage (38-48 h post invasion), budding nuclei and cytoplasmic organelles from the main parasite mass form individual merozoites.

During the intra-erythrocytic stage of the life cycle of the malaria parasite degrades the hemoglobin. Hemoglobin degradation by the parasite during the intra-erythrocytic cycle has been studied through experimental techniques and mathematical models and simulations. Studies suggest that hydrolysis of globin provides the principal source of amino acids for erythrocytic development and also provide sufficient space for the parasite growth [66]. Hemoglobin degradation is also essential to maintain osmotic stability of the intra-erythrocytic parasite [34]. Breaking down of hemoglobin is a complex process which involves transport of hemoglobin from cytosol to the parasite food vacuole, disruption of hemoglobin tetramers, removal of heme, detoxification of heme by the formation of hemozoin and the hydrolysis of globin by a number of proteases into amino acids. The malaria parasite *Plasmodium falciparum* introduces mechanical changes in the host red blood cell [69-71] making it difficult for the cells to pass through the vessels. This indeed affects the oxygen transporting capability.

2.2.1 Merozoite structure and its invasion of erythrocytes

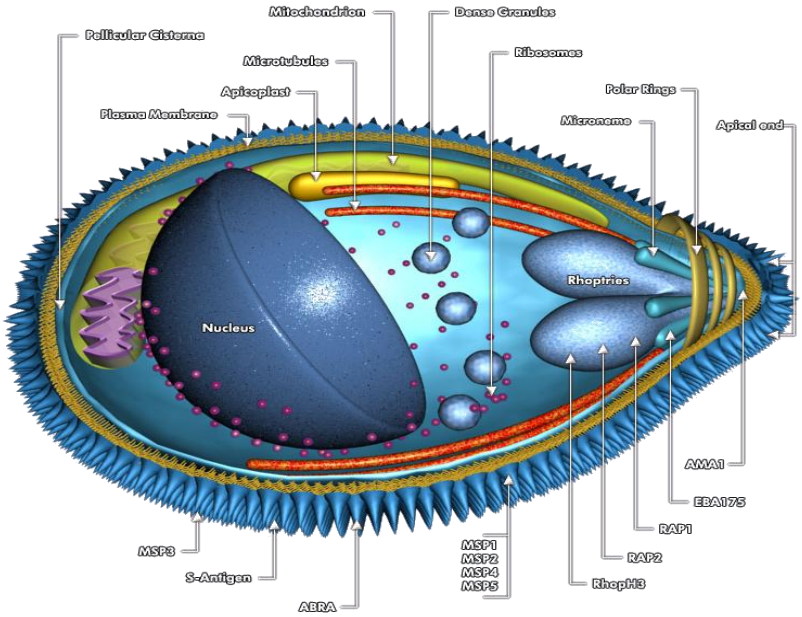

Figure 4 Structure of merozoite [72]

Merozites are 1.5- 2.5 μm long and 1-2 μm wide ovoid eukaryotic cell with a plasma membrane, nucleus and other intracellular organelles [72]. They are broader at the posterior end than the anterior apical pole. The specialized apical pole has three polar rings composed of cytoskeletal matrix surrounding the area from which the parasite molecules are egressed during invasion. Microtubules are present in a localized area of the parasite which allows timely and effective expulsion of the parasite molecules. These microtubules are attached to the basal member of the apical rings. Studies suggested the presence of numerous intra-membranous particles in the merozoite's plasma membrane and intra cellular organelles membrane. Presence of two other membranous structure forming cisterna has been confirmed through electron

micrographs. The surface coat of the plasma membrane is shown to contain spike like structures. These structures help attaching to the erythrocyte while the parasite is released inside the host cell through the apical end.

As a merozoite invades a RBC it starts forming an invasion pit surrounding itself lined with a parasitophorous vacuole membrane to separate itself from the host cell's cytosol. Once inside the host cell the parasite takes the form a ring enclosed within three membranes: parasite plasma membrane, parasitophorous vacuole membrane and the erythrocyte membrane. The parasite then initiates hemoglobin degradation (discussed later in detail) inside the food vacuole. The amino acids released are used to transform the parasite from the quiescent ring stage to the trophozoite stage. After the parasite matures the nucleus divides resulting in the production of more merozoites and the parasite is said to enter the schizont stage. As these merozoites develop, their apical end faces the erythrocyte plasma membrane ready to invade other erythrocytes upon rupture of the host cell.

The whole phase of merozoite invasion can be categorized into three phases [66, 73]. First phase involves identification of an appropriate host cell, followed by the second phase in which merozoites attached to the erythrocytes realign themselves through apical attachments. The final phase involves modification of the parasite environment in order of its growth into trophozoite stage. The process of invasion takes place on the time scale of 30-60 seconds and the conversion into the ring stage on the time scale of 10-20 minutes. The extra cellular merozoites are short lived with parasitophorous vacuole membrane protecting the parasite from external immune system. Studies show that initial adhesion between merozoites and the erythrocyte can occur at any point on the merozoite's surface. They can get detached and can readhere to other

erythrocytes during this step. These interactions are suggested to be molecularly mediated between specific receptors in the erythrocyte membrane and ligands of the merozoite.

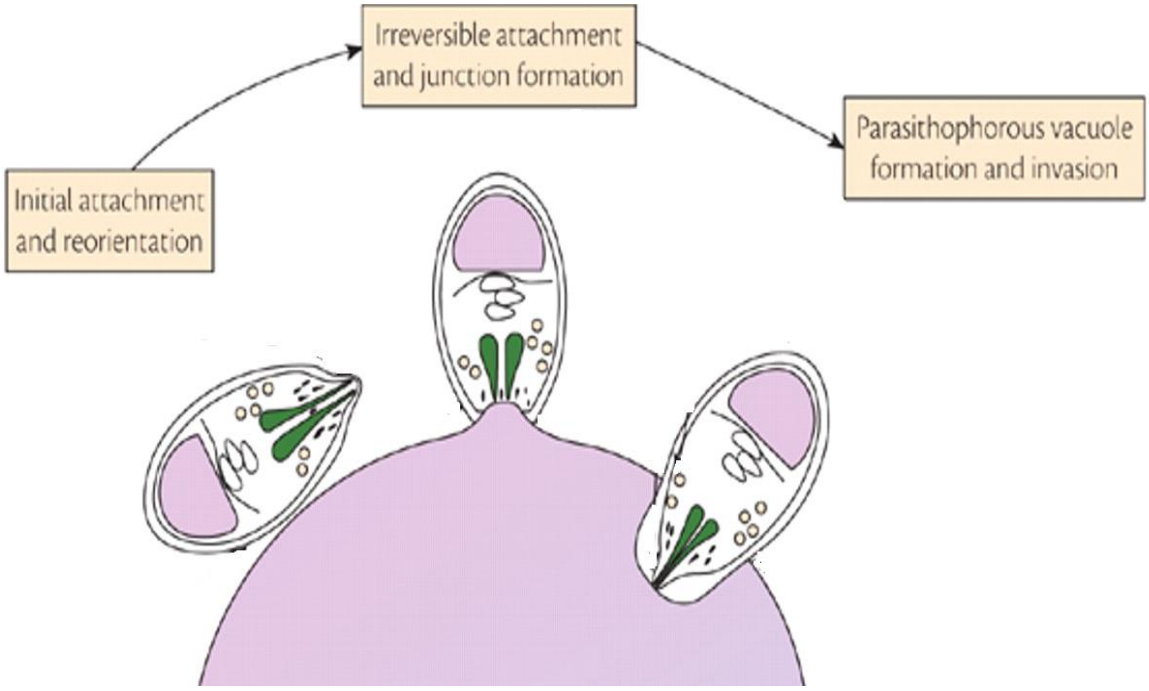

Figure 5 Cartoon showing merozoite invasion of a red blood cell [74].

Figure 5 shows a schematic of merozoite invasion of a red blood cell [74]. After initial attachment, the merozoite realigns itself so that the apical pole is facing the erythrocyte membrane. The studies suggest oscillations in the RBC membrane at the initial contact extending around the merozoite to facilitate reorientation. This positioning of the merozoite's apical pole towards the RBC membrane results in a tight junction, which is irreversible, and allows the merozoites to enter the host cell. Though numerous studies have been performed to identify the specific adhesive and molecular interactions, there is much to be discovered with regards to various molecules involved both as ligands and receptors.

The entry phase of merozoite after the formation of tight junction is a multi step process initiated by merozoites [75]. Electron micrographs show that upon initiation of merozoite entry an indentation appears in the host cell membrane at the site of tight junction. The junction begins to move posteriorly over the merozoite's surface [76]. Parasitophorous vacuole begins to form between the merozoite and the host cell beyond the junction. The parasitophorous vacuole membrane expands inward as the junctional band continues to encircle over the merozoite pushing it into the parasitophorous vacuole. The surface coat is absent in the region of merozoite which gets enclosed in parasitophorous vacuole. Studies revealed that the contents of rhoptries are released into parasitophorous vacuole which contains a mixture of proteinaceous and lipid material that assist in the invagination and restructuring of the host cell membrane and further results in the formation of parasitophorous vacuole membrane. Parasite proteases also play a crucial role in the invasion of erythrocytes with the rupture of membranes to release merozoites. When the merozoite is inside its host cell, it is entirely enclosed by parasitophorous vacuole membrane and the junction fuses to close any connection between parasitophorous vacuole membrane and the erythrocyte membrane. Once invasion is complete the merozites release the sense granules which attach to the cytoplasmic surface of the RBCs membrane and alter the environment assisting in the transition to trophozoite stage.

The malaria parasite inhabits terminally differentiated and enucleated human erythrocytes. To survive within the red blood cell environment, the intracellular parasite extensively modifies the erythrocyte cytoplasm and induces the development of various membrane-bound compartments that serve as sorting stations for exported proteins. These include the multiple single-membrane limited structures called Maurer's clefts (MC) and the complex network of

tubovesicular (TVN) compartments [33, 77-80]. The parasite also induces changes in the membrane structure.

The erythrocytic cycle of the malaria parasite *Plasmodium falciparum* is marked with structural, mechanical and biochemical modifications to the host red blood cell. The parasite degrades the hemoglobin of the host cell and hydrolyzes it into hemozoin [81-83]. We investigated healthy and infected erythrocytes in situ using spatially resolved absorption spectroscopy. The electronic absorption spectrum of a single cell is measured and spectral changes are related to the parasite life cycle. In parallel to micro-absorption, the effect of malaria parasite on fluidity of the host cell membrane is investigated in situ through high pressure experiments.

2.3 Model heme proteins

Proteins are biological macromolecules, consisting of tens or hundreds of amino acids, that play crucial roles in virtually all biological processes [84]. Many proteins are enzymes that catalyze biochemical reactions and are vital to metabolism. They also perform structural or mechanical functions in muscles and also help in maintaining the cell shape. Many small ions and molecules are stored and transported by specific proteins. Other proteins are important in cell signaling, immune responses, cell adhesion, and the cell cycle.

The primary structure of a protein consists of a linear chain of amino acids linked together by peptide bonds. Amino acids, the building blocks of the proteins, are built around a carbon atom connected to a carboxyl group, an amino group, a hydrogen atom and a side chain. The carboxyl (COOH) and amino group (NH_2) are responsible for linking the amino acids to other building blocks in the chain and

the residue group (R) determines the specific properties of an amino acid. The peptide bond that links the amino acids together is covalent in character. The sequence in which the amino acids are linked together is determined by the genetic codes. Even slight discrepancy in the sequence can lead to formation of an abnormal mutant.

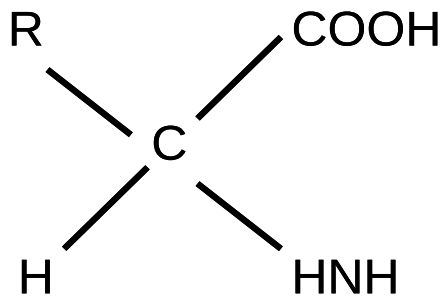

Figure 6 General Structure of an amino acid

Protein structure can be categorized into four levels. The amino acid polypeptide chain forms the *primary structure* of a protein. The *secondary structure* describes 3-D structures stabilized by hydrogen bonds. The most commonly found secondary structures are α-helix and β-sheets. The protein folds into a complete 3-D structure defining the overall shape of the molecule and providing spatial locations to all residues. This comprises the *tertiary structure* of a protein and is responsible for basic function of a protein. The highest structural level is the *quaternary structure* which is formed by non-covalent bonding of tertiary subunits.

Protein molecules are complex systems that can assume a myriad of conformational states, which vary slightly in their 3-D structures and function with different rates [23]. They are dynamic systems which fluctuate between its equilibrium conformations in their native states. This distribution of various confirmation states brings in the concept of energy landscape [85, 86]. The energy surface is highly

degenerate. It can be assumed that a given primary sequence can fold into a large number of different conformational substates, which are separated by free energy barriers [87]. All possible substates together form the energy landscape, where a substate is pictured as a valley in the landscape [86]. During a rebinding reaction, the system undergoes a series of sequential transition states [26, 88]. Measurements of the rate coefficients for the transitions between these states yield the barrier heights. The reaction landscape of the binding is produced by plotting these barrier heights versus a 1-D reaction coordinate [23].

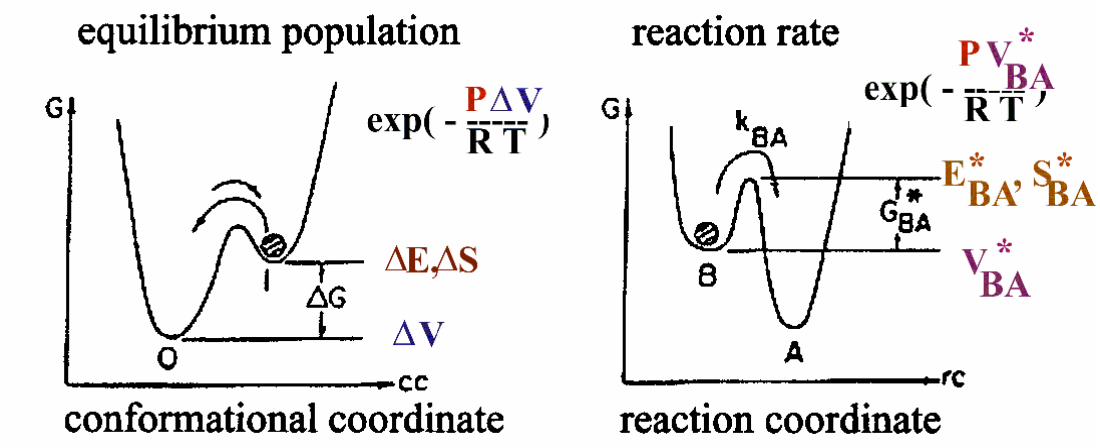

Figure 7 Energy landscape showing different conformational states (left panel) and the binding kinetics intermediate states projected along the reaction coordinate (right panel) [107].

Assuming protein has two states A and B and two conformations 0 and 1. In each of the conformational sub states protein can make a transition from B to A. Now, at equilibrium the ratio of the populations of the two conformational states at a temperature T is given by $e^{-\Delta G''/RT}$ where $\Delta G''$ is the difference between Gibb's free energy between the two sub states. Thus, if the reaction $B \rightarrow A$ occurs

in a conformation state, then the reaction rate coefficient is given by $k = \upsilon e^{-G''/RT}$, where G'' is the activation Gibb's free energy and υ is the frequency factor in that substate.

The existence of substates has been demonstrated by various experiments [89] and by computer simulations [90, 91]. An understanding of how protein structure and dynamics determine protein function is a major goal in biophysics. A static picture of proteins is incomplete and a thorough understanding of proteins dynamics in the light of external parameters such as temperature and pressure is required to understand protein dynamics. An applied pressure P shifts the equilibrium ratio of two conformations by the factor exp (-PΔV), where ΔV is the (conformational) volume difference. Pressure also affects the reaction rate. Within a single conformational state the reaction rate coefficient can be written as $k_{BA} = \nu$ exp ($-G^*_{BA}$ / RT). Here $G^*_{BA} = E^*_{BA} + PV^*_{BA} - TS^*_{BA}$ is the activation Gibbs free energy and ν is a frequency factor. The reaction rate can either speed up or slow down by the factor exp ($-PV^*_{BA}$ / RT) depending on the sign of the activation volume PV^*_{BA}.

A heme protein is a metalloprotein containing a heme prosthetic group bound to the protein itself. The iron in the heme can undergo oxidation and reduction. The two extensively studied heme proteins are myoglobin and hemoglobin. While myoglobin stores oxygen in muscles [92], hemoglobin is the principal means of delivering oxygen to various tissues via blood.

In contrast to the single polypeptide chain of myoglobin, hemoglobin consists of four subunits linked together by non-covalent interactions. Each subunit is composed of a protein chain tightly associated with a non-protein heme group and has a molecular weight of about 17,000 Da, for a total molecular weight of about 68,000 Da. The protein chain arranges into a set

of alpha-helix structural segments that are folded to form a pocket that strongly binds the heme group. It contains a porypherin ring with an iron atom at the center of the heme group [92]. The porphyrin ring is unsaturated with 22 delocalized π electrons. The entire protein molecule is surrounded by a 0.4 nm thick hydration shell. The iron atom is bound to the four nitrogens of the heme and to the proximal histidine of the protein backbone. The backbone is formed of 8 α helices. The ferrous ion prefers to be surrounded by six ligands in octahedral coordination. Nitrogen atoms of the heme provide four of these ligands and proximal histidine forms the fifth ligand. A pocket is formed on the distal side the heme from which ligand binds reversibly to the sixth coordination position of the iron. The iron ion and the four nitrogen atoms in the center of the ring all lie in one plane. The iron is also bound strongly to the globular protein via the imidazole ring of the F8 histidine residue below the porphyrin ring. The heme prosthetic group is same in both.

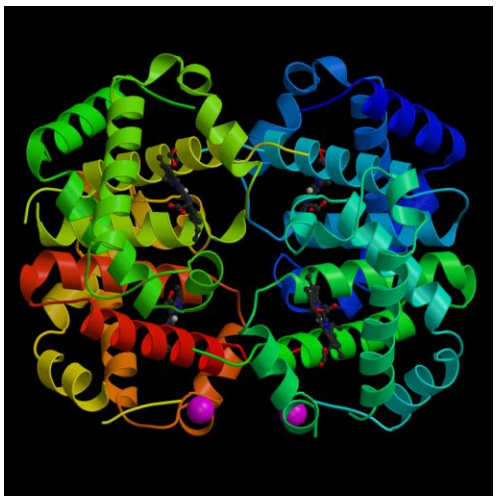

Figure 8 Structure of Hemoglobin: PDB:4HHB

Hb can exist in two distinct structural states [30] characterized by an energy difference for binding oxygen between the high-affinity (R) and low-affinity (T) structures. A sixth position can reversibly bind oxygen by covalent bond. The oxygen diffuses through the cell membrane of RBC and attaches to the heme group of hemoglobin. During binding, oxygen temporarily oxidizes (Fe^{2+}) to (Fe^{3+}). A hemoglobin molecule can bind to four oxygen molecules. It has high oxygen affinity at high pH and low oxygen affinity at lower pH. Also, the binding of first O_2 is slower while the binding of later O_2 is faster. This is termed as collective behavior of the protein in which binding of the molecule increases the affinity for further binding. This effect makes the hemoglobin more complex.

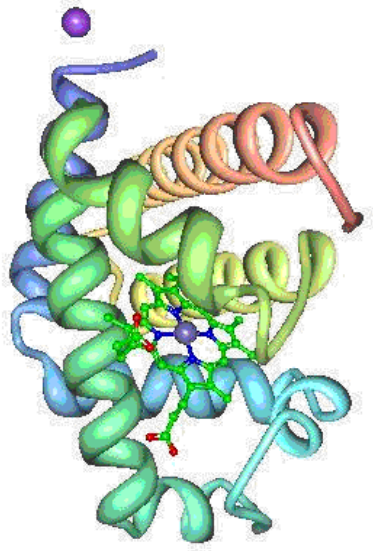

Figure 9 Structure of Myoglobin: PDB :3HC9

Mb consists of 153 amino acids and has a molecular weight of 17 KDa[17] and dimensions of 4x4x2 nm^3[93]. At low pH Mb also catalyzes NO [17]. During the process of reversibly binding the ligand, the chromophore and the protein undergo conformational changes.

X ray structural data show that ligand binding to myoglobin displaces iron atom by 0.45 Å closer to the heme plane [94, 95].

Kinetic experiments have played a crucial role in the history of hemoglobin [96]. The ligand binding kinetics is a key marker to probe its function in situ, and it has been shown to be very sensitive to conformational changes [97-101]. Gibson conducted flash photolysis experiments, which showed that the rebinding rate of CO to deoxy Hb produced after flash is 30 times, faster than the binding rate with deoxy Hb [97]. The deoxy Hb produced after photolysis has a spectrally altered structure [97]. The ligand dissociation and association can be explained by a two state allosteric model. The spectral changes found after photolysis occurs in microsecond to millisecond time regime [97].

Myoglobin and hemoglobin are responsible for storing and transporting small molecules (ligands). Thus, one of the reactions of particular importance is protein interaction with different ligands. The binding between a ligand and the protein occurs by weak reversible bonds. Ligand binding is associated with the conformational changes in the protein.

2.4 High pressure studies

Pressure and temperature are fundamental thermodynamic variables that affect the functional and structural properties of cells and bio-molecules [102]. Pressure between 10 - 100 MPa can exert powerful effects on growth and viability of organisms [19, 103]. For example, Bartlett et al. found that that the stress response of E. coli to elevated pressure of 53 MPa resulted in the induction of 55 proteins [104]. Despite the fact that the basis of all pressure effects arise from a single perturbation, namely the change in

system volume that accompanies a physiological or biochemical process, high pressure exerts many influences on living organisms, making it difficult to pinpoint pressure-points in cell growth and viability [19]. Ocean's depth varies from an average of 3800 m to a maximal of 11000 m, thus having a pressure ranging from 38 - 110 MPa. It is a fundamental thermodynamic variable, which on one hand can deactivate enzymes and kill bacteria and on the other hand affects both the equilibrium constant and the rate of a biochemical reaction [8]. Pressure can unfold proteins and introduce conformational changes in the protein. It is important for the understanding of physical forces that stabilize native structures. To understand the life under deep sea, it is crucial to study the pressure effect on proteins.

Functional properties of biological molecules and cells are affected by high pressure environment [7]. Recent investigations have explored the effect of pressure on proteins [102, 105-110], lipid membranes, vesicles [111, 112], microbes [19, 103] and cellular systems [7]. On the cellular level, studies shows that the bacteria E. coli undergoes elongation of shape and inhibition of colony formation at elevated pressure [113]. Application of high pressure affects the cell morphology and thus affects the functions of the organisms whose native environment is at ambient pressure. The mechanical behavior of the muscle fiber is reported to change with increase in pressure [114, 115].

A Red blood cell is composed mostly of protein hemoglobin which is a complex bio-molecule. Protein molecules are surrounded by water molecule. This hydration water plays an important part in the activity of the protein. An application of hydrostatic pressure is to modulate the interaction between the protein and the hydration water. NMR studies reveal that high hydrostatic pressure does not affect the primary and secondary of structure of the protein but just increases the structural fluctuations of protein molecules [6]. The pressure induced effects are suggested to be caused by clustering of the water

molecules around the hydrostatic and hydrophobic parts of protein. This implies that the elevated pressure modulates protein function and structure without use of any chemical other than water molecules [116].

At ambient pressure, temperature is a widely used as a perturbant. However an increase in temperature can cause irreversible change in protein structures in solutions and can have simultaneous changes in volume and thermal energy in a way that's hard to separate, pressure can isolate the effects that depend solely on volume. It can provide a continuous controlled way for molecule environment perturbation [18]. Even a single protein is a complex system with large number of conformational substates. Pressure can either act on a given substate or effect the distribution of conformations influencing protein structure, function and dynamics [107]. For high pressure studies of protein, we use a simple reaction and a well characterized protein. The experiments performed investigate ligand binding kinetics to heme proteins in the light of variable pressure.

2.5 Ligand binding reaction in heme proteins

At physiological temperatures, each molecule can fluctuate between different conformational states, while at low temperatures, each protein is frozen into a particular conformational state [24]. Dynamics is essential as oxygen cannot enter or leave Mb if the atoms were fixed in their equilibrium positions [117]. As the temperature increases the proteins breathe and moves from one conformational state to another and the ligand rebinding to Mb sees an average barrier height rather than a distribution leading to exponential time dependence [25]. At higher temperatures and lower pressures the ligand gains enough energy to transit through the pathways and escapes to the solvent. Once in the solvent all the ligands present are eligible to bind at the heme atom. The nature of the solvent plays an important role in rebinding [26]. This exponential process S involves rebinding from the solvent.

The first X-ray structural data of intermediates of a reaction obtained showed that ligand binding to myoglobin is accompanied by a ≈ 0.35 Å displacement of the iron atom close to the heme plane [118]. The complexity of rebinding kinetics and different intermediate states has been supported by the low temperature crystallography data [119].

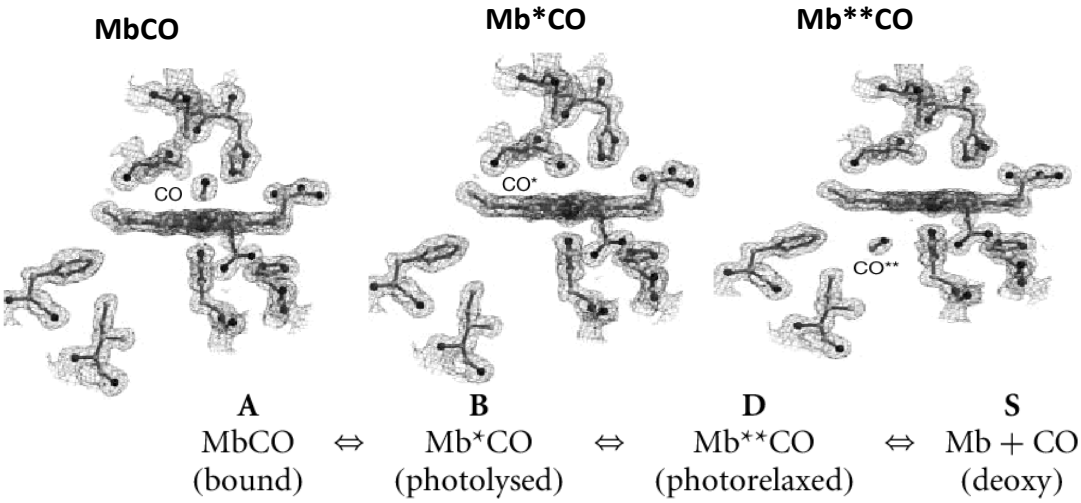

Figure 10 Low temperature X-Ray crystallographic data [119] of myoglobin reaction intermediates.

Low temperature X-ray crystallography of the photolysed state [119] shows that initially the system has CO bound to the heme iron to form carbonmonoxy myoglobin. The above X-ray picture shows that immediately following photolysis, the system is in the photodissociated state; the heme and the pocket are assumed to be in the bound conformation, but the dissociated ligand occupies the heme pocket. Rebinding and relaxation of the protein to the deoxy structure then occur simultaneously. After photolysis, the CO migrates inside the heme pocket to a primary docking site. It becomes photo relaxed when the second docking site becomes populated as ligand moves to the proximal side of heme. At high temperature and after long times, the ligand escapes the protein matrix to the solvent and we get deoxy myoglobin.

At ambient pressure the non-exponential intermediate processes have been attributed to intramolecular kinetic states indicating that ligand migration occurs through a limited number of pathways with docking sites [120]. In experiments performed at higher temperatures CO has been found in protein cavities which are also binding sites for xenon, particularly on the proximal side. Evidence for ligand migration toward the xenon-binding cavities has come from ambient pressure flash photolysis studies of MbCO and MbO_2 including mutants [121, 122] and experiments where docking sites are blocked by xenon [123]. Conformational relaxation and motion of the F-helix following ligand dissociation has recently been observed with time-resolved x-ray crystallography [124]. Since there are significant differences in the static x-ray structures of MbCO and Mb, these multiple intermolecular processes have also been modeled by protein coupled barrier changes [125]. A recent theoretical and computational investigation [126] finds that Mb has more than one exit to and from the heme binding site and that the network of cavities may have an influence in tuning the different ligation properties of various gas ligands.

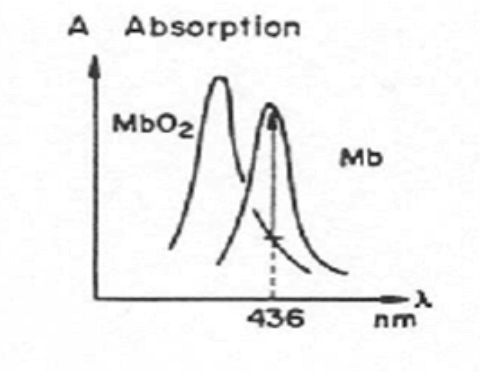

Figure 11 Soret Absorption Band of ligated and unligated states of myoglobin [17]

The underlying concept for studying the heme protein rebinding kinetics via flash photolysis is that the chromophore absorption in the myoglobin is sensitive to the ligation state [102]. The Soret absorption band is at 434 nm for Mb, 423 nm for MbCO and 418 nm for MbO_2 [23]. A blue LED provides the monitor beam at 440 nm. The light intensity passing through the sample before and after photolysis is recorded. The sample is monitored at 440 nm beam with a photo multiplier tube. The difference in the absorption spectrum of ligated and unligated Mb allows us to follow the subsequent rebinding optically.

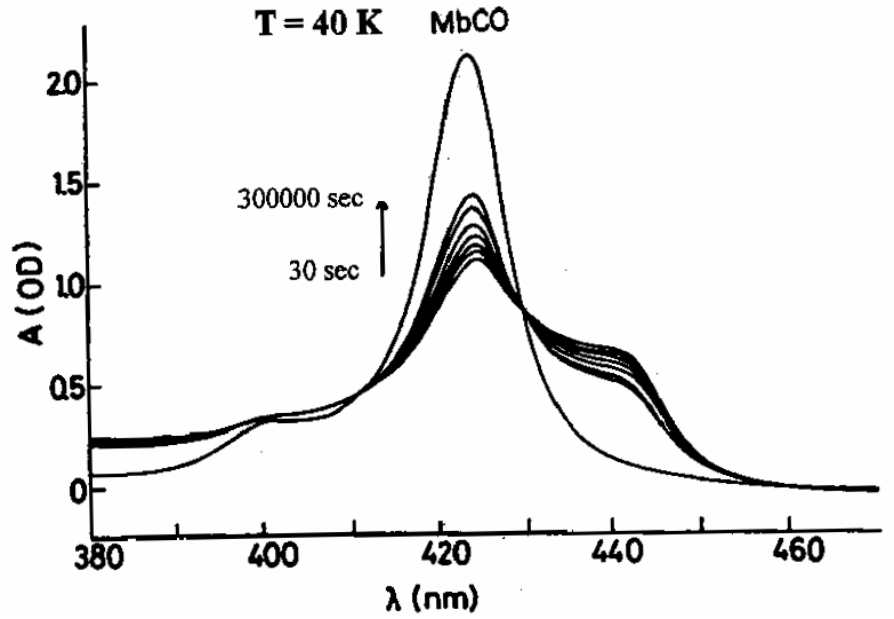

Figure 12 Absorption spectra following Mb CO photolysis at low temperature [127]

Figure 12 shows the absorption spectrum of MbCO at 40 K before and after the flash photolysis at 40 K and spectra taken at subsequent time (30sec-30000sec) following flash photolysis. The increase of the absorption at 423 nm (MbCO) and decrease near 440 nm (Mb^*) indicates the binding kinetics [127].

A few static X ray measurements at variable pressure [128] have been available recently, most time resolved measurements are done at ambient pressure. Sub Angstrom changes can be resolved using spectral assignments through vibrational spectroscopy [9]. Static X ray structures and electron density data confirms the presence of docking sites [129]. It also suggests that the ligand once photolysed initially lies flat on the heme plane and later migrates to occupy the pocket on the proximal side of the heme plane. Tetreau in 2004 explored ligand migration and competition of ligands with Xe to occupy these docking sites [123]. Recent time resolved X ray crystallographic studies carried out after flash photolysis of CO to Mb suggest that structural changes under pressure can be interpreted as change in the populations of conformational substates [128].

Additional structural information from high pressure X-ray data is available [129], however these measurements may not resolve the small differences detected by rebinding kinetics experiments. The ligand binding reaction has been studied by various methods such as time resolved spectroscopy, low temperature spectroscopy, stopped flow technique etc [92, 130]. Ligand rebinding processes encompass both slow and fast reaction which go over more than nine orders of magnitude in time [23]. It involves fast process extending from nano seconds to 10^{-3} seconds and slow process with rapid drop off at several seconds [131]. Thus, we employed the flash photolysis technique extended in three directions: time, pressure and temperature.

CHAPTER 3. RESEARCH DESIGN AND METHODOLOGY

3.1 Challenges and experimental approach to high pressure studies

High-pressure spectroscopy of bio-molecules is a unique technique for exploring and understanding biological systems [132]. Specialized pressure cells have been introduced for NMR studies [133] and studying protein kinetics [107].

To extend high pressure applications to sub-cellular level, there has been a growing interest to combine high pressure applications with imaging techniques. Diamond anvil cell has been used to directly visualize biological and chemical probes during high pressure application. Due to uncorrected aberrations for diamond window, spatial resolution is quite poor [134] and the assessment of exact pressure inside the diamond anvil cell was inaccurate. Because of the thick optical windows, it further required longer working distance microscope objective and thus limits NA [135]. To overcome these constraints a high pressure vessel with higher resolution has been introduced which uses sapphire optical windows [136]. A specialized high pressure vessel with improved image quality when using large working distance have been employed to study single fibers of skeletal muscles using confocal fluorescence microscopy [137]. The HPDS high pressure cell employs an inverse light microscope coupled to CCD camera has been adapted to directly monitor cells under pressure [138]. A modular system for high resolution fluorescence microscopy has been employed to image the growth of E. coli at higher pressure. Salmon

developed a stainless steel high pressure microscopy chamber with strain free optical windows to examine the pressure related changes in the biological systems directly [139] which has been successfully employed to study polymerization-depolymerization of microtubules. Using this conventional high pressure chamber the effect of high pressure on the structure and function of cytoskeletal proteins have been studied [116].

These conventional pressure cells pose a problem in in-situ studies of individual cells. The optical windows of the pressure cell usually have a thickness of 1 mm or more. Single molecule detection requires high NA and small working distances (<0.5 nm). A novel approach to high pressure studies was introduced that employed fused silica micro-capillary as a high pressure cell for fluorescence [132] and Raman spectroscopy [140-142]. The dimensions of the capillary made it possible to be used as a microscopic sample holder and the wall thickness makes it compatible with high NA. We couple the micro-capillary technique with a camera to enable direct optical imaging in real time at variable pressure. In the following section I briefly describe the two pressure cells involved during the high pressure experiments reported in this dissertation.

3.2 Direct Optical imaging at high pressure

3.2.1 Micro-capillary high pressure cell

In the micro-capillary based pressure chamber, the capillary walls serve both as a mechanical support and optical window. Pressure robustness is achieved by using the capillaries with high outer-to-inner-diameter ratio and wall thickness compatible to high NA is maintained. The cell [140-142] provides optical access and is derived from a design first used for fluorescence correlation spectroscopy by Mueller

and Gratton [132] and in the imaging of giant vesicles [112]. In developing high pressure chambers for live cell imaging we couple a high pressure square geometry micro-capillary to a confocal microscope. The capillary chamber used for live cell imaging has to be flat-geometry as the curved capillary walls introduce significant image aberrations. Use of confocal microscope also helps in increasing the contrast and providing better spatial resolution for imaging.

A fused silica micro-capillary of square geometry (Polymicro, WWP050375) with an inner bore of 50 μm and outer diameter 350 μm was used as a nano liter sample holder. These capillaries can handle a pressure of upto 700 MPa [132]. Using either nitrogen gas or an inert liquid as the pressurizing medium, the pressure can be continuously varied. The advantage of the micro-capillary based high pressure cell is that it allows measurements with minuscule amounts of sample and is well suited (due to the small volumes involved) for pressure jump experiments. It is also compatible with high numerical aperture (short working distance) microscopes objectives. The micro-capillary is coupled with a hand driven pressure pump through a pressure plug [141]. The hydrostatic pressure pump uses 3M Fluorinert (FC-84) as the pressurizing medium. To make the high pressure cell, the micro-capillary tubing is cut to a length of 9 inches by placing it on your finger and making a slant cut at 45^0 using the non serrated side of the specialized cleavage stone. It was then pulled horizontally to break it along the cleavage. An improper cut may lead to a fault that can lead to easy breaking of the micro-capillary upon stress.

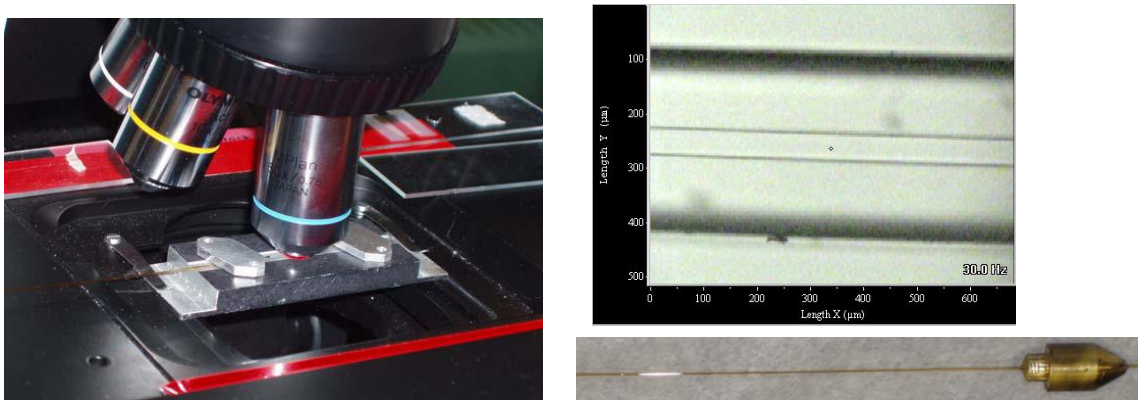

Figure 13 Camera view of the micro-capillary mounted on the microscope stage (left), a picture of fused silica micro-capillary with optical window for viewing the cell (right bottom). The top right panel view shows a microscopic image of the optical window.

A small hole is made in the conical pressure plug and the capillary is inserted into the hole and secured using the glue. The glue employed was a combination of two glues mixed evenly in equal proportions and kept at room temperature for 30-45 minutes. The pressure plug is heated using a plate heater so that the glue can be easily poured into the hole. The hole was filled up with glue and the capillary is inserted through the wider side. Caution has to be taken that it is aligned at the center of the plug. The plug along with the micro-capillary is kept on the heating plate and rotated slowly so until the glue gets hard and the capillary is fixed into the plug. The piece is kept at room temperature for at least 12-14 hours before employing it into the experiment.

To visualize the sample inside the capillary an optical window is required. The silica coating is burned using a matchstick and wiped with ethanol to get the optical window. The sample is loaded in micro-capillary by dipping one end in the sample culture allowing capillary action to draw the cells up and also by employing vacuum pump if required. The micro-capillary is sealed at the free end using an acetylene lamp which fuses the silica together.

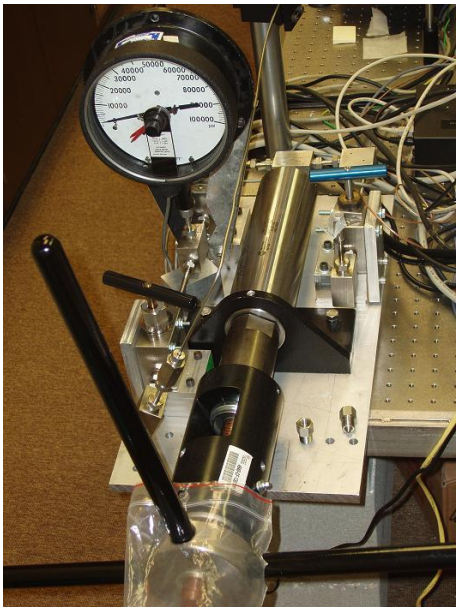

Figure 14 Hand driven Pressure pump

The other end of the capillary which is attached to the pressure plug is connected to the steel tubing which couples the home built pressure generator to the micro-capillary. A standard pressure gauge is connected to the pump for reading the applied pressure.

Optical microscopy has always been a powerful tool in monitoring and studying biological samples. Conventionally, it is done by putting the sample on a glass slide and putting it under microscope. We extended the micro-capillary approach to study the sample close to physiological conditions. A micro-capillary technique has several advantages over conventional slide method. On a slide, a sample may get dried up while in the micro-capillary it can be kept alive for longer periods of time. Using a micro-capillary allows the sample to be closer to the conditions of their native environment. The small sample volumes allow investigating individual cells without interference from adjacent neighboring cells.

3.2.2 Microscopic-imaging at high pressure

Bio-molecular dynamics and stability are predominantly investigated in vitro and extrapolated to explain the function in the living cell. A micro-capillary as a pressure cell provides a tool to study the cells in an environment more closely resembling their native environment [140]. It allows keeping cell alive and enabling the study of the same cell through the whole pressure cycle. The photomicrography setup combines commercial confocal microscope (Olympus BX 41) with self made high pressure setup. The microscope employs a 100 x dry objective (NA=0.92). The apparatus has 1 µm lateral and 2 µm axial resolutions.

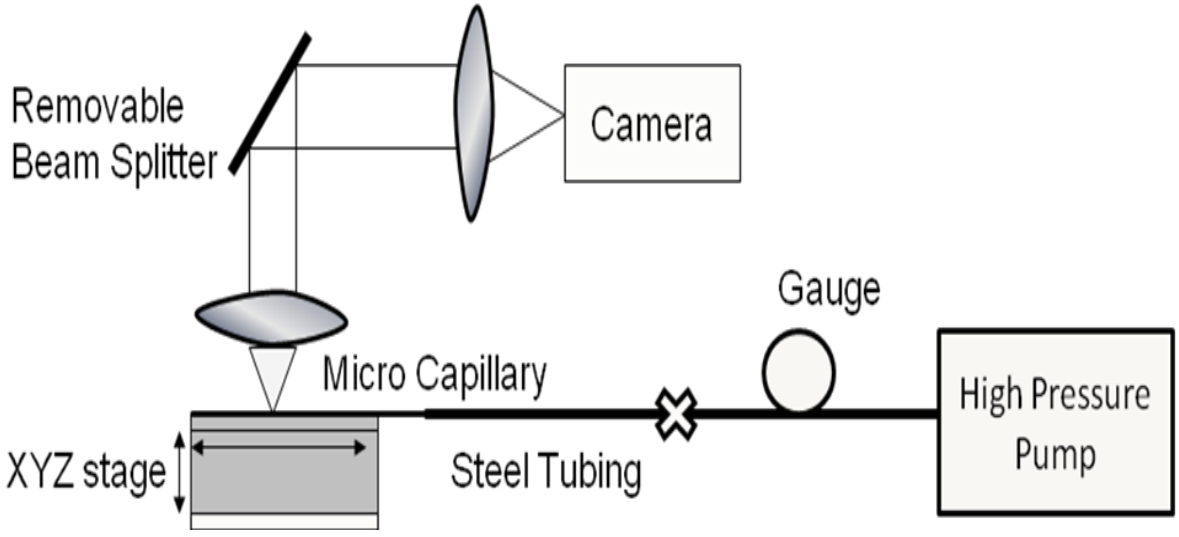

Figure 15 Schematics of high pressure setup employed for investigating morphological changes in red blood cells in real time

The loaded micro-capillary is placed in the slide groove mounted on motorized XYZ stage and positioned under the microscope attached to a TV camera (Sony CSC790) for direct optical imaging. Caution has to be taken while aligning the micro-capillary in the groove that the plane side of the capillary and not the edge faces up. A lot of readjustments may lead to additional stress making the micro-capillary

fragile and easy to break upon pressurizing. Using the camera a real time movie was made while the sample was slowly pressurized up to 200 MPa and then de pressurized back to ambient pressure. The image was taken at a pressure step of every 2 k Psi (13.7 MPa).

With a 50x objective (NA=0.75), a lateral resolution of 0.4 μm is achieved that allows to easily obtain the images of the red blood cells. The micro-capillary allows monitoring the same cell throughout the pressure cycle. Since there is no limit to the time taken to measure the diameter of the cell once the pictures are taken, the measurements can be done with more accuracy as compared to the measurements done directly under microscope. Also, as the images are permanent, so, the measurements can be rechecked for the errors by any number of users.

The above setup allows us to investigate high pressure effects on the structure of a red blood cell in healthy and pathological conditions. The novel use of capillaries enables studies of both healthy and pathological cells under conditions closely resembling their native environment. The same cell can be investigated over the life cycle of either the cell or an infecting agent. In the case of an erythrocyte and its parasite this may lead to a clearer understanding of the cell degradation process and provide data that will be useful in the development of anti-malarial therapies.

3.3 Flash photolysis experiment at variable pressure

3.3.1 Copper beryllium cell for optical spectroscopy

To investigate protein-ligand binding reaction at variable pressure a compact high pressure cell that can be attached to the cold head of a refrigerator was employed. Prepared samples were sandwiched between two sapphire windows using a doughnut shaped Teflon spacer of 1 mm thickness and 3 mm diameter hole inside a beryllium copper sample holder and placed in the high-pressure cell for measurements.

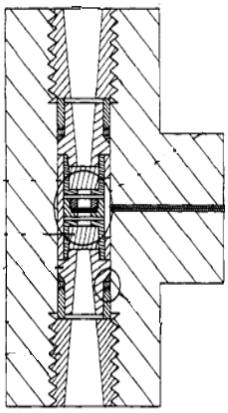

Figure 16 High Pressure Cell [107]

The experimental setup is similar to the one used previously for Raman measurements [102, 143]. The pressure cell is constructed of beryllium copper that combines the ability to resist high pressure (up to 400 MPa) with good thermal conductivity. Sapphire windows allow measurements from near UV to near IR region. The windows are held in place on the mushroom plug using an unsupported area seal which can withstand pressures upto 400 MPa and temperature from 30 K – 350 K. High pressure was generated by an air-operated diaphragm-type compressor obtained from Newport Scientific (Jessup,

MD), which is rated for a maximum operating pressure of 200 MPa. Nitrogen or helium gas is used as the pressurizing medium. With the present setup the pressure could be raised from 0.1 MPa (1 atm) to 170 MPa within 100 s. For cryogenic measurements the pressure cell is mounted to the cold head of a closed-cycle refrigerator (Model 22, CTI Cryogenics, Waltham, MA). To minimize the heat leakage at the pressure tubing/cold head interface a cold head bell adapter is used. The sample temperature is measured with a Si diode on the high pressure cell [107] and is stabilized to 0.1 K with a temperature controller (RC-93C, Lakeshore, Westerville, Ohio). The sample is held in place using a doughnut shaped Teflon spacer sandwiched between the sapphire windows [102].

3.3.2 Transient absorption following photolysis at variable pressure

There are two major experimental requirements for transient absorption experiments in erythrocyte suspension: i) measure the absorption spectrum of a cell suspension or an individual cell, and ii) record binding kinetics over many orders of time and amplitude. We have demonstrated that both are feasible with our experimental setup. As protein dynamics extends over many timescales, another key consideration is that pressure effects can be probed over a wide dynamic range (10 decades in time) in a single experiment. The technical challenge is to contain the very high pressure at variable pressure while allowing access by optical or other non-destructive probe.

The kinetics of ligand binding to myoglobin at variable pressure was studied using flash photolysis technique. A frequency doubled Nd: YAG laser is used to photolyze the sample at a wavelength of 532 nm. The covalent bond between the ligand and the Mb is broken by the absorption of

a visible photon. The setup is designed to measure changes in the absorption spectrum of the sample in the nanosecond to several seconds timescale after photo dissociation.

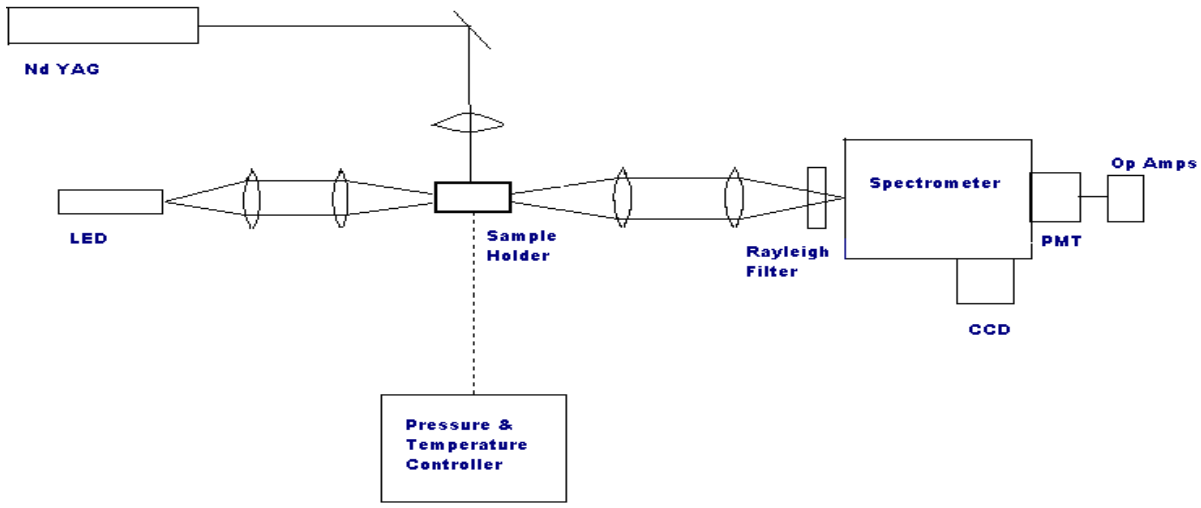

Figure 17 Schematics of flash photolysis setup

Before reaching the sample the monitor beam is passed through a pair of lenses and an interference filter to get a well focused collimated beam. The photomultiplier tube connected to the spectrometer collects the light. Hamamatsu photomultipliers R955 has been used in the setup. It is a side on photomultiplier tube with synthetic quartz window. It has a broad wavelength range of 160nm to 900 nm and a gain of 10^7 with an operating voltage of 1000V and average anode current of 0.1mA. The PMT signal is further amplified for significant signal detection. The PMT output can be fed into a storage oscilloscope and the data can be taken from scope tracing. But, the time bases of oscilloscope are linear, thus only a limited time range can be observed from a single flash which doesn't satisfy the requirement of having wide dynamic range of several decades to unravel the complex processes. Thus, the output of

the PMT is fed to a current to voltage converter. As the light reaches the anode of the PMT, an avalanche of electrons is created which generated a current of several micro amps at the cathode.

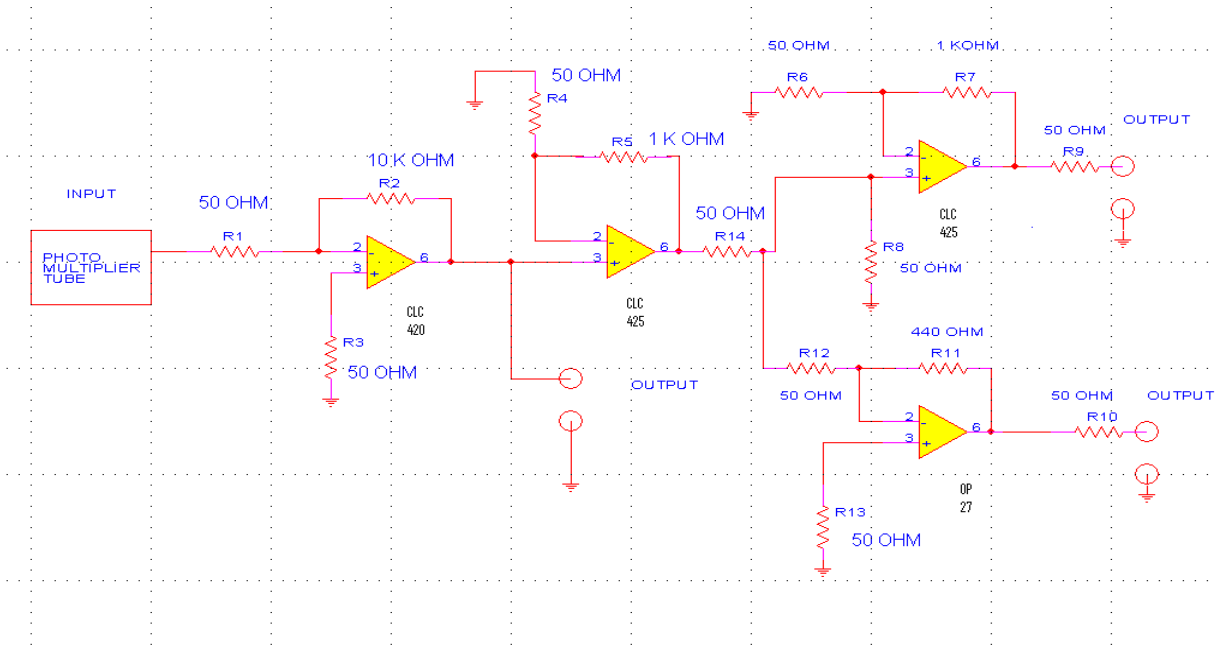

Figure 18 Diagram of the amplification circuit

This cathode current was given as an input to the first opamp, CLC 420, called PMT socket opamp. This amplifier acts as a *current to voltage converter*. The CLC420 is an operational amplifier designed for transimpedance amplification. It offers a 300MHz bandwidth and an input offset current of 0.2µA. The low input offset current and current noise makes the CLC420 ideal for photo multipliers amplifiers. The output of the PMT socket amplifier was fed as an input to the *first stage amplifier*. As we are dealing with wide frequency range, an amplifier with wide bandwidth and low noise was required for the purpose. CLC 425 combines a wide bandwidth (1.9GBW) with a very low input noise ($1.05nV/\sqrt{Hz}$, $1.6pA/\sqrt{Hz}$) to provide a very precise, wide dynamic range op amp offering closed-loop gains of greater than or equal to 10. It also offers great flexibility with its externally adjustable supply

current [144]. The CLC425's combination of ultra low noise, wide gain bandwidth, high slew rate and low dc s enabled us to achieve maximum high frequency signal-to-noise ratios.

The output of the first stage amplifier is fed further as the inputs to the *second stage amplifiers.* Second stage amplification was characterized into two branches: *High frequency:* As discussed earlier, the combination of ultra low noise, wide gain bandwidth, high slew rate and low dc s enabled us to achieve maximum high frequency signal-to-noise ratios. Thus, CLC 425 was employed as a high frequency amplifier. *Low frequency:* The OP-27 precision operational amplifier combines the low offset of 25μV with high speed and low noise of $3.5nV/\sqrt{Hz}$, making it ideal for accurate high-gain amplification of low-level signals. A gain-bandwidth product of 8MHz provides excellent dynamic accuracy in high-speed data-acquisition systems. These characteristics make it ideal for use as a low frequency opamp in our circuit. The outputs from the second stage amplifiers were hooked up to oscilloscope. Signal is digitized by a combination of a digital oscilloscope and a data acquisition card. The fast channel output is fed to the scope channel and the slower to the A/D card. Thus kinetics at a longer time range can be observed.

Observing kinetics at longer time range is achieved by logarithmic averaging which is presently done in the software. The basic principal behind it is that a trigger is used to fire the laser and start a logarithmic clock. This logarithmic clock emits signals in exponentially increasing intervals. The first m intervals have a length Δ; the second m intervals have length 2 Δ and the nth m interval have a length 2^{n-1} Δ. The sum is divided by 2^{n-1} and the result is stored. So even when the interval length increases exponentially with time, a constant input signal generates a constant output signal [23, 145]. The optical density is computed from observed intensity as a function of time. The measured absorption change ΔA is converted to N (t), the fraction of Mb molecules that have not rebound CO at the time t after the flash

using $N(t) = \frac{\Delta A(t)}{\Delta A(0)}$. The difference in the absorption spectra at the selected wavelength of 436 nm, ΔA (t), for the bound and unbound sample monitors subsequent rebinding [146].

3.4 Sample preparation

The samples were obtained from the laboratory of Dr. Debopam Chakrabarti, UCF and prepared with the help of his graduate student Jennifer Mauser. In this section I briefly describe the sample preparation for the healthy erythrocytes and the synchronized stages of malaria parasite.

3.4.1 Healthy erythrocytes

Freshly drawn blood is collected over an anticoagulant. The blood is mixed with an isotonic salt solution and erythrocytes are washed by centrifugation several times. Finally a thick suspension of erythrocytes was obtained. Since the preparation is done in the presence of air, it is obtained as oxygenated derivative. 1X Phosphate Buffer Saline (pH 7.4) is added to achieve the sample at required concentration. The sample was prepared by diluting the red blood cells in RPMI 1640 culture medium by a factor of 5.

3.4.2 Synchronized stages of malaria parasite

Parasites were maintained in human A+ erythrocytes at 5% hematocrit in complete

RPMI-1640 (Invitrogen) supplemented with 0.5% Albumax (Gibco) at 37^0C in a humidified CO_2 (5%) incubator with medium change every 24 h, requiring subculture by addition of fresh erythrocytes every 4-5 days [147, 148]. Cultures were split every other day to maintain a parasitemia of 2-5%, as monitored by Geimsa stained smears, and freshly washed RBCs were added. A+ whole blood was obtained from Florida Blood Centers on a monthly basis. Whole blood was washed in incomplete RPMI to remove unnecessary components and RBCs were resuspended in complete RPMI-1640 to 50% (2% Dextrose, 15mg/L Hypoxanthine, 0.2% Sodium Bicarbonate, 25mM HEPES, 25ug/ml gentamycin). Parasites were synchronized on a MACs LD Separation Columns (Miltenyi Biotec) in late trophozoite stage. Columns were placed on a magnetic stand and equilibrated with 5ml of complete media. Parasite cultures were pelleted and resuspended in 5 ml fresh media and applied to the column. Flow through containing uninfected RBCs, ring and early trophozoite stage parasites was discarded; late trophozoites remained bound to the column. The column was then washed with 5ml of complete media. The column was removed from the magnetic stand and parasites were diluted with 5ml complete media. Freshly washed erythrocytes were added to the synchronized culture to obtain 4% hematocrit. The following day Geimsa stained smears of the culture were prepared to evaluate parasitemia.

CHAPTER 4. CONFOCAL ABSORPTION MICROSCOPY: A NOVEL TECHNIQUE

When a beam of light passes through a sample, its intensity falls off exponentially, depending on the dielectric properties. This loss of intensity is due to absorption. Molecules usually display a selective absorption band, which means that if a white light beam passes through a sample, it absorbs certain wavelengths more than the other. Optical absorption is a well established technique for studying and characterizing dielectric materials and biological samples [149].

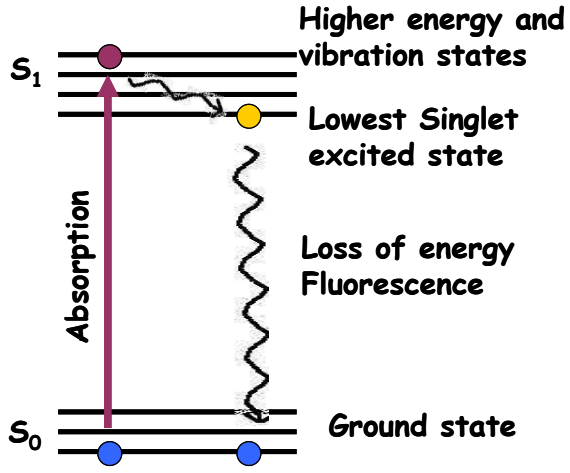

Figure 19 Jablonski Energy Diagram

Figure 19 depicts a schematic energy diagram and electronic transitions for absorption. The electron at lower energy level absorbs a photon and moves to a higher energy level. This absorption of photon results in loss of intensity and thus forms absorption bands in the spectrum.

Two parameters characterize an absorption band: the position of the maximum (λ_{max}) and the extinction coefficient (ε). The relationship between extinction coefficient and concentration is given by Beer-Lambert law stating $I = I_0 10^{-\varepsilon lc}$, where I and I_0 represents the transmitted and incident light intensity, l is the optical path-length the beam travels inside a specimen, ε is called the extinction coefficient and c is the concentration of the sample [149]. In other words, log I/I_0 is the absorbance.

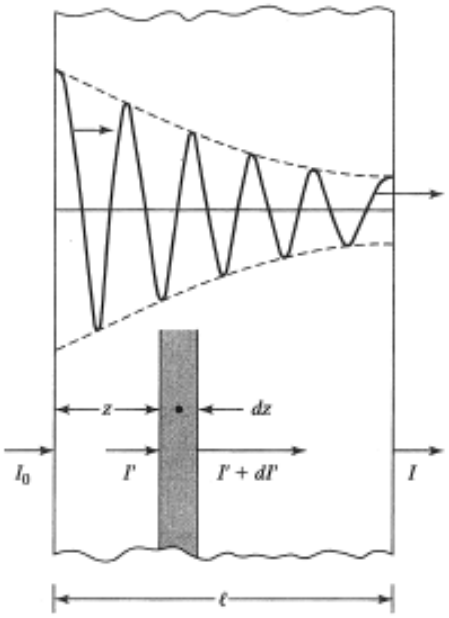

Figure 20 A beam of light traversing a sample of absorbing molecules loses its intensity exponentially [147].

Expressed in terms of differential increments, the Beer-Lambert law says that successive increments of absorbing molecules in a light beam will absorb equal fractions of light. If the increment of absorbing molecules is Ndz, where N is the number of molecules in the light beam per unit volume and dz is a thin slice of the path, then the fraction of light absorbed is dI/I, where

I is the intensity of light and the Beer-Lambert equation can be expressed as $Ndz = \frac{-1}{\sigma}\frac{dI}{I}$ where minus sign indicates absorption and σ is the absorption cross-section [150, 151].

The electronic spectrum is usually presented as a plot of absorbance versus the wavelength of irradiation. The extinction coefficient is a measure of the absorbing power of the compound and is related to the transition probability at a given wavelength.

Though there is a range of sampling techniques available to determine the absorption of macroscopic samples, to perform such an experiment at microscopic level pose a challenge. Various methods for sensitive absorption detection have been explored in past decade.

The development of confocal microscopy has provided advantages of better optical resolution by limiting the field of view over conventional wide field microscopy. The confocal imaging differs from conventional imaging in that it illuminates and images the sample one point at a time. It illuminates one point on the sample through a pin hole and the light reflected from the sample is imaged by the objective back on the pin hole. If an image gets defocused, it does not pass through the pin hole to the detector on the other side and thus disappears rather than getting blurred, providing better edge definition [152]. Remarkable advances have been made in confocal microscopy over last few decades [153]. Confocal laser scanning microscope (CLSM) provides advantage of imaging thin optical sections within thick fluorescence labeled specimens [154]. Even though confocal microscopy is mainly performed in fluorescence mode [155] there are areas of interest which requires study of the samples with direct methods without employing exogenous labels [156]. Absorption measurements provide a convenient label free way for characterizing unknown material [157]. Though, advancements have been made in multidimensional imaging, standard confocal microscopy so far lacks direct optical absorption profile measurements.

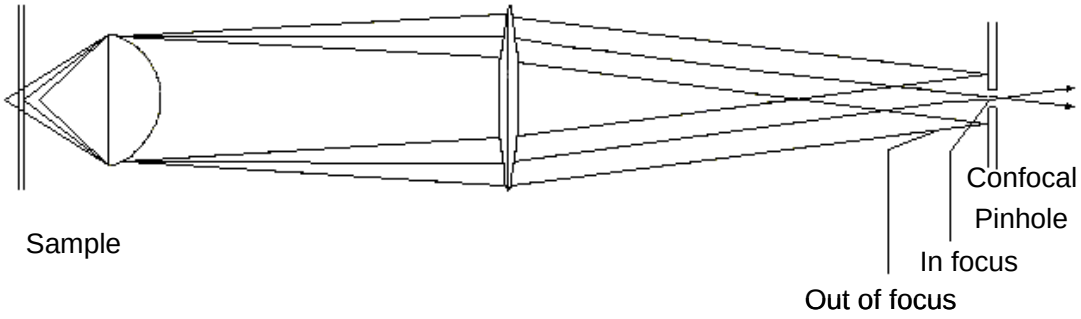

Figure 21 Confocal Schematics

Confocal microscopy provides enhanced resolution due to elimination of out of focus rays by a spatial filter (pinhole) or by multi-photon excitation [152]. For confocal detection a pinhole is located in the conjugate plane of the focal plane (defined by the collection optics) which enables optical sectioning along the axial direction [158]. Fluorescence probes employing confocal or other geometries are well established; however they generally require labeling and are limited by photobleaching and quenching [159]. On the other hand, micro-spectroscopy [157, 160] based on absorption measurements provides a convenient label free way for characterizing an unknown material. Though light scattering has been used recently as a source of contrast [156], standard confocal microscopy so far lacks direct optical absorption profile measurements. A difficulty for measurements with axial resolution is presented by the 'missing cone' problem [161] discussed later in this chapter.

To provide spatial discrimination in the axial direction a confocal laser absorption microscope has been proposed [153]. An excitation laser pulse irradiates the sample so that ground-state molecules transit to the excited state, thus creating a spatial distribution of molecules, similarly to what is used in confocal fluorescence. The absorption to higher energy

levels is then probed by a monitoring laser beam introduced coaxially. An excited state absorption profile is obtained by scanning the sample. In general the absorption of the laser beam due to electronic transitions from the ground state is assumed to be negligible, although the attenuation of the propagating light could provide a mechanism for contrast in the axial direction. In the following we will employ spatial variation in light intensity as it passes through the sample as a source of contrast [16].

By exploiting the spatial variation of the intensity due to Beer-Lambert law we demonstrate a novel approach to obtain ground state absorption spectra with a spatial resolution of better than 2.1 μm in the lateral and 3.6 μm in the axial direction [16]. The method employs a confocal detection system to probe and spectrally resolve the attenuation of a white light beam in the axial direction. It enables the measurement of absorption spectrum of biological assemblies at the single cell level and small samples with a thickness of few microns. Confocal absorption microscopy (CAM) is nondestructive and is capable of collecting both spatial and physical information based on light absorption by microscopic structures.

4.1 The optical transfer function and the missing cone problem

In many 3-D applications it is necessary to understand how an imaging system can provide information on the structure of an object in the direction perpendicular to the image plane. In microscopy the shape of a 3-D object can either be determined by focusing through the object-that is, by examining a succession of images with different parts of the object in focus, usually termed as optical sectioning and then reconstruct the 3-D image through suitable tomographic technique. However, this technique of optical slicing has the disadvantage that each

slice is obstructed by out-of-focus noise, which enters each image from adjacent slices [162]. Another useful way to determine the shape of the 3-D object is through a framework based on optical transfer functions (OTF): the image intensity distribution is given by the 3-D convolution of the object and a 3-D point spread function (PSF); equivalently, in 3-D Fourier space the image spectrum is the product of the object spectrum and a 3-D OTF [163].

The basic idea of Fourier optics is to study classical optics using transform functions. Fourier transforms are widely used in analysis of linear electric filter circuits to describe their behavior in terms of a transfer function, which indicates how a network transmits signals as a function of frequency [164]. A time varying signal can be expressed as X(ω) in terms of its frequency spectrum. If the network has a frequency response H(ω), then the output spectrum is given by X(ω)H(ω) and the final signal can be given by inverse Fourier transform of X(ω)H(ω). In optical circuits, instead of time varying input signal, we have the object f(r) and the frequency content is now measured in terms of spatial frequency with lens acting as a spatial frequency filter.

The relation between the object as a function of position f(r) and resulting image g(r) is given by:

$$I[f(r)] = g(r) \tag{1}$$

where I is the imaging operator and r is the position coordinate (x,y,z).

An object can be represented as $$f'(r) = \int_{-\infty}^{\infty} f(s)\delta(r-s)ds \tag{2}$$

where $\delta(r-s)$ is a set of regularly spaced sampling points with spacing ds.

The Point Spread Function e(r) is defined as image of a point $\delta(r)$. So, mathematically

$$I[\delta(r)] = e(r)$$
$$I[\delta(r-s)] = e(r-s) \tag{3}$$

Thus

$$I[f'(r)] = I[\int_{-\infty}^{\infty} f(s)\delta(r-s)ds] \tag{4}$$

I is the linear operator so can be taken inside the integral. Then,

$$I[f'(r)] = \int_{-\infty}^{\infty} f(s)I[\delta(r-s)]ds$$

$$I[f'(r)] = \int_{-\infty}^{\infty} f(s)e(r-s)ds \tag{5}$$

$$I[f'(r)] = g(r)$$

The image thus is convolution of the object with the point spread function. Or mathematically,

$$g(r) = f(r) \otimes e(r) \tag{6}$$

Also according to convolution theorem, Fourier transform of a convolution is the product of individual transforms of the functions. Thus, Fourier transform of the image is given by

$$G(s) = F(s)E(s) \tag{7}$$

The lateral resolution is determined by wavelength of light used and the NA of the objective lens. In conventional optical microscopy, the out of focus light either gets lost or is present with very less contrast, thus limiting the depth of field resolution for large structures.

Using dimensionless coordinates in the lateral direction as $v = \frac{2\pi}{\lambda} n \sin\alpha \sqrt{x^2 + y^2}$ and axial direction as $u = \frac{8\pi}{\lambda} n \sin^2 \frac{\alpha}{2} z$, we get the intensity distribution in point spread function is independent of NA of the lens.

Actual focal field distribution in these coordinates is given by [165]:

$$h(u,v,\psi) = A \exp\left(\frac{iu}{4\sin^2\frac{\alpha}{2}}\right) \int_0^1 \int_0^{2\pi} P(\rho,\theta) \exp\left\{-i\left[v\rho\cos(\theta-\psi) + \frac{u\rho^2}{2}\right]\right\} \rho d\rho d\theta \qquad (8)$$

Mathematically, the pupil function, P(ρ,θ), describes the deviation from the perfect lens behavior of transforming a plane wave into a converging spherical wave [166]. For the aberration free case the pupil function can be set equal to 1. Integral over θ can be done using well known Bessel's function.

$$\frac{i^{-n}}{2\pi} \int_0^{2\pi} \mathrm{e}^{ix\cos\alpha}\, e^{in\alpha} d\alpha = J_n(x) \qquad (9)$$

Thus, Integral over θ can be reduced to:

$$\int_0^{2\pi} \mathrm{e}^{-iv\rho\cos(\theta-\psi)}\, d\theta = 2\pi J_0(v\rho) \qquad (10)$$

Substituting back in $h(u,v)$ we get

$$h(u,v) = 2\pi A \exp\left(\frac{iu}{4\sin^2\frac{\alpha}{2}}\right) \int_0^1 \exp\left(-i\frac{u\rho^2}{2}\right) J_0(v\rho)\, \rho d\rho \qquad (11)$$

where parameter u in the above equation corresponds to the defocus of the lens. Assuming that the lens is focused on the object plane, we can set u=0 [167].

$$h(v) = 2\pi A \int_0^1 J_0(v\rho)\,\rho d\rho \tag{12}$$

Using first order Bessel's function

$$\frac{d}{dx}\left[x^{n+1} J_{n+1}(x)\right] = x^{n+1} J_n(x) \tag{13}$$

We get, for aberration free lens:

$$\begin{aligned} h(v) &= 2\pi A \int_0^1 \frac{1}{v\rho} \frac{d}{d(v\rho)} \left(v\rho J_1(v\rho)\right) \rho d\rho \\ &= \frac{2\pi A}{v} \int_0^1 \frac{d}{d\rho} \left(\rho J_1(v\rho)\right) d\rho \\ &= \frac{2\pi A}{v} \left[\rho J_1(v\rho)\right] \\ &= \frac{2\pi A}{v} J_1(v) \end{aligned} \tag{14}$$

If the Fourier transform of the PSF is small at high spatial frequencies, the components of the object corresponding to these frequencies are attenuated in the image. Thus, the OTF is forming a torus with a missing cone corresponding to attenuation of low spatial frequency along optical axis and thus lack of axial resolution.

The 'missing cone' problem poses a difficulty for measurements with axial resolution [161]. The optical transfer function is angularly band limited [168, 169], so that the longitudinal resolution in the axial direction is degraded.

Confocal microscopy uses a pinhole as a spatial filter to eliminate out of focus light from detection and thus provide axial sectioning and fine image contrast. Due to this rejection some of the light emitted by the specimen is rejected though specimen is illuminated completely which leads to bleaching of fluorochrome and photo-toxicity of living cells. Deconvoluting the stacks

of the wide-field image is thus an alternate way to achieve depth resolution which also allows recording of up to 30% more light emitted by the specimen as compared to confocal microscopy.

Considering the traditional confocal arrangement for which bright-field image intensity is given by [170, 171] the convolution can be written as :

$$I = \left| h_1 h_2 \otimes \tau \right|^2 \tag{15}$$

where, h_1 is the point spread function of the illuminating light, h_2 is the amplitude point spread function of the detection light, τ as amplitude transmission function of the object. Whereas if the system is imaging in fluorescence, image formation properties are completely different and are given by:

$$I = \left| h_1 h_2 \right|^2 \otimes f \tag{16}$$

where f is the distribution of fluorophores.

In confocal laser induced absorption microscopy, the excitation laser light is focused on the sample using an objective lens. It excites the molecules such that the concentration is proportional to the photon density and thus having a spatial variation. An absorption monitoring laser is introduced coaxially. Since, the monitoring light passes through the same region as the excited laser, the absorbance varies as a function of axial coordinates and thus provides depth discrimination to the samples. The capability of 3-D imaging is described mathematically using optical transfer functions [153] which is based on the paraxial approximation for excitation and monitoring systems and neglecting multiple scattering in an object [163, 172].

The point spread function of the excitation system in coordinates z_1(axial) and x_1(lateral) is given by:

$$e(x_1, z_1) = \iint P_{e1}(\rho_1) P_{e1}^*(\rho_1') \exp\left[-2\pi i x_1 \left(\rho_1 - \rho_1'\right)\right] \exp\left[-\pi i z_1 \lambda_e \left(\rho_1^2 - \rho_1^{2'}\right)\right] d^2\rho_1 d^2\rho_1' \quad (17)$$

where, λ_e is the wavelength of excitation light, $P_{e1}(\rho_1)$ represents the pupil function for the objective lens with the wavelength λ_e.

The diffraction of the laser by the 3-D structure of the object can be expressed as scattering distribution function as [172]:

$$t(x_1, z_1) = \delta(z_1) + c(x_1, z_1) e(x_1, z_1) + d(x_1, z_1) \quad (18)$$

where the first term represents the unscattered light, second is the contribution of transient absorption by excitation light and third the steady state absorption of the ground state molecules. When the object is moved by a displacement (x_0, z_0), the scattering function is altered and the intensity distribution is given by:

$$i(x_2; x_0, z_0) = \left| \iint h_1(x_1, z_1) t(x_1, z_1; x_0, z_0) \times h_2(x_2 - x_1; -z_1) d^2 x_1 dz_1 \right|^2 \quad (19)$$

where h_1 and h_2 are the 3-D point spread functions of the illumination and the detection systems, respectively.

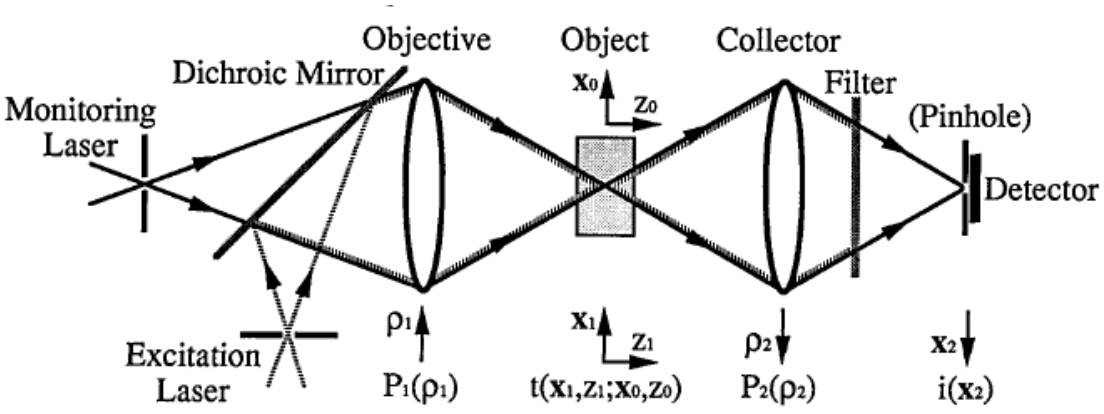

Figure 22 Optical diagram of confocal laser-induced absorption microscope [151]

On the basis of weakly scattering theory the bilinear terms in the point spread functions are neglected which yields intensity function as [153]:

$$\begin{aligned} i(x_2;x_0,z_0) &= \left|G(x_2)\right|^2 \\ &+\iint\left[F(x_2;\rho,\zeta)***E(\rho,\zeta)\right]C(\rho,\zeta)\times\exp\left[2\pi i\left(x_0\rho+z_0\zeta\right)\right]d^2\rho d\zeta \\ &+\iint\left[F^*(x_2;\rho,\zeta)***E^*(\rho,\zeta)\right]C^*(\rho,\zeta)\times\exp\left[-2\pi i\left(x_0\rho+z_0\zeta\right)\right]d^2\rho d\zeta \\ &+\iint F(x_2;\rho,\zeta)D(\rho,\zeta)\exp\left[2\pi i\left(x_0\rho+z_0\zeta\right)\right]d^2\rho d\zeta \\ &+\iint F^*(x_2;\rho,\zeta)D^*(\rho,\zeta)\exp\left[-2\pi i\left(x_0\rho+z_0\zeta\right)\right]d^2\rho d\zeta \end{aligned} \quad (20)$$

where *** denotes the 3-D cross correlation. The equation can be written in terms of Fourier transforms as:

$$\begin{aligned} i(x_2;x_0,z_0) &= \left|G(x_2)\right|^2 \\ &+\iint H_C(x_2;\rho,\zeta)C(\rho,\zeta)\exp\left[2\pi i\left(x_0\rho+z_0\zeta\right)\right]d^2\rho d\zeta \\ &+\iint H_D(x_2;\rho,\zeta)D(\rho,\zeta)\exp\left[2\pi i\left(x_0\rho+z_0\zeta\right)\right]d^2\rho d\zeta \end{aligned} \quad (21)$$

where

$$\begin{aligned} H_C(x_2;\rho,\zeta) &= F(x_2;\rho,\zeta)***E(\rho,\zeta)+F^*(x_2;-\rho,-\zeta)***E^*(-\rho,-\zeta) \\ H_D(x_2;\rho,\zeta) &= F(x_2;\rho,\zeta)+F^*(x_2;-\rho,-\zeta) \end{aligned} \quad (22)$$

Assuming the excitation and the monitoring wavelength to be same, the pupil functions can be described by the disks of same radius. The spatial frequency cutoffs calculated for the above functions shows that $H_D(x_2;\rho,\zeta)$ is not only a low pass filter but also has an angularly band limited region. On the other hand $H_C(x_2;\rho,\zeta)$ has no missing cone as shown in the Figure 23.

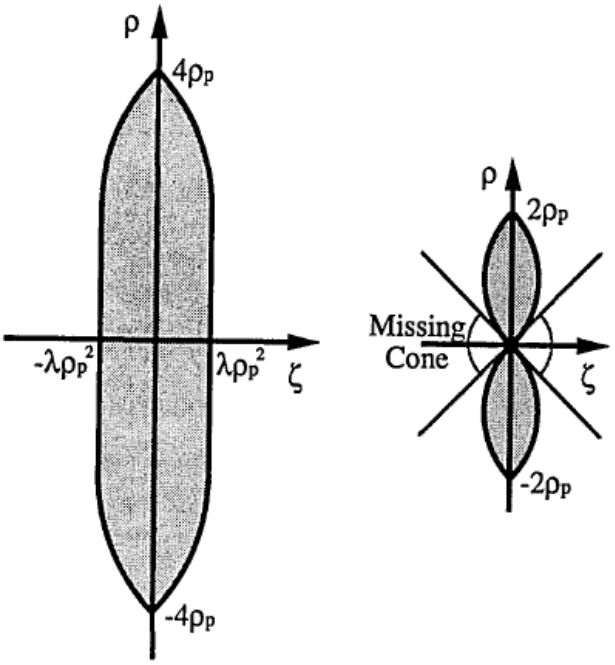

Figure 23 Spatial frequency cutoffs of $H_C(0;\rho,\zeta)$ and $\overline{H_C(x_2;\rho,\zeta)}$ for the transient absorption (left) and $H_D(0;\rho,\zeta)$ and $\overline{H_D(x_2;\rho,\zeta)}$ for the steady-state absorption (right) [151]

By exploiting the spatial variation of the intensity due to Beer-Lambert law we demonstrate a novel approach to obtain ground state absorption spectra with a spatial resolution of better than 1.4 μm in the lateral and 3.6 μm in the axial direction. Our method employs a confocal detection system to probe and spectrally resolve the attenuation of a white light beam in the axial direction. The attenuation of the light beam in the axial direction due to absorption provides a mechanism for contrast.

4.2 Experimental setup and characterization

Conceptually, the measurement of absorption spectrum is straight forward. To obtain absorption spectra of microscopic samples one needs to compare the intensity of transmitted light with and without the sample in its path. The problem of removing any stray light affecting the measurements can be solved via several different approaches. One could either limit the light by using a microscope objective between the light source and the sample or could limit the area of excitation using apertures. Here we demonstrate that by limiting the plane of view and exploiting spatial variation of transmitted intensity (Beer-Lambert law) enables high spatial resolution and absorption sensitivity. This provides a simple and direct approach with high sensitivity over wide spectral range to measure micro-absorption spectra with 3-D spatial resolution.

A schematic diagram of the CAM instrumentation is shown in Figure 23. Our setup couples a commercial Labram system with broadband white light excitation source. Light illuminates the sample through an optical fiber (core diameter 400 microns, N.A.= 0.22). The optical fiber is mounted in a cylinder for precise alignment. An aperture of size 5 μm to 100 μm is positioned at the illuminating end of the fiber. The fiber cylinder topped with illuminating aperture is seated at the centre of the sample slide. The slide has a groove at the centre for aligning the micro-capillary with outer diameter of 350 μm and inner bore of 50 μm. The illuminating aperture limits the stray light and illuminates only the sample inside the micro-capillary. The slide is then mounted on motorized XYZ stage.

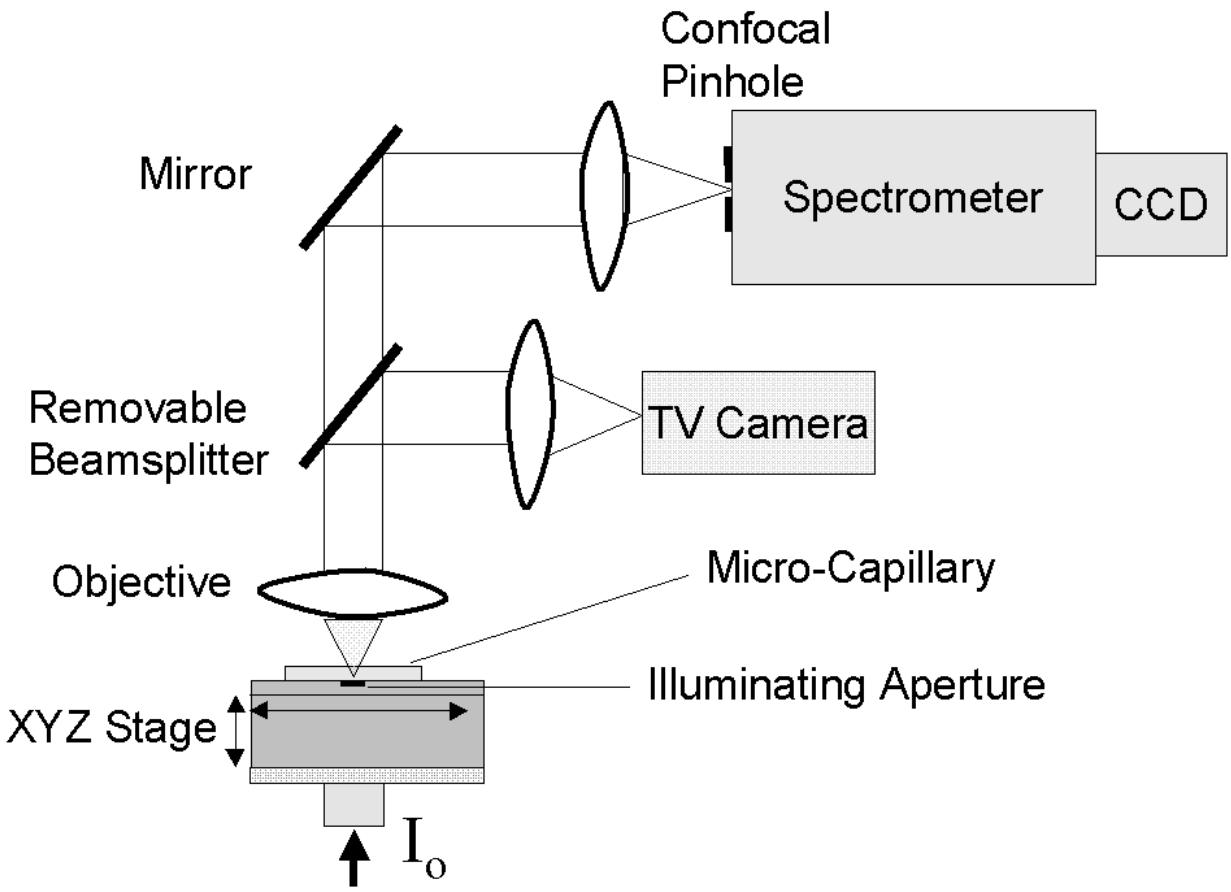

Figure 24 Schematics of the prototype spatially resolved confocal absorption setup

The transmitted light is collected through 50x objective lens (NA=0.75) and is then either transmitted through the removable beam splitter to the camera for optical imaging, or reflected to the spectrometer. The reflected light is focused on the confocal pin hole which transmits it to the other side to the detector. An aperture with 5 μm to 25 μm opening limits the field of view to provide better optical resolution. The spatial resolution, however, is determined by the confocal pinhole at the entrance to the spectrometer is demonstrated by employing three different illuminating apertures.

One possible approach is to use different size apertures at the sample position to determine the excitation area. In the first set of experiments, the confocal pin hole of the spectrometer was fixed. The 25

μm illuminating aperture with no sample was scanned through the beam along the axis for maximum transmitted light intensity. The light intensity inside the aperture varies by less than 7% inside the 20 μm diameter. At the edge of the hole the intensity increases from 10 to 90 % over a distance of 1 μm. The tests were repeated with apertures having opening of 5 and 10 μm with the same results. The spatial resolution (10 to 90% points) is determined by the confocal pinhole on the detection side while the aperture limits the illuminated area on the excitation side. Constant light intensity was achieved across the excitation area of 10 microns diameter with 25 microns illuminating aperture.

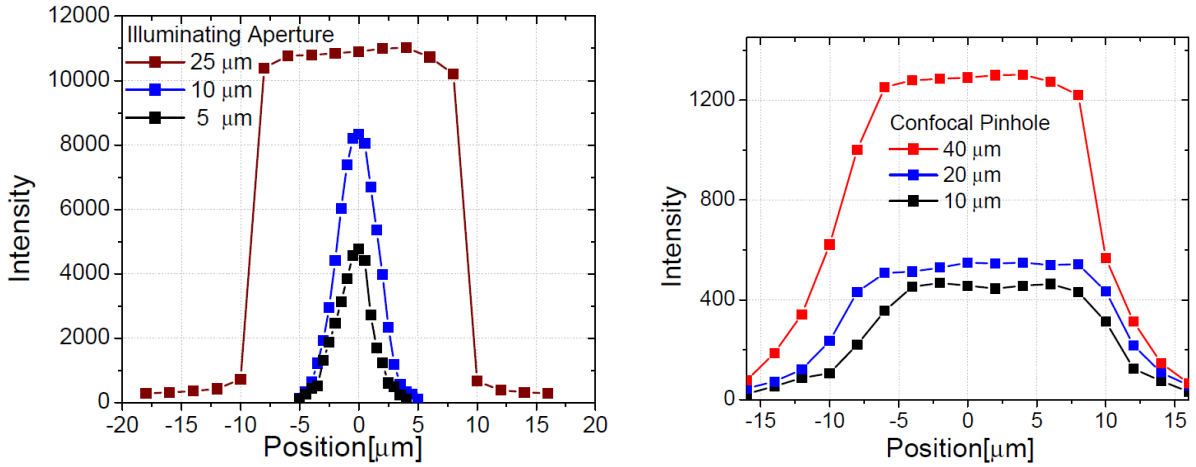

Figure 25 Effect of different illuminating apertures on maximum transmitted intensity along the axis (left) and effect of different confocal pin hole on maximum transmitted (right)

The most efficient way to achieve high spatial resolution is to simply use the confocal pinhole at the entrance of the spectrometer. Therefore we conducted a second set of experiments with an illuminating aperture of 25 microns and the confocal hole was varied from 10 to 50 microns. It was demonstrated that the light intensity plateaus inside the aperture. The steepness of plateau depends on the size of the confocal hole. The setup showed lateral spatial resolution of better than 3 microns.

4.2.1 Spatial resolution

Combining the two above mentioned results illuminating aperture was fixed at 25 µm and confocal pinhole was fixed at 50 µm. To determine the spatial resolution of the system we required a small absorbing object. In a first experiment polystyrene beads were used. However, the fluorescence signal from the beads distorts the absorption spectrum. Therefore, we employed red blood cell with diameter 7 µm. Red blood cells were immobilized on a cover slip that was mounted on the slide assembly. The slide assemblies with and without cells were scanned in the lateral and axial direction and light intensity as a function of position is recorded. The back counts of CCD was subtracted from the intensity and the signal was corrected for the base line. Using the formula $\Delta A = -\log\left(\frac{I}{I_0}\right)$, the absorbance was calculated at each spatial location. The peak absorbance (at 415nm) is plotted for both lateral and axial direction.

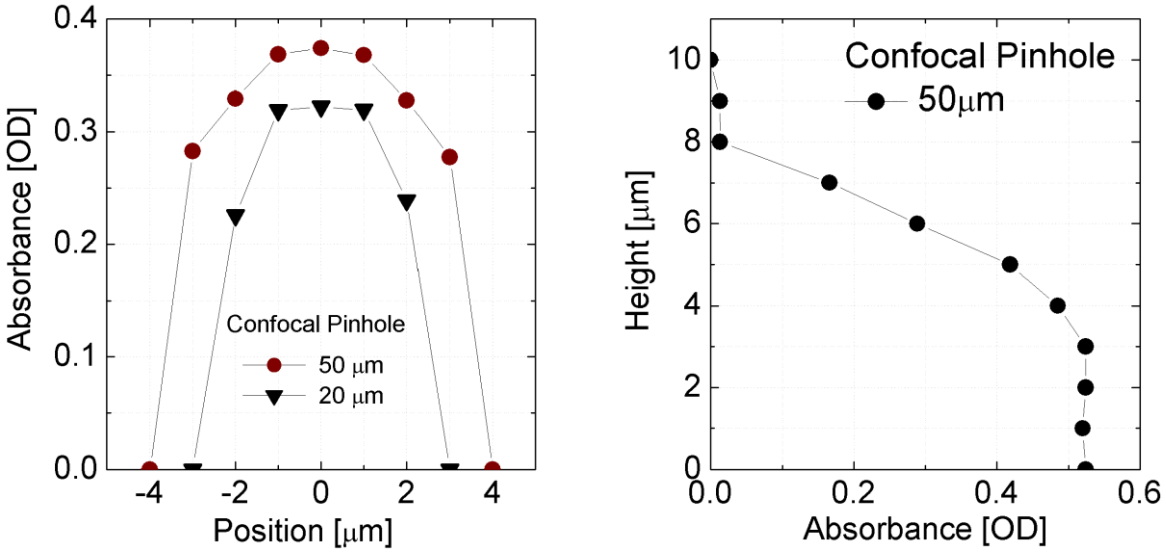

Figure 26 Spatial variation of absorbance of a red blood cell (see text) at the peak position of the Soret band. Scans are shown in the lateral (left panel) and axial (right panel) directions.

In the lateral direction, it was observed that absorbance increases and then decreases. The width of the plot gives the diameter of the red blood cell. As we increased the confocal pin hole size the absorption plateaus. The lateral resolution was determined from 10% and 90% intensity points and is found to be better than 1.4 microns with a confocal pin hole size of 20 microns. In the axial direction, the absorbance increases within the erythrocyte and then stays constant. An axial resolution better than 3.6 microns can be achieved using 50 micron pin hole.

To establish the accuracy of Confocal Absorption Microscopy and its ability to determine the absorption spectrum of nano liter samples I conducted a set of experiments to determine the effect of concentration on the optical absorption of calcein dye and Met Mb solution.

4.2.2 Micro-fluidics application

The measurements were performed on solutions of lypholized horse muscle Mb (Sigma M 0630; Molecular Wt.: 17.6 K Da; $\varepsilon = 188\ mM^{-1}cm^{-1}$), a globular protein with Soret peak at 409 nm. The sample was prepared by dissolving 35.2 mg of the Mb powder in 500µl of De ionized water. The solution was stirred with magnetic stirrers slowly for 10 minutes. It was passed through a micro-filter to remove any impurities. The final concentration of 4 mM stock solution was achieved which was brownish red in color. Calcein solution was prepared using analogous methods.

For comparison the optical absorption of the solution was measured at various concentrations in a 1 cm cuvette using conventional UV-VIS spectrometer (Cary 500i). The required volume of stock solution was dissolved in required quantity of potassium phosphate buffer (pH 7.05) to obtain 3ml samples with final concentrations between 0.3 µM to 3 µM. For CAM, the sample was loaded into a

micro-capillary of nominal inner diameter 50 ± 5 μm. The loaded micro-capillary was positioned in the slide groove and was illuminated by the broad spectrum white light source using the optical fiber through 25 μm illuminating aperture. The transmitted light was collected through the 50x objective and focused on the 50 μm confocal pin hole.

The data is first corrected for the CCD dark counts. Tungsten halogen lamp with black body curve goes to zero below 360nm. In order to do the baseline correction, we measured the ratio between I and I_0 at 650nm and then multiplied I with that factor. This gives us the baseline corrected transmitted intensity. Using this corrected data, absorbance was calculated.

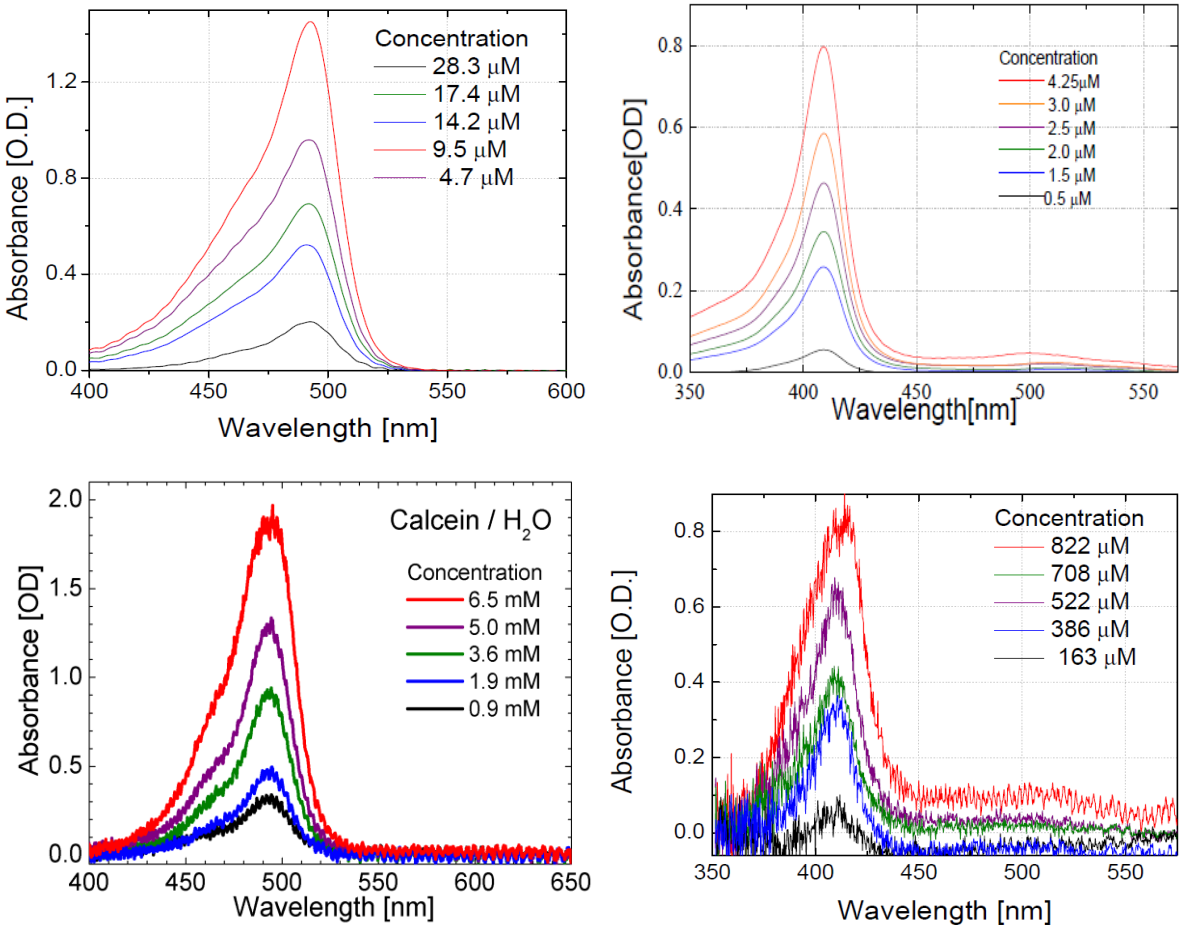

Figure 27 Absorption spectrum of calcein(left) and met myoglobin(right) obtained with confocal absorption microscopy setup (bottom) and obtained with Cary UV-Vis spectrometer(top) . The data acquisition time was 60 seconds for Cary 500i. For confocal absorption microscopy, it is 1 sec for Mb solution and 2 sec for calcein solution.

The absorption spectrum obtained in the micro-capillary is in excellent agreement with the spectrum measured in conventional 1 cm cuvette. Data acquisition times for spectra were 2 seconds for the micro-capillary in the micro-absorption setup and 60 seconds for the cuvette on a scanning spectrometer. The figure above shows that absorption spectra of protein and dye solutions can be obtained in a micro-capillary (micro-fluidics application).

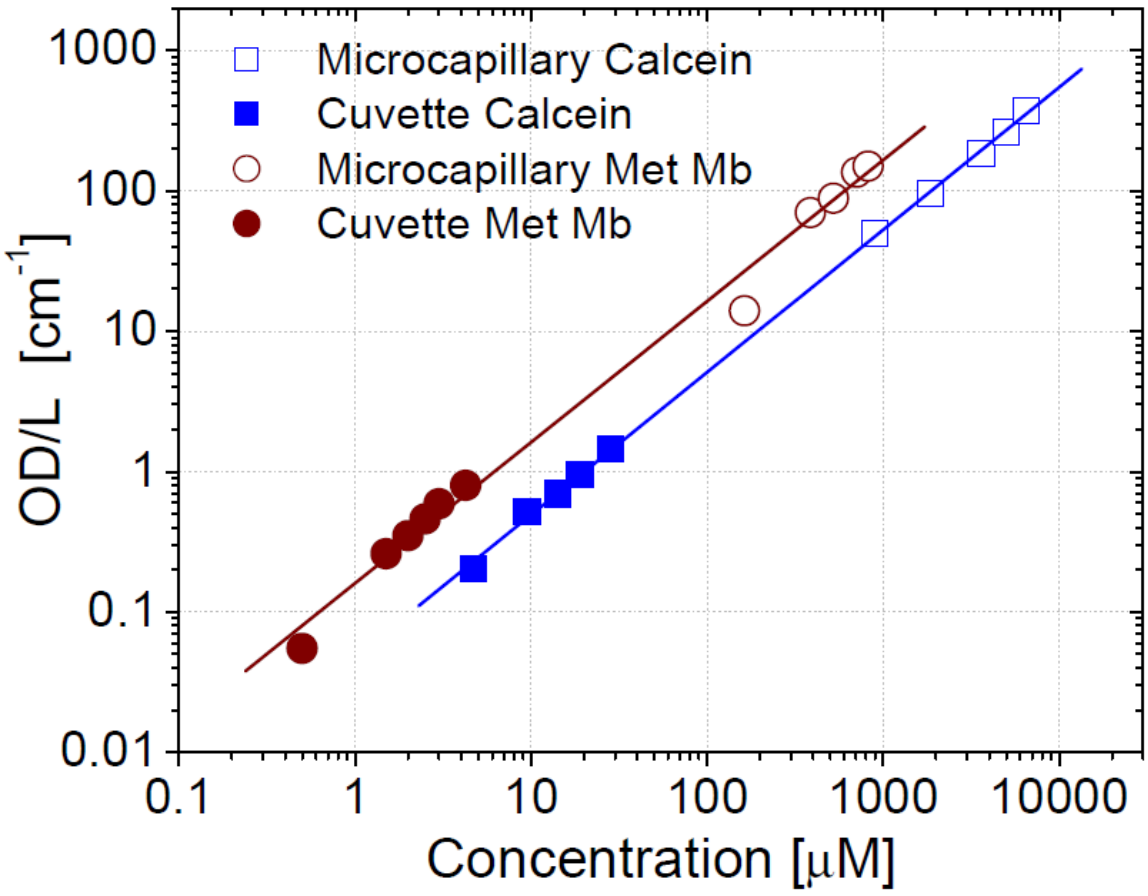

Figure 28 Peak absorbance ΔA divided by pathlength L as a function of concentration

The absorbance ΔA depends linearly on the concentration c according to $\Delta A = \varepsilon L c$. Here, ε and L denote molar extinction coefficient and pathlength, respectively. The results are plotted in the form ΔA / L vs. concentration on a double-logarithmic scale. The data are plotted in the form of ΔA /L, so, the slope corresponds to the extinction coefficient of the solutions. Due to the log-log representation the curves are shifted by the difference in the extinction coefficients of the two compounds. The slope calculations yield the ε to be 0.0549 $\mu M^{-1}cm^{-1}$ for calcein(actual value 0.0551 $\mu M^{-1}cm^{-1}$) and 0.187 $\mu M^{-1}cm^{-1}$ for met Mb (actual value 0.188 $\mu M^{-1}cm^{-1}$). Using the slope of the graph, the path length was determined to be 94 mm

for the conventional method and 47.5 µm for the micro-capillary. The data in Figure 28 show that absorption spectra of solutions can be obtained in a micro-capillary and suggest applications in diagnostics and micro-fluidics.

4.2.3 Spatially resolved Beer-Lambert law

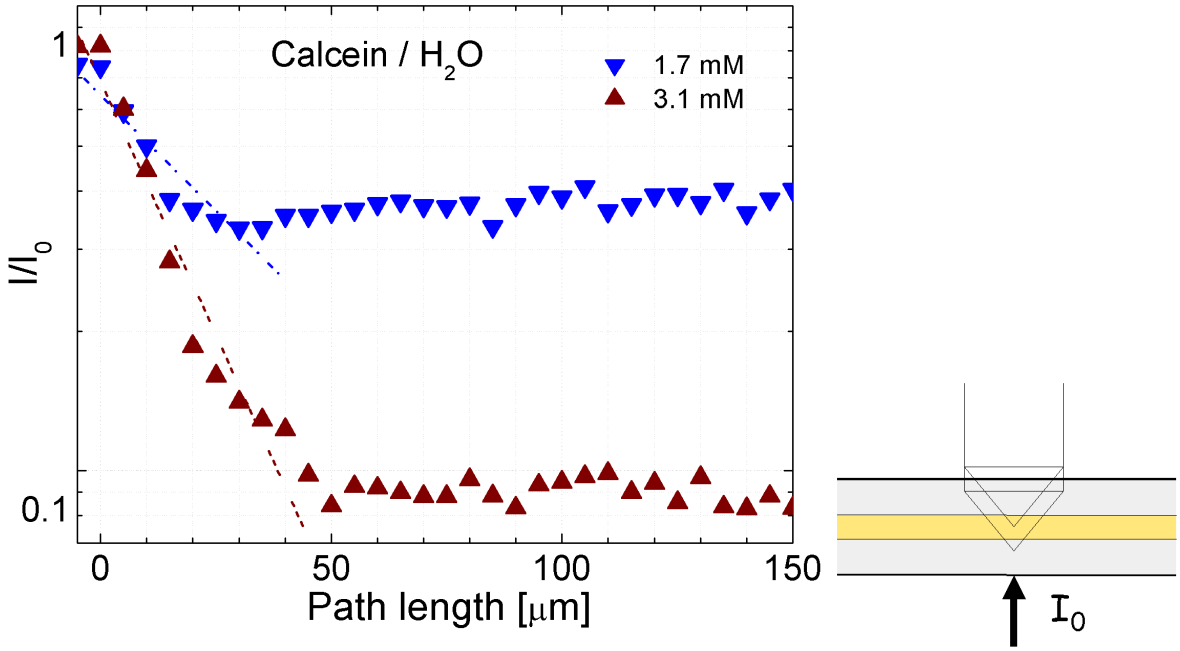

Figure 29 Dependence of the transmitted intensity ratio I/I_0 on the optical pathlength in the micro-capillary. Note the logarithmic scale on the vertical axis. The dashed lines indicate least-squares fits to Beer-Lambert law. The right panel shows a schematic of the axial sampling.

Within the micro-capillary the intensity should decrease due to absorption by dI over a distance dz according to Beer-Lambert law: $dI = - \alpha I dz$. This provides a further test for spatial resolution. Calcein dye loaded in a micro-capillary was employed to establish that CAM is capable of spatially resolving Beer-Lambert law inside a sample. The micro-capillary loaded with 3.1 mM calcein solution was placed

in the slide groove and scanned along the axial direction. The transmitted light intensity profile with buffer (I_0) and with dye solution (I) was measured at every 5 microns starting from under the sample position. I/I_0 plotted on log scale with pathlength shows absorption increase with pathlength inside the sample and then stays constant. The downward slope of the plot inside the sample corresponds with εC which is calculated to be - 0.017 μm^{-1}. The same trend was observed with a lower concentration of 1.7 mM and the slope was measured to be - 0.011 μm^{-1}. The linear relationship between log (I/I_0) and pathlength inside the sample demonstrates a spatially resolved attenuation according to Beer-Lambert law.

In conclusion, we have demonstrated a new approach to confocal absorption microscopy (CAM) by combining confocal detection and broadband illumination in a transmission geometry. The attenuation of the light beam in the axial direction due to absorption provides a mechanism for contrast. The method has been used to study cells in their native environment and other biological assemblies. Variations in composition of inhomogeneous samples (e.g. thin films) may be determined from spatially resolved absorption spectra. Because no marker dyes are required and has no photo bleaching effect, it can be used to study live viable cells and biological assemblies. Using CAM, we were able to obtain absorption spectra of single live red blood cells and of nano liter solutions in micro-capillaries.

4.3 Extension to single cell flash photolysis experiments

The setup is very flexible and enables transient absorption measurements following photolysis. It requires a monitor and a photolysing beam. The photolysing beam is coupled into the setup via beam splitter, so that is counter propagating through the sample with the monitor beam.

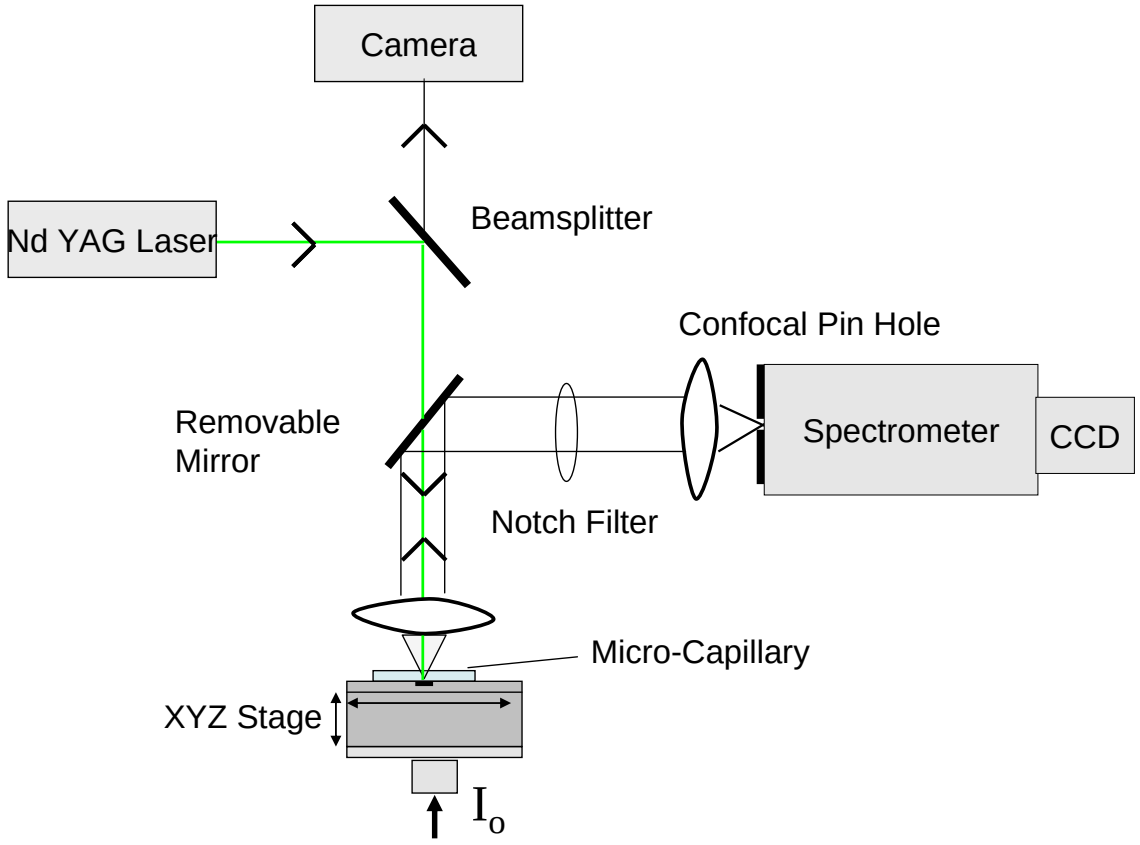

Figure 30 Schematics of single cell flash photolysis

The system is coupled with an Olympus BX 41 microscope with a 100x dry objective (NA = 0.9). The external laser beam is coupled into the optical path by a set of mirrors and beam splitters and focused through a lens onto the sample. The monitoring beam is introduced coaxially to the laser beam. The absorption signal is collected by the microscope objective through a holographic notch filter to the 50 μm confocal pin hole of the spectrometer. Spectra are recorded between 350 and 700 nm with a resolution of 0.5 nm using a multichannel detector.

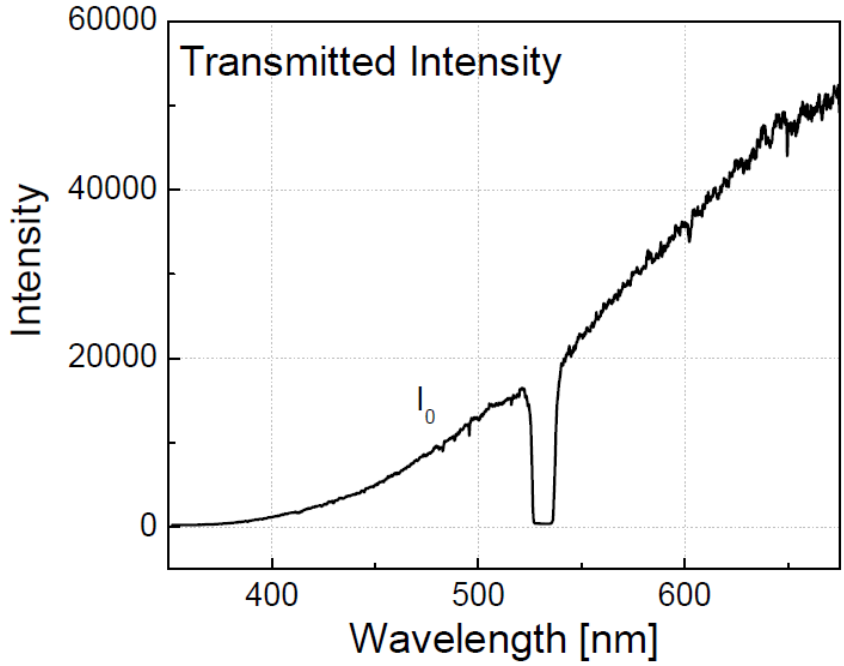

Figure 31 Transmitted intensity of the lamp through 532 nm notch filter

Figure 31 shows the transmission curve of the notch filter for the output of the tungsten halogen lamp. we conducted the preliminary experiment to find out whether the absorption spectra in the presence of a photolyzing laser beam can be acquired.

For these measurements, the red blood cells are immobilized on a coverslip with poly-lysine solution using the method described in section 6.1. A continuous wave frequency-doubled Nd-YAG laser is used to photolyze the hemoglobin and the absorption spectrum is measured without and with laser illumination using confocal absorption microscopy.

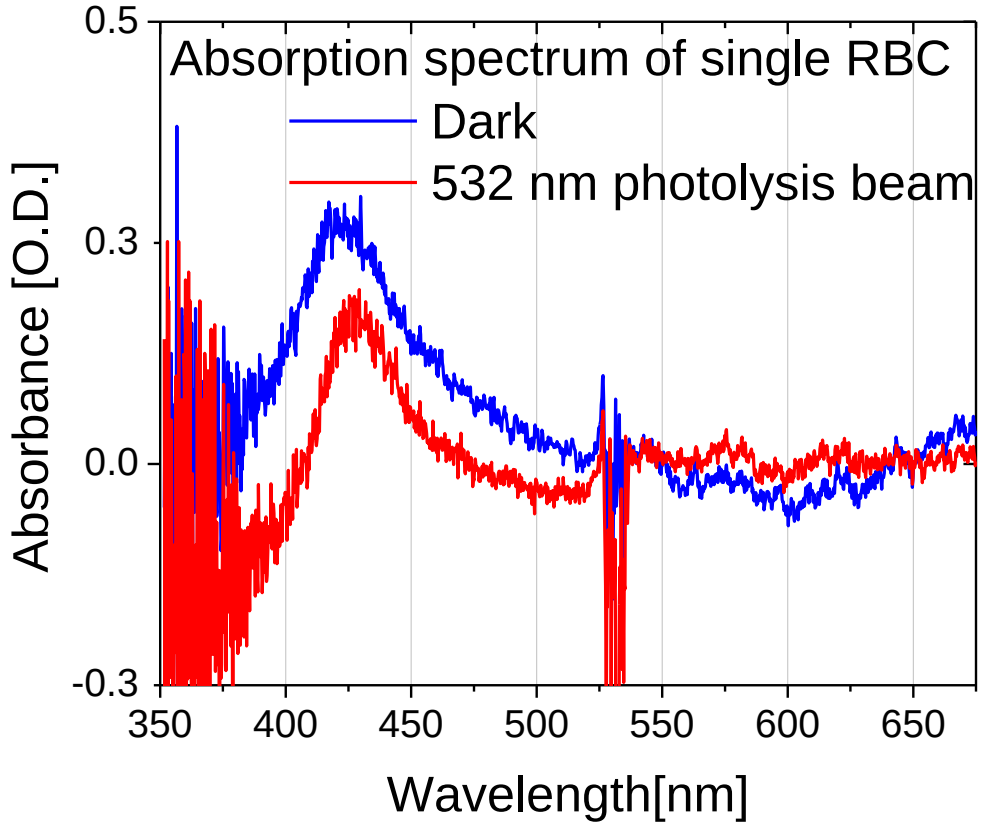

Figure 32 Micro-absorption spectrum of single erythrocyte showing photodissociation.

Figure 32 shows the results of the preliminary experiment to measure the hemoglobin photoproduct in a single erythrocyte. A spectrum of the oxygenated hemoglobin is taken with the photolysis beam blocked. The photolyzing laser (532 nm) is then switched on and the spectrum with laser illumination (2 mW) is recorded. The acquisition time for the spectrum was 20 seconds. The spectrum is a superposition of the oxygen bound and deoxy hemoglobin spectra.

The Soret peak shifted from 415 nm to 428 nm with laser illumination. There are consistent changes in the β- and α- band region. The literature value of the Soret band position for the deoxy Hb in solution is 430 nm [92, 102]. The photostationary equilibrium is determined by the photolysing rate and the rebinding rate of oxygen to hemoglobin. The experiment suggests the feasibility of measuring the ligand binding kinetics to hemoglobin in a single erythrocyte.

CHAPTER 5. MORPHOLOGICAL CHANGES IN RED BLOOD CELLS WITH HIGH PRESSURE PROBED BY DIRECT OPTICAL IMAGING

Red blood cells and their main protein, hemoglobin, provide a model how the cellular environment modulates function. They are excellent candidates for high pressure studies at the cellular level, since they are very simple cells, devoid of nucleus or organelles: they are made of a lipid bilayer linked to a cortical cytoskeleton, used to transport hemoglobin.

In the following, the effect of hydrostatic pressure on individual cells shape and size was recorded through photomicrography inside the fused silica micro-capillary and the images in real time are recorded using a TV camera. The red blood cells showed a decrease in lateral diameter with increase in pressure. Through analysis of several cells we demonstrate that the effect of variable pressure on the size of healthy erythrocyte is reversible and the cells stayed intact after the pressure cycle of up to 210 MPa.

5.1 High pressure microscopy of living erythrocytes

The red blood cells were loaded in a fused silica micro-capillary of inner diameter 50 microns and kept close to physiological condition. They were subjected to a hydrostatic pressure of up to 210 MPa and monitored with direct optical imaging in real time. It was observed that the healthy cells maintained their shape and size up to a pressure of 35 MPa, after which further

increase in pressure lead to a decrease in diameter. The healthy cells went back to there original size when the external pressure was removed. The cell stayed intact after the pressure cycle.

The volume of the sample employed for micro-imaging was nanoliter. The micro-capillary was aligned under the microscope with flat side up and was focused for best image quality. An image of the cell was taken at ambient pressure. The TV camera coupled to the microscope was set to record the movie as the hydrostatic pressure was slowly increased to 210 MPa. From the recorded movie, a frame was taken at a step of every 2000 Psi. The pressure was accurately read through the pressure gauge attached to the pressure pump. Figure 27 shows the representative frames taken from the movie. Their radius along the disc decreases with pressure. Pressure also decreases the mobility of red blood cells. This is evident from the response of many cells.

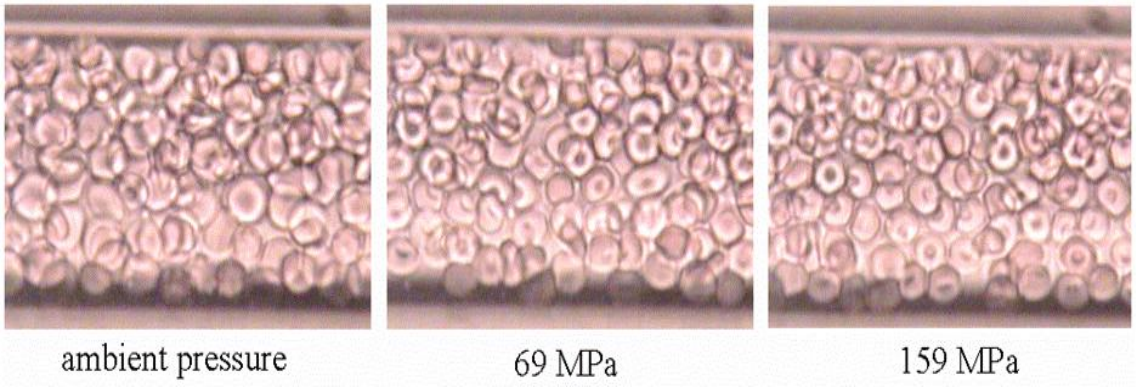

Figure 33 Optical images showing morphological changes in red blood cells at variable pressure

For calibration an image of a scalebar is acquired with the same parameters and is examined to determine the magnification of the setup. Then the image of an empty micro-capillary is used to further ensure the accuracy of the magnification. The final measurement is

made with a 10 mm scale, divided to 1 mm. This scale is placed over the image of the cells in such a way that the diameter can be read off. It must be noted that the 1 mm corresponds to 0.4 μm of the actual size, thus the measurement is accurate within 0.4 μm.

The radii of several cells from every set of experiments were measured and the results are displayed in Figure 34. Upto a hydrostatic pressure of 35 MPa, the radii of the cells do not change. Incidentally, the average pressure under sea at a depth of 3800 m is 38 MPa, this may suggest that during deep sea diving there is no significant change in erythrocyte's size upto this depth. As pressure is increased further a non-linear decrease in radius with increase in pressure was observed up to 210 MPa. This covers the range of maximal sea depth of 11000 m with a pressure of 110 MPa. The cells were intact up to a pressure of 210 MPa (maximum pressure achieved in these experiments). The pressure was then reduced back to ambient pressure. The effect on the size change was found to be reversible. The cell reaches its original size after the pressure cycle. The cell shape remains a discocyte during the whole experiment [173].

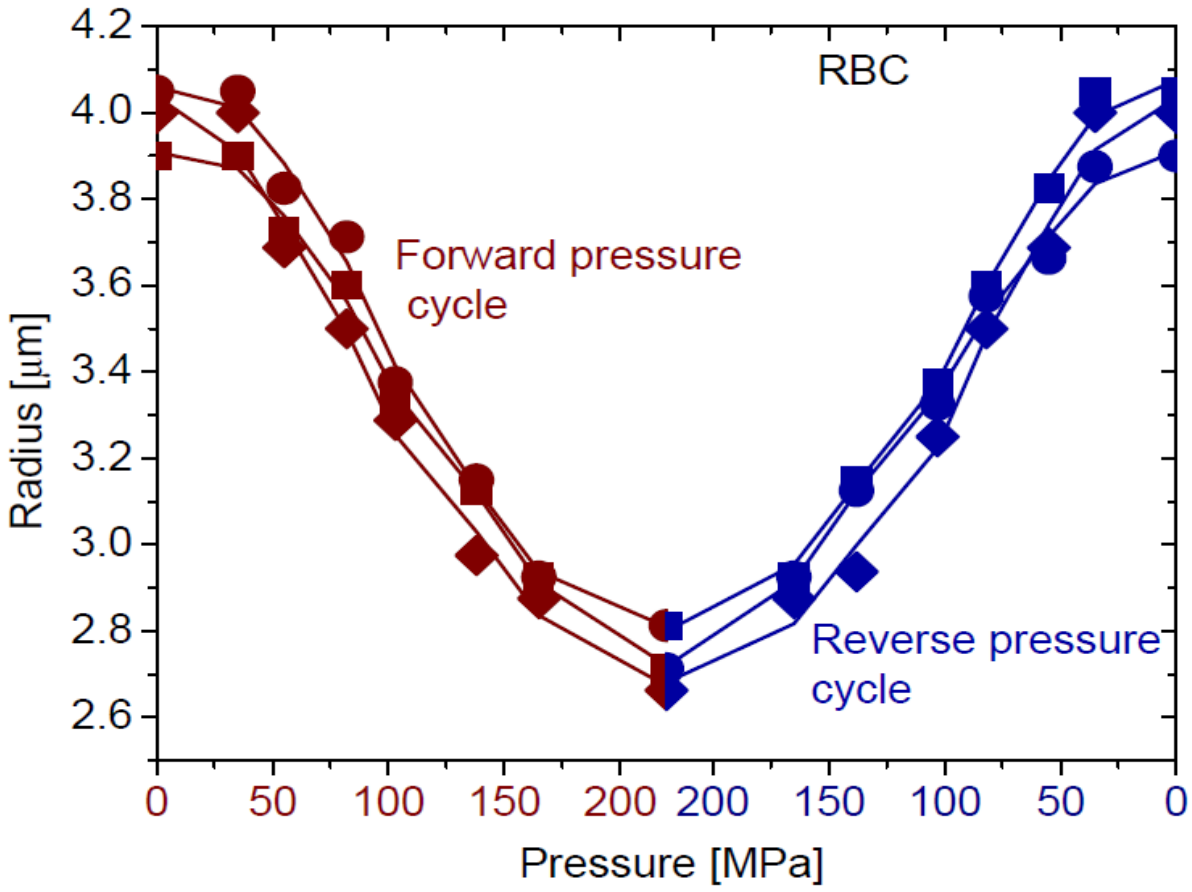

Figure 34 Effect of hydrostatic pressure cycle upto 210 MPa on the radius of red blood cells as seen through live cell imaging under variable pressure.

The compressibility describes the isotropic elastic response of the system to pressure. It is defined as the relative volume change with respect to pressure. Since the pressure is changed rather slowly on the time scale of seconds, we measure the isothermal compressibility $\beta_T = -\frac{1}{V}\left(\frac{\partial V}{\partial P}\right)_T$ in these experiments. On the other hand, if the period of perturbation is short compared to the time required for thermal equilibrium of the sample, the process is adiabatic and

reversible[106]. The adiabatic compressibility is defined as $\beta_{ad} = -\frac{1}{V}\left(\frac{\partial V}{\partial P}\right)_S$, where V and P are the volume of the sample and the pressure respectively. The compressibility is given by the ratio of specific heats C_P and C_V, at constant pressure and constant volume, respectively. For an ideal gas $C_P - C_V = nR$ [174].

Adiabatic compressibility values of the proteins have been reported suggesting them as an incompressible liquid [175]. The low value can be explained by the fact that amino acids have a negative apparent compressibility while it has been reported that globular proteins have an apparent positive value. However, no direct measurements of compressibility of red blood cells as a function of pressure have been available.

In a protein solution, there are several contributions (volumes) to the compressibility [106]. The total volume of a solution is given by $V_T = \sum_i N_i V_i = V_T \sum_i v_i$, where N_i/V_T is the molar concentration and v_i is the fractional volume of the i^{th} species. The adiabatic compressibility is then defined as:

$$\beta_{ad} = -\frac{1}{V_T}\left(\frac{\partial V_T}{\partial P}\right)_S = -\frac{1}{V_T}\sum_i \left[N_i \left(\frac{\partial V_i}{\partial P}\right)_S + V_i \left(\frac{\partial N_i}{\partial P}\right)_S \right] = \sum_i \left[(v_i \beta_i) - \frac{V_i}{V_T}\left(\frac{\partial N_i}{\partial P}\right)_S \right] \qquad (23)$$

where β_i is the adiabatic compressibility of i^{th} species.

The first term corresponds to the fact that total compressibility of the solution is the volume average of compressibility of the components whereas the second term is the characteristic of the system under consideration and depends upon the chemical relaxation process. In particular, if one existing equilibrium is pressure dependent, it contributes to the solution adiabatic compressibility [106]. The equation has a relaxational and a non relaxational

term. The relaxational term depends upon the frequency determined by the reaction constant and can be neglected here. The non relaxational part contains three parameters: intrinsic protein compressibility, bound water compressibility and fractional volume of bound water with respect to the protein [106].

Using the data plotted in figure 34, the compressibility values were calculated to be -5.54 $\pm 0.4\ 10^{-9}\ Pa^{-1}$ as compared to the compressibility of water – $5.1\ 10^{-10}\ Pa^{-1}$ at 0 ^{0}C and ambient pressure [176]. Results show that the intrinsic protein compressibility is very low.

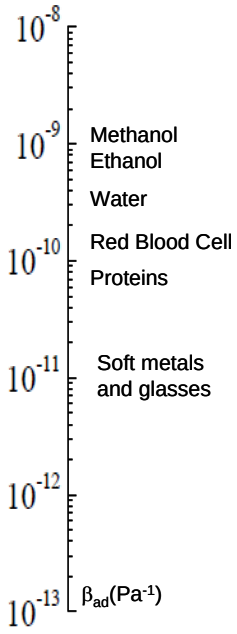

Figure 35 Known values of adiabatic compressibilities of some materials compared with that of red blood cells.

Comparison with the compressibilities of known materials [177] shows that the red blood cells compressibilities are lower than those of liquids and solid polymers but larger than those of metals. The value is near to that of water, but the red blood cells are less compressible. It points

towards relatively fluid interior [61]. To elucidate the effect of variable pressure on the morphology of red blood cells and the fluctuations in volume associated with the dynamic process taking place in the system [178, 179], it is important to understand the structure and composition of the red cell membrane.

5.2 Role of membrane and spectrin network

Our experiments have demonstrated the deformability and elasticity of red blood cells. They show that erythrocytes appear as soft elastic media and can undergo large reversible changes when under external stress. We propose the following hypotheses to support our experimental results.

The excess surface of approximately 40 μm^2 allows the cells to undergo large deformations [35, 50]. They can go up to extensions double their normal size or contractions to half of there normal size. The net deformability of the cell is determined by the intrinsic viscoelastic properties of the cell, cell geometry and viscosity of the cell contents. When hydrostatic pressure is applied it may lead to folding and unfolding of the spectrin molecule. The red blood cells are highly permeable to anions and water molecules which are exchanged readily. The cell maintains their constant volumes through energy dependent active membrane pumps, gradient driven passive transporters and various channels. These channels along with the aquaporin channels maintain the hydration of the cell and thus keeping the visco-elastic properties under check.

The resilience of the cell is attributed to the mechanical properties of the cell membrane. It is comprised of three layers, the glycocalix at the exterior which controls cell's interaction with other cells;

the lipid bilayer and the cytoskeleton consisting of spectrin tetramers connected to the bilayer via membrane proteins [180]. The relatively stable spectrin tetramer network tethered to a phospholipid bilayer [44] allows the cell to regain its biconcave shape when the stress is removed. In healthy conditions the skeleton allows the cell to undergo large deformations while maintaining membrane structural integrity [181]. The connectivity of the spectrin network experience extensive remodeling as the cell undergoes large deformations [44].

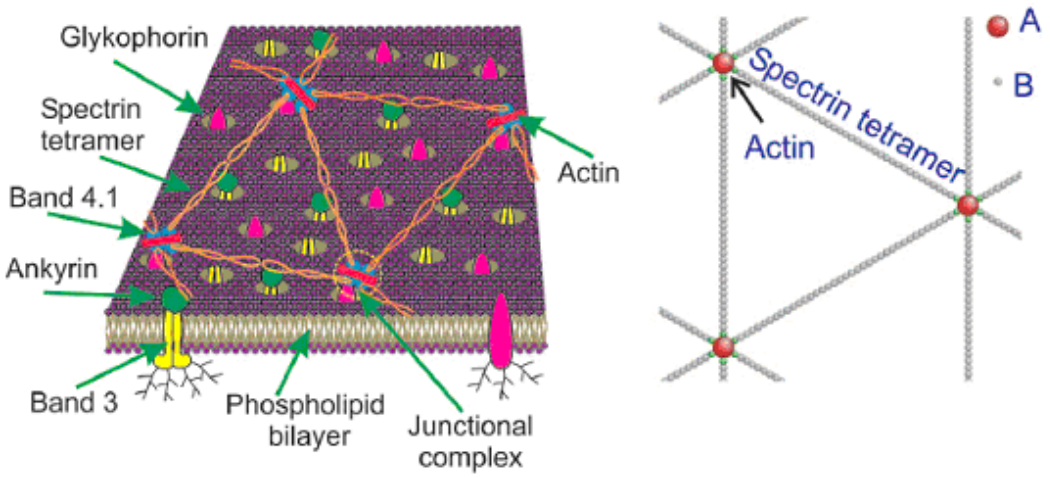

Figure 36 Schematic of cytoskeleton of the human RBC (Left) in a minimal physically realistic model with breakable actin–spectrin interaction. According to Li et al [44] A (red sphere) represents an actin protofilament, and B (green and gray spheres) represents a spectrin segment. Only the two ending spectrin units (green spheres) of a spectrin chain can bind to A [44]

Figure 36 shows a schematics of cytoskeleton of the human red blood cell membrane as according to Li et al. [44]. Two structural features that affect membrane mechanical properties are the intrinsic elasticity of the spectrin molecule and the geometric organization of spectrin molecules within the skeleton [181]. Spectrin is a flexible, 100 nm rod shaped molecule which forms a meshwork underlying the cytoplasmic surface of the plasma membrane. It is composed of two parallel polypeptide chains: (α- and β- chain), that are intertwined side by side to form a

dimer. It is attached to the lipid bilayer in association with ankyrin. The anchoring protein is further connected with the anion transporter which is an integral membrane protein. Additional association between spectrin and glycoprotein through band 4.1 has been suggested [50]. Spectrin hetero- dimers self-associate to form tetramers such that no α- α and β- β contact occur. Higher oligomers of spectrin are also present in the cytoskeletal meshwork [182]. The tetrameric species of spectrin tend to predominate the membrane skeleton. The tail end of the spectrin tetramer is connected to actin oligomer composed of 12 monomers. On average, six spectrin ends associate with each actin oligomer to create an irregular network with a hexagonal lattice. Each spectrin actin junction is stabilized by formation of a ternary complex with protein 4.1, which is composed of 622 amino acids.

There may be several possible mechanisms to membrane deformability and elasticity as observed in the data. Firstly, for the membrane to deform normally the skeletal network undergo conformational rearrangements including folding and unfolding of spectrin molecules [183]. Secondly the exchange of water molecules through aquaporin channels may lead to alteration in the size of the red blood cell during pressurization and de-pressurization. Though studies have been conducted to measure the shear modulus and young's modulus of the red blood cell [51], the direct measurement of compressibility of the red blood cell through live cell imaging has been successfully done for the first time (to the best of our knowledge). The results open a new avenue for experiments addressing questions on cell elasticity. Our experiments have been extended to study the cells in pathogenesis with high pressure imaging. Red blood cells infected with the malaria parasite were probed in the same way as healthy cells. The erythrocytic stages of the parasite life cycle, namely, ring stage, trophozoite stage and schizonts stage were studied.

5.3 Volume changes in erythrocytes infected with the malaria parasite

The volume of the erythrocyte may play a significant role for the metabolism and abnormal cell function. For instance, in red blood cells the polymerization reaction of sickle cell hemoglobin is highly concentration dependent [184]. The experiment was performed on malaria infected cells to see if the parasite has any effect on the spectrin network of the cell membrane and thus the deformability of the host cell. The malaria parasite *Plasmodium falciparum* is an example of a microorganism invading a red blood cell. Parasitization leads to structural, biochemical, and mechanical modification of the host cell. Hemoglobin is degraded inside the digestive vacuole of the parasite into toxic free hem and denatured globin. The process of detoxication involves the conversion of iron-protoporphyrin IX (FePPIX) to hemozoin, also known as malaria pigment, which is an insoluble compound located in the food vacuole of the parasite complex. Volume expansion plays an important role in the intra-erythrocyte development of the malaria parasite [185] and its multi-stage life cycle [73, 186].

We investigated the effect of pressure on the morphology of red blood cells infected with the malaria parasite using the same experimental protocol as for healthy cells. The preparation of the malaria infected cells is described in Chapter 3. The optical images and the real time movies made at different stages of infection were measured and the data was analyzed for change in shape and size of the host red blood cell. Measurements were repeated on several cells in each stage of infection.

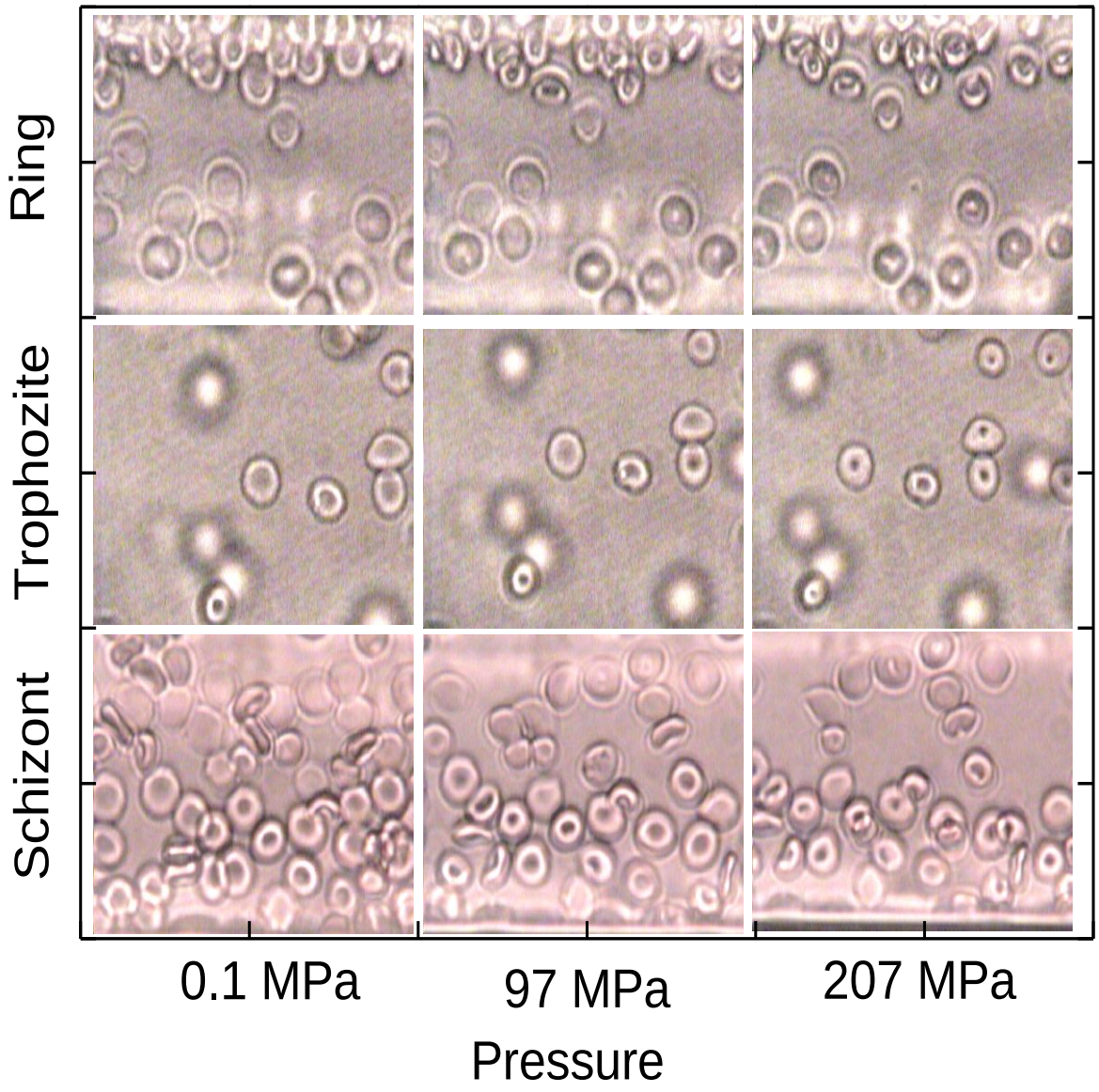

Figure 37 Optical images of the three stages of malaria infected cell at variable pressure.

Figure 37 shows optical images of the intra-erythrocytic stages of parasite multiplication probed with high pressure. Pressure is plotted on the horizontal axis and the stage of malaria

infection on the vertical axis. The top panel shows the ring stage (1-18 hr post invasion), the middle panel is the trophozoite stage (18-28 hr post invasion) and the bottom panel shows the schizonts stage (28-38 hr post invasion), respectively. The measurements show that the lateral radii of the cells decreases with pressure.

Studies of malaria infected cells at variable pressure reveals that the cells are more rigid as compared to the healthy cells. Different stages respond differently to the pressure stimuli. The different stages of the parasite infection cycle vary in terms of onset of change in shape, compressibility and mean volume of the host cell. The results suggest that the malaria infected cells become rigid and gets difficult to pass through narrow capillaries. The deformability was found to be lower in the case of infected cells [61]. There is a volume increase during the multiplication cycle of the parasite, particularly in the trophozoite stage, where hemozoin accumulates.

However, the change in size was observed to be reversible in the case of healthy erythrocytes, clear differences between compression and decompression curves were observed in case of the infected cells. The images taken at ambient pressure before and after the pressure cycle were compared. It was seen that the infected cells become less spherical after the decompression cycle. The results revealed that the different stages of the parasite life cycle may have different effects on the decompressibilty cycle.

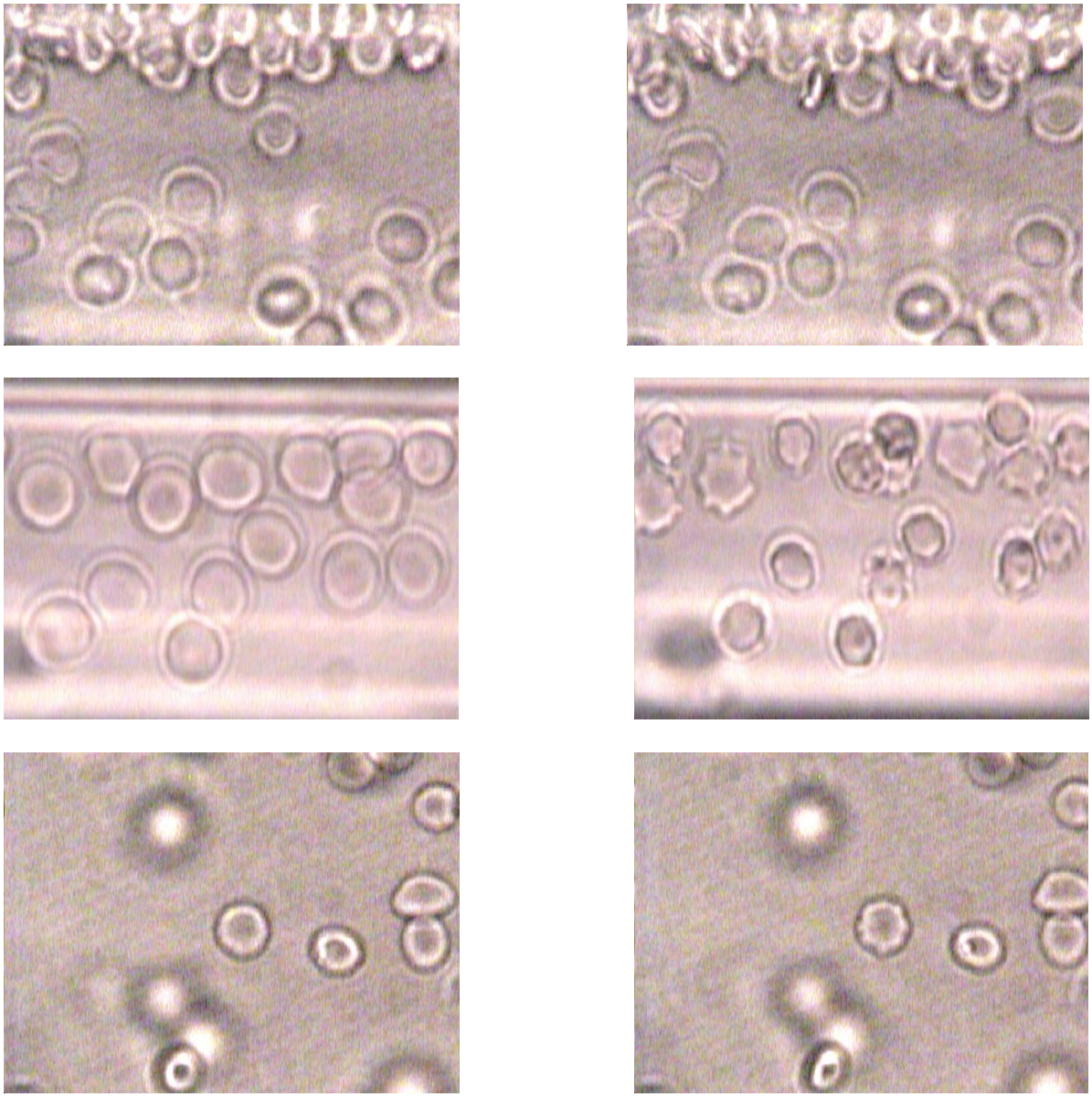

Figure 38 Optical images of malaria infected erythrocytes at ambient pressure loaded in a micro-capillary. The image at the left was taken before the pressure cycle and the image at right is taken after the pressure cycle of 210 MPa. The three stages of intra-erythrocytic stages are shown as: ring stage(top panel), trophozoite stage(middle panel) and the schizonts stage(bottom panel). The cells display knobbing on release of pressure in infected cells.

Figure 38 shows the images of the three stages of parasite infection at ambient pressure taken before and after the pressure cycle. The left column has the images before the pressure cycle. The pressure is increased upto 210 MPa and then lowered back to ambient pressure. The right column shows the images after the pressure cycle. The infected cells deform during the decompression cycle. When the pressure was decreased back to ambient pressure the change was found to be irreversible. The cells in the trophozoite and schizonts stage started to burst and displayed knobbing upon release in pressure. The effect was seen to be more prominent in the case of trophozoite stage. The cells in ring stage did not display knobbing but did not get back to the original size either.

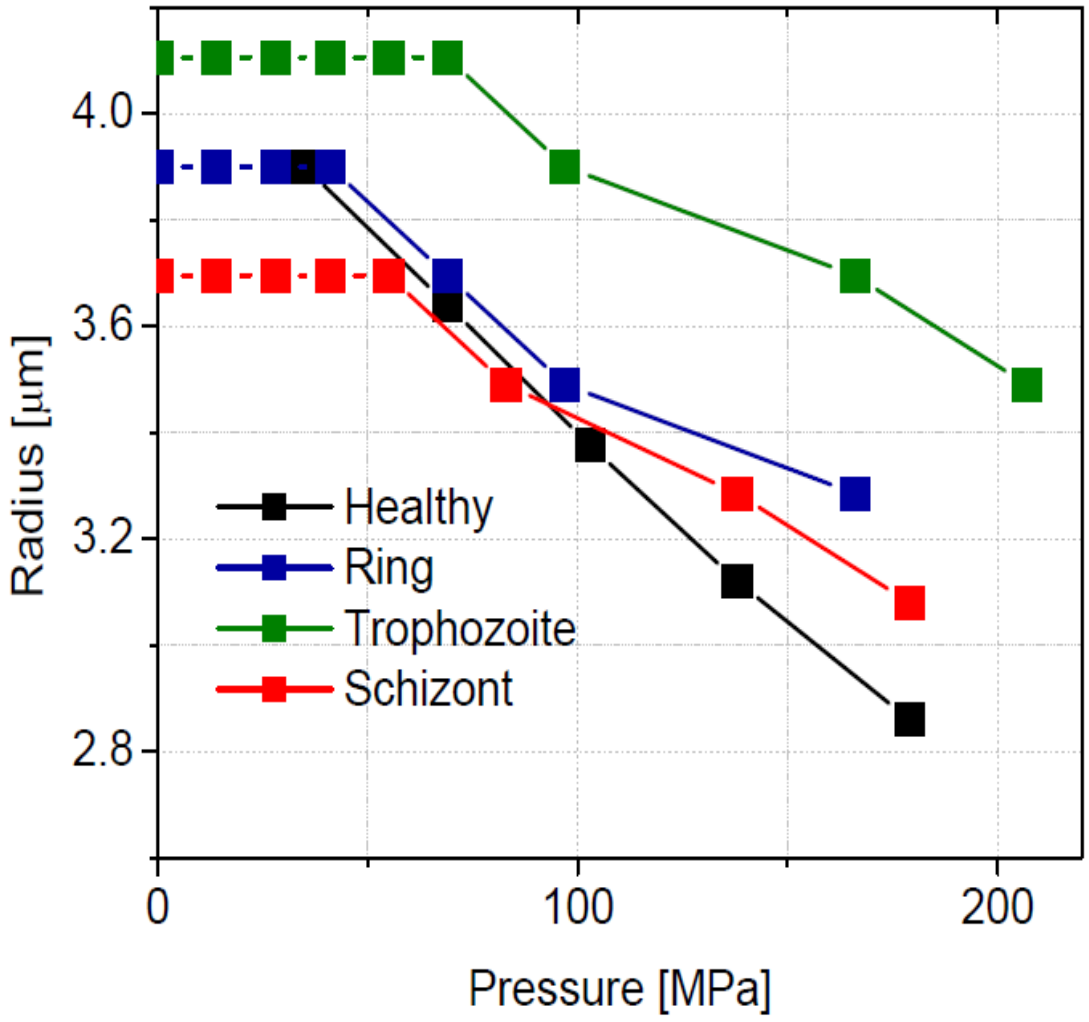

Figure 39 Effect of high hydrostatic pressure on the radius of red blood cells infected with malaria parasite

From optical images, the radii along the disc were determined as described earlier. The lateral radii of the healthy cell and the infected host cell as a function of forward pressure are plotted in the Figure 39. The horizontal axis shows the hydrostatic pressure and the lateral radii are shown on the vertical axis. The data reveals that the size of the host cell during the ring stage is comparable to the healthy erythrocyte. Whereas an increase in lateral diameter was observed at

the trophozoite stage of the infection cycle, the cell's diameter decreased when the parasite reaches the schizont stage. This suggests that as the parasite grows there are new permeation pathways that get activated so that the excess ions are transported out and the cell does not swell up and lyse immaturely. The data show that the mean volume of the cells in ring stage is comparable with the mean volume of a healthy cell, while the mean volume of trophozoite is more and that of schizonts is less than that of a healthy cell [21, 185, 187]. There are two major factors that might cause a Plasmodium-infected cell to swell [33]. The first is the physical presence of the growing parasite which, as it matures from the early ring-stage to the late-stage trophozoite, expands from occupying an estimated 4% of the intracellular volume [188] to occupying most of it. The second arises as a result of the parasite-induced increase in the ionic permeability of the erythrocyte membrane. A considerable amount of hemoglobin is digested by parasites during intraerythrocytic development and converted into insoluble polymerized form of heme known as hemozoin [189]. Recent measurements of the shear module G of RBC membranes using diffraction phase microscopy find an increase of G for ring and schizont stage relative to healthy cells. The plot in the Figure 39 shows that the onset of change in shape varies with the stage in the parasite multiplication cycle. Ring stage, the quiescent stage did not alter in size up to a pressure of 69 MPa, while trophozoite stage, the metabolically most active stage was found to have highest onset of 97 MPa; whereas the schizonts stage showed shrinkage initiation at 83 MPa.

The compressibility of the infected cells was calculated using the slope of the graph in the linear region of the radius versus pressure curve. The rate of compressibility is different for different stages of the parasite cycle. For the ring stage the value is $-3.76\ 10^{-9}\ Pa^{-1}$, trophozoite -

3.26 10^{-9} $Pa^{-1}$and -4.03 10^{-9} Pa^{-1} for schizonts. The results of high pressure imaging of healthy and infected erythrocytes are summarized in Figure 40.

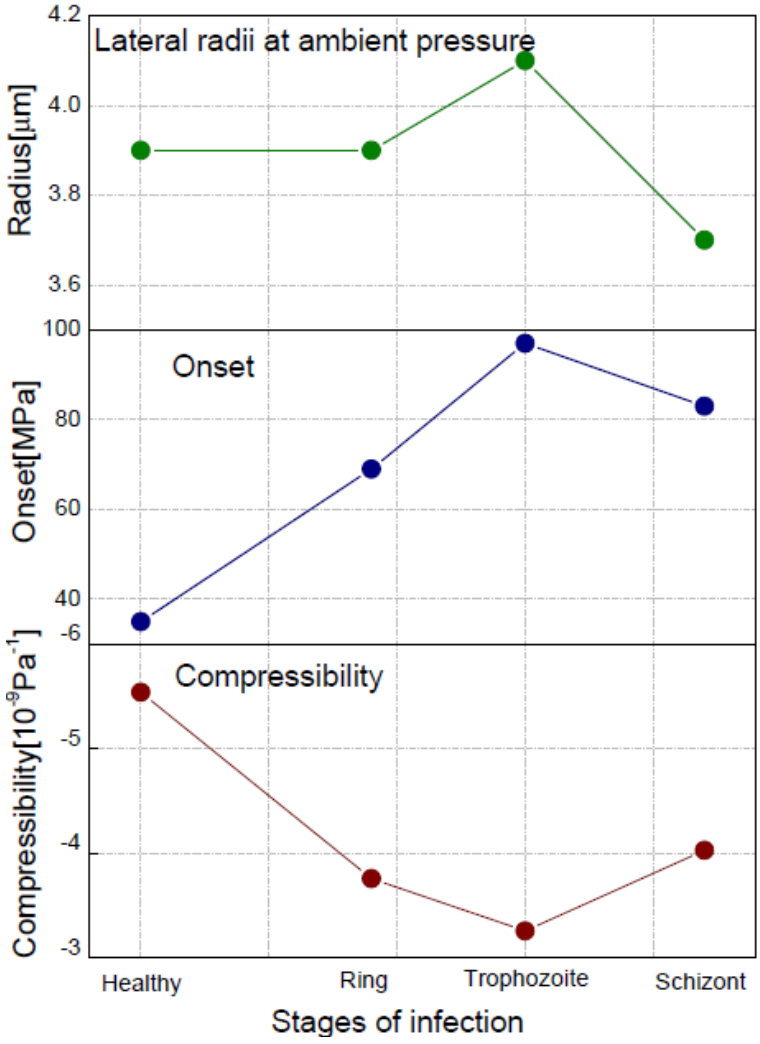

Figure 40 Structural changes probed with pressure upon malaria infection

The three panels in Figure 40 show the changes in lateral radii (top panel), onset of compression(middle panel) and the compressibility(bottom panel) with response to high pressure as seen with the progression of malaria parasite cycle. The horizontal axis shows the intra-

erythrocytic stages of the parasite cycle. As the malaria grows the host cells become less deformable and the membrane compressibility may be correlated with the parasite multiplication cycle. In following section the variations in the structure of the membrane with the parasite growth is explored.

5.4 Possible mechanisms for cell membrane modification upon pathogenesis

Our intent here is to provide a contemporary view of the relation between red blood cell membrane molecular architecture and mechanical properties in healthy and pathological conditions.

In the host cell, the parasite grows and divides to generate upto 36 daughter parasites during its 48 hour life cycle. For this successful growth and multiplication, the parasite needs to duplicate the structural components [190, 191]. To identify the abnormalities in red blood cells associated with pathogenesis we first address the changes in the membrane composition with parasite invasion.

The predominant lipids constituting the red blood cell membrane have been reported [73, 192-194], however it is difficult to learn about the lipids present in trace amounts such as neutral lipids, phosphatidic acid and phosphatidylglycerol. Studies with Plasmodium falciparum grown in vitro or isolated from patients with malaria have revealed profound changes in membrane composition and structure. Following parasite invasions of the host cell, a six fold increase in phospholipid content is observed with large increases in phosphatidylcholine, phosphatidylethanolamine and PA. Phosphatidylcholine and phosphatidylethanolamine forms the major content of the phospholipid composition in the infected host cells with 40 to 50% and 35

to 40% of the total phospholipid content, respectively [66]. The neutral lipids that are found in the trace amounts in healthy erythrocytes however dramatically high increase in percentage is observed upon invasion [193, 194]. This increase is attributed to the active synthesis of neutral lipids by enzymatic machinery during its growth. These neutral lipids are known to play a crucial part during merozoite release or invasion [195, 196].

Several studies reveal that malaria infection accelerates the signs of aging in the erythrocyte by reduction in phospholipid and cholesterol content and increase in lipid peroxidation of the uninfected cells around the infected cell [197, 198]. This could be the result of the proteins secreted by the parasite to change the composition and structure of uninfected cells, a mechanism to facilitate future invasion. It may also be the result of the high nutritional demand of the parasite that the composition of serum is altered which in turn results in changes in the membrane composition of the uninfected cells present in the vicinity. The lipid biogenesis is a crucial step as the byproducts provide the ingredients for the composition of food vacuole inside the host cell.

The parasite causes major reorganization of the host cell membrane during its intra-erythrocytic development [66, 73]. It remodels the molecular species of membrane phospholipids and also inserts newly synthesized proteins into the bilayer. These changes results in altered lipid packing, modification in membrane rheology, decreased micro-viscosity and higher membrane fluidity. It also causes functional modifications in the membrane by introducing new permeability pathways. Our data reveal a decrease in deformability with infection which may be due to a decrease in cholesterol content in the host cell membrane. The degree of saturation of

the fatty acids attached to the phospholipid glycerol is also changed causing decrease in the deformability of the host red cell.

The asymmetric composition of the inner and outer monolayer is also affected during parasitization. Phosphatidylserine which is present in the inner layer in healthy erythrocytes has been reported to flip to the outer layer on pathogenesis [199]. One probable reason for this exposure of phosphatidylserine to the outer layer is the influx of calcium which stimulates bidirectional phospholipid migration across the membrane. This loss of asymmetry increases with the increase in parasitemia. This asymmetry leads to binding of phosphatidylserine receptors on macrophages and subsequent phagocytosis of the cell [200]. This also contributes to the cyto-adherence of parasitized erythrocyte [201].

Another important aspect that can affect the host cell deformability and elasticity upon parasite invasion is creation of new permeation pathways in the host cell membrane for the parasite growth. During the intra-erythrocytic cycle of the asexual growth of the parasite, it enters a hostile environment where insufficient amount of nutrients are present and exist chances of critical buildup of the hazardous metabolic end products. Duplication into daughter parasites requires more energy from the host cell. The membrane transporters present naturally in the erythrocyte membrane are geared to optimize the respiratory function and maintain cell homeostasis at minimal metabolic cost. Thus, to survive within the cell, the parasite alters the permeability of the host cell membrane by up regulation of existing carriers and by creating new permeation pathways. For the parasite to grow it obtains most of the nutrients from within the cell's cytosol, however several essential amino acids are not present in the cell and thus have to be imported from outside. For some of these nutrients there exist channels in the cell which

needs to be up regulated while for other new pathways needed to be made. Thus with the growth of the parasite the transport properties of the membrane gets greatly modified [202, 203]. These transport pathways increase the permeability to various solutes, amino acids and monovalent inorganic ions. These pathways also have an important function in maintaining the osmotic balance of the cell and volume regulation. It removes the lactate produced from glycolysis of hemoglobin which is important for the parasite growth, as if accumulated it can be toxic and can lead to swelling and bursting of the cell before even the parasite growth cycle is completed. In addition to the two above mentioned factors the membrane is also deformed by accumulation of parasite protein secretion along the inner layer of the host cell membrane.

Membrane speculation could be a probable reason for the infected cells to burst when the pressure is removed. According to the coupled bilayer hypothesis, tight packing of membrane lipids and integral proteins in 8 nm thick membrane is very critical in maintaining the shape of the cell. During flipping of phosphatidylserine, if the outer monolayer expands or the inner monolayer shrinks then it results in echinocyte formation due to exocytosis. Our data show similar features on the depressurizing cycle as in echinocyte formation suggesting the effect of exocytosis and the role of permeation pathways and aquaporin channels. If the spectrin associations are increased or the proximity of the spectrin network to the lipid bilayer is increased, it inhibits the ability of spectrin molecules to undergo the necessary structural rearrangements and thus the deformability decreases.

The critical modification factors in deformability are adenosine triphosphate, adenosine triphosphatase and calcium. It has been shown that red blood cell deformability is dependent on the level of intracellular ATP and when the ATP content is decreased, increased free calcium is

bound to membrane proteins, resulting in increased rigidity of the red blood cell membrane [204]. The use of ATP via the parasite leads to excess calcium concentration inside the cell. This calcium gets accumulated at the inner surface of the phospholipid bilayer increasing the rigidity of the cell. This accumulation of the calcium changes the membrane permeability by blocking the important water and anion channels. Due to a decreased exchange of the water molecules, the cell gets dehydrated and the cytoplasmic viscosity of the cell increases. The proximity of spectrin network to the phospholipid bilayer increases as the parasite grows and multiplies. This inhibits the ability of spectrin molecules to undergo necessary rearrangements when stressed. Increase in intermolecular and intra-molecular associations of spectrin hinders the conformational changes and thus decreases the deformability.

The red blood cell membrane consists of phospholipids that generally contain unsaturated acyl chains and are loosely packed in the bilayer. This provides rapid rotational and lateral movement of integral proteins. On contrast, parasite membranes consist of glycerophospholipids and sphingolipids which contain long saturated acyl chains. These lipids pack tightly in the membrane forming quasi gel membranes with reduced movements.

In summary, the stiffness of the red blood cell is found to increase with the parasite invasion. With application of hydrostatic pressure, the deformability of the parasitized cell is significantly reduced compared to that of healthy red blood cell. Thus the infected red blood cell also undergoes a shape change to display knobbing compared to the biconcave shape of the healthy red blood cell. Membrane studies performed on the cells in pathological conditions may open new pathways to drug delivery. The parasite *Plasmodium falciparum* has been reported to

alter the membrane deformability via altering the lipid composition, flip flop of integral proteins and opening new permeation pathways [66, 73].

The above results show that the healthy red blood cells are highly deformable which allows them to flow through narrow capillaries during circulation. Upon parasite invasion, modification of the plasma membrane with parasite multiplication into daughters leads to reduced fluidity of the cell. These results offer a mechanistic rationale for the erythrocyte cytoskeleton mechanical function under loading. Shape changes may be related to molecular structure that affects mechanical properties.

In the following chapter, the micro-imaging measurements are complemented by micro-absorption spectroscopy to determine changes in the hemoglobin. In parallel to micro-imaging, using confocal absorption microscopy the effect of parasite on the spectra of the host cell is examined. The measured micro-absorption spectroscopy points to a potential diagnostic tool for malaria infection in single erythrocytes.

CHAPTER 6. SINGLE CELL ABSORPTION SPECTROSCOPY OF HEMOGLOBIN IN HEALTHY AND INFECTED CELLS

Our goal here is to measure micro-absorption spectra of live erythrocytes healthy and infected with a malaria parasite and to investigate molecular changes which occur during differentiation of the parasite inside the cell.

6.1 Micro-absorption spectrum of healthy red blood cell

For micro-absorption measurements the red blood cells were immobilized on a coverslip using standard procedures. The coverslip was rinsed with 70 % Ethanol followed by 1X Phosphate Buffer Saline (pH 7.4). Sufficient 1mg/ml poly-L-Lysine HBr was applied to coat the coverslips which were then kept at room temperature for 15 minutes. Coating solution was removed and the coverslips were rinsed with 1X PBS. The erythrocytes suspended in 1 X PBS were added to the coverslips and were allowed to adhere at room temperature for 20 minutes. Excess liquid was drained from the coverslip.

The transmitted intensities without (I_o) and with a red blood cell (I) were measured at the center of a single red blood cell with a spectral resolution of 0.5 nm. Spectra were acquired with an integration time of 5 seconds.

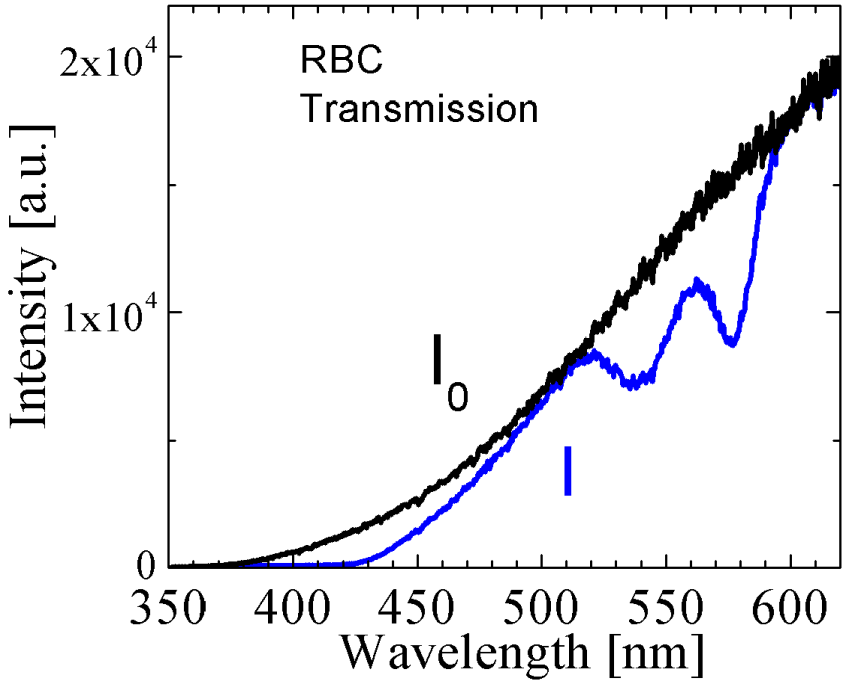

Figure 41 Transmitted intensity spectrum without (I_o) and with red blood cell (I)

Figure 41 shows the transmitted intensity I_0 through the coverslip coated with poly lysine and buffer solution. It corresponds to the spectra of the tungsten-halogen lamp which is a black body curve. A single spectrum is acquired over the range from 350nm to 700 nm within 5 seconds. The transmitted intensity I measured at the center of the red blood cell coincides with I_0 in the range between 600 and 650 nm. In this range the absorption is absent. At wavelengths 415 nm, 541 nm and 577 nm the transmitted intensity shows dips which corresponds to the chromophore absorption bands of hemoglobin. Using I and I_0 the absorbance was calculated using the relation $\Delta A = - \log (I/I_o)$.

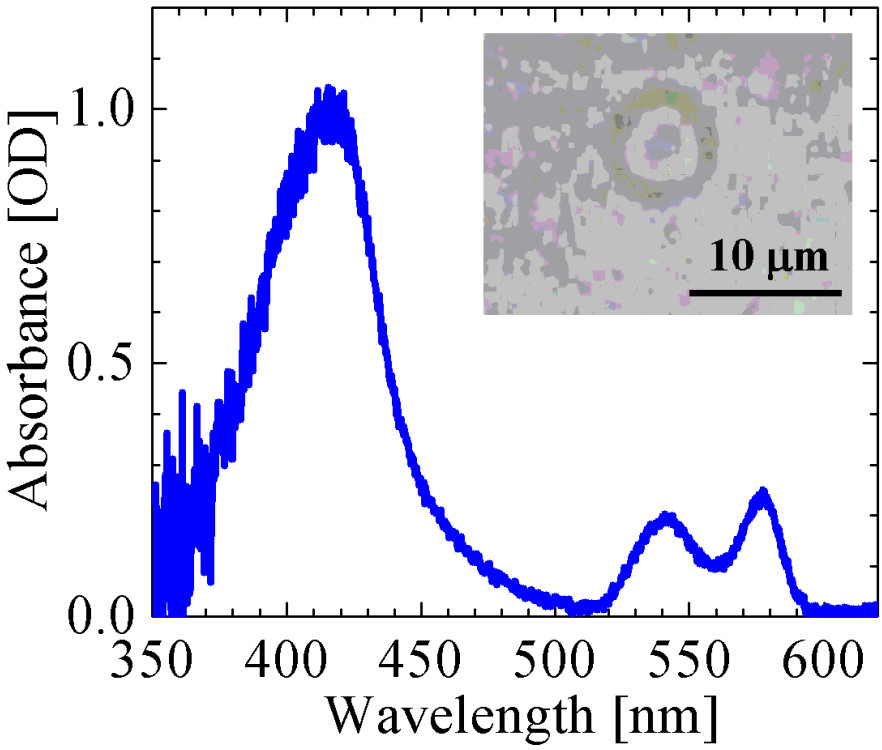

Figure 42 Absorption spectra of a single RBC

The spectrum was obtained over the visible range from 350 to 700 nm. The electronic absorption spectra of porphyrins are characterized by the intense Soret transition near 400 nm and two weak visible transitions near 555 nm [205]. The intense absorption bands result from to π to π^* transitions and can be distinguished from the weak bands due to charge-transfer transitions. The spectra depend on the electronic configuration of the iron cation and can be correlated to the spin state [205]. The absorption spectrum of the healthy red blood cell is indicative of oxygenated hemoglobin with the Soret band at 415 nm and β- and α-bands at 541 and 577 nm, respectively. The ratio of relative intensities of β- and α-bands was calculated to be 0.87 as compared to the literature value of 0.92 [92].

Following the methods described previously, slides with synchronized stages of the malaria parasite multiplication cycle were prepared. The slides were examined for spectral changes associated with intra-erythrocytic development of the malaria parasite and corresponding heme degradation.

6.2 Effect of malaria parasite cycle on the absorption spectrum of red blood cell

The malaria parasite degrades large quantities of hemoglobin during the multiplication cycle. To study the effect of heme degradation inside a host cell, the spectral changes at different intra-erythrocytic stages were probed using Confocal Absorption Microscopy technique. Change in relative intensities of the β- and α- bands was observed which can be correlated to the parasite life cycle. The Soret peak shifts to higher wavelength as the parasite grows. The experimental studies focus on characterizing and interpreting the effect of malaria parasite growth inside the host cell.

Optical microscopy images of healthy human RBC and RBC infected with malaria inducing parasite *Plasmodium falciparum* are shown in Figure 43. The cells are contained in a micro-capillary of inner bore 50 μm. Image on the right shows the cell with the parasite in it at 24 hr post invasion. It is difficult to discern healthy from infected cells through optical images without stains and to correlate them to parasite multiplication cycle. The results that follow show the potential of micro-absorption as a diagnostic marker for different stages of parasite multiplication cycle.

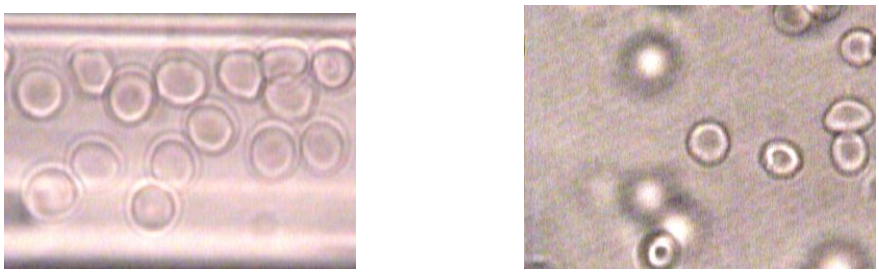

Figure 43 Erythrocytes in a micro-capillary: healthy (left) and infected (right). The diameter of a single cell is ~ 7 μm.

Absorption spectra for each stage of the multiplication cycle of the parasites were measured as described is section 6.1. The absorption spectra were measured along the lateral direction. An individual live erythrocyte under physiological condition was illuminated using broadband excitation and the transmitted light intensity was collected using the spectrometer with 5 seconds acquisition time. The following stages were synchronized for measurements: 14–20 h (ring stage), 20–36 h (trophozoite stage), and 36–48 h (schizont stage) after merozoite invasion. Figure 44 shows the micro-absorption spectrum of an individual erythrocyte in the healthy state and the three stages of the parasite multiplication cycle.

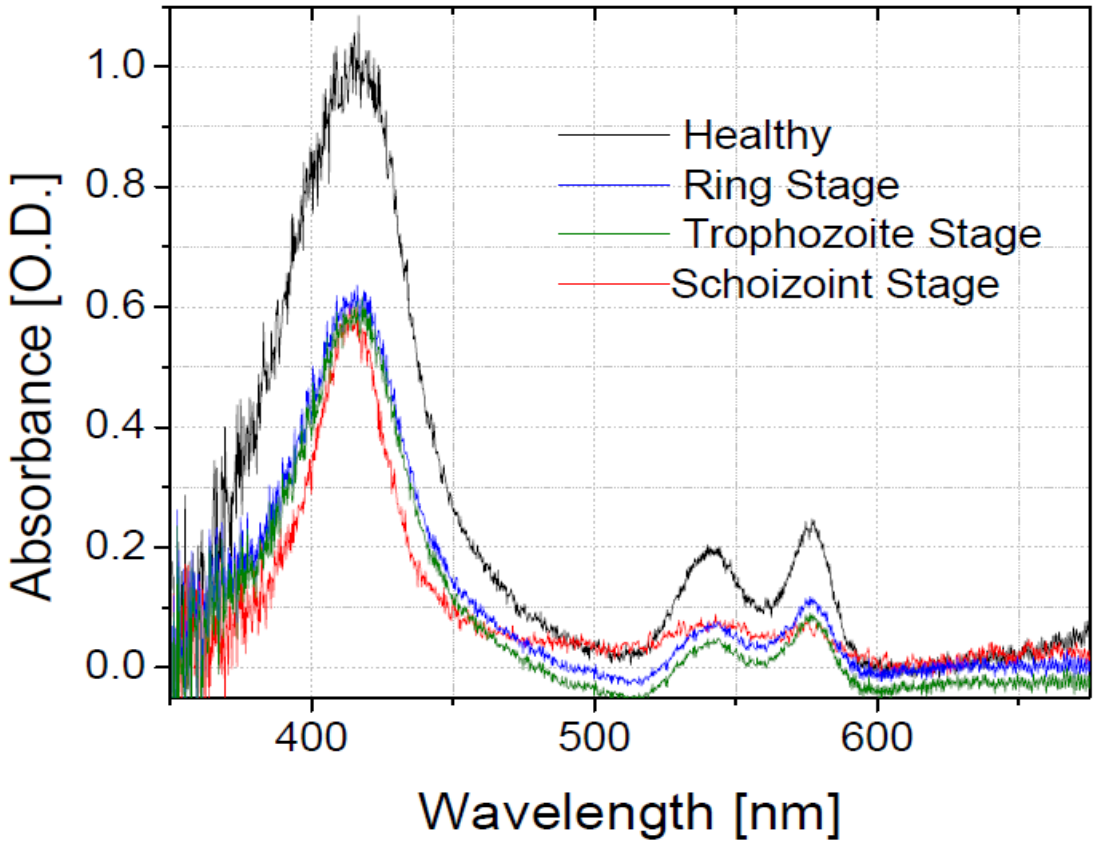

Figure 44 Micro-absorption-spectra of single erythrocytes. The spectra are from a healthy erythrocyte and from erythrocytes infected with malaria parasite *Plasmodium falciparum.* The data acquisition time is 5 seconds.

Changes in peak positions and relative peak intensities were observed in the case of cells in pathological conditions. The intensity of the Soret band was weaker than in uninfected sample and the ratio of the relative intensities of the β- and α- bands changed. The spectral bands were generally broader and less intense in the infected cells. The spectral changes with infection are summarized in Figure 45.

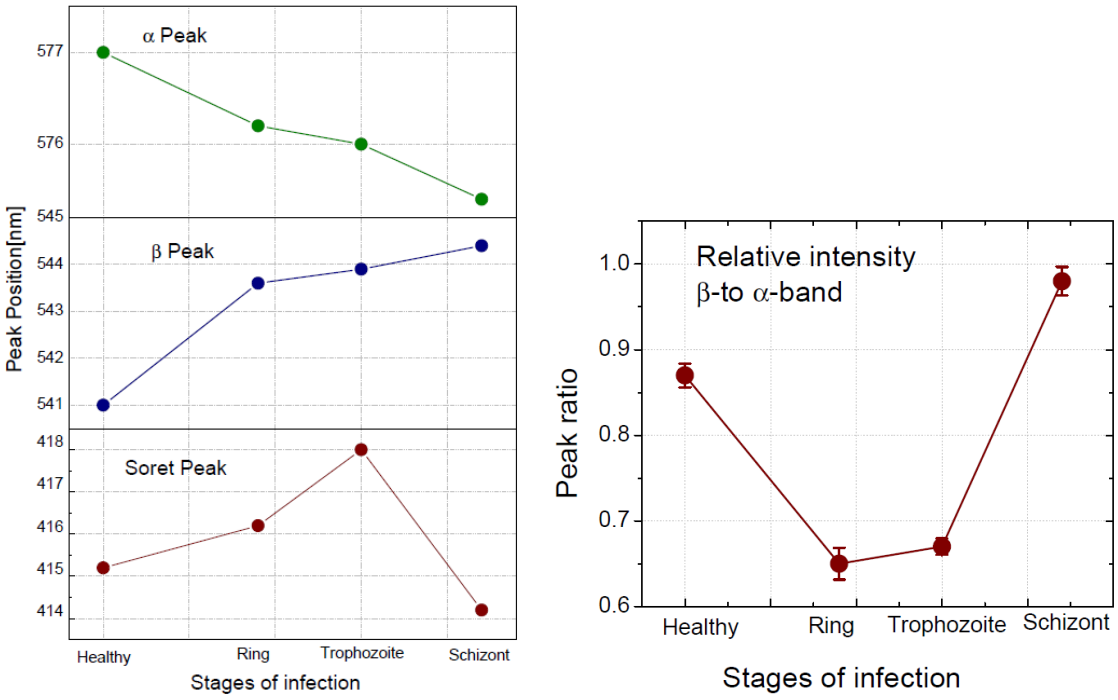

Figure 45 Change in peak positions of absorption spectrum upon infection (Left Panel). Change in relative peak intensities of β- and α- bands upon infection with malaria parasite *Plasmodium falciparum.*

The left panel of the figure 45 shows changes in the peak positions of the hemoglobin absorption spectrum upon invasion with malaria parasite. There is a 3 nm shift observed at a spectral resolution of 0.5 nm. In the post invasion, micro-absorption spectra changes in peak positions were observed as early as in the ring stage of the infection cycle. The Soret band and the β-band shifted to higher wavelengths, 416 nm and 544 nm, respectively. The ratio of the β- to α-bands was found to be 0.65. The Soret band further shifted to 418 nm at 24 hour post invasion and as the parasite multiplied it shifted towards the lower wavelength (414 nm at 36 hour post invasion). The β- and α-bands moved to 543 and 576 nm, respectively during the trophozoite stage. A shift to 544 nm and 575 nm was observed in β- and α-bands positions as the

parasite got into the schizonts stage of the life cycle. The ratio of the relative intensities of the two bands decreased to 0.67 during trophozoite and increased to 0.98 at the schizonts stage of infection. As the hemoglobin is broken down by the parasite, the protein chain fragments are transported away for further digestion. The remaining toxic heme is then oxidized to a ferric state. The release of the heme from the protein is the first step in the formation of hemozoin. The changes in the spectra could be the result of this degradation and the changes in the vibrational modes of the now free heme. As the heme rings are no longer bound within the pocket of the protein the constraints on the various bonds will be much more random which accounts for the broadening of the bands.

6.3 Spectral changes and mechanism of hemoglobin degradation

Hemoglobin processing is a complex process, including transport of hemoglobin from erythrocyte cytosol to the parasite food vacuole, disruption of hemoglobin tetramers, removal of heme from hemoglobin, detoxification of heme with formation of hemozoin, and hydrolysis of the globin into individual amino acids [66]. In the discussion that follows I will explain these constituent processes which complete the proteases of hemoglobin.

Pinocytose of the hemoglobin rich erythrocyte cytosol into small vesicles has been reported to start as early as in ring stage [206, 207]. By the onset of trophozoite stage two structures, namely the food vacuole and the cytosome, specialized for hemoglobin transport and processing, appears in the host cell. Cytosome are tubular structures that contain apposed parasite and parasitophorous vacuole membrane and functions to take up the host cell's cytosol. The food vacuole results from the fusion of small vesicles that bud from the cytosome. The

hemoglobin breakdown is suggested to start inside the transport vesicles itself [207, 208]. The food vacuole is an acidic compartment that slowly denatures hemoglobin [209-211] and releases heme. The acidic pH of the vacuole is maintained by two proton-pumping mechanisms, a H^+-ATPase and a H^+- pyrophosphatase [212]. The heme is then separated from the globin using aspartic and cysteine protease activities. The small globin-derived-peptides are then transferred to parasite's cytosol for further hydrolysis by cytosolic proteases.

Studies show that hemoglobin content reduced by almost 75% or more in cells infected with malaria parasite. During the parasite life cycle, the free amino acids content increased significantly and the composition of these amino acids matched those of the hemoglobin [213]. A percentage of amino acids released on hemoglobin degradation is used in the parasite growth and the rest is expelled out of the cell through parasite transport pathways. The parasite is also capable of acquiring amino acids from outside the cells through transport channels and permeation pathways discussed in section 5.1.4. Studies have also revealed that if specific precursors are available, the parasite has capacity to synthesize some amino acids [214]. Thus, even if all the amino acids from the hemoglobin hydrolysis are not utilized and parasite is capable of acquiring and synthesizing few amino acids, the need for some essential amino acids might obligate the parasite to hydrolyse the hemoglobin.

Hemoglobin hydrolysis releases amino acids, heme and iron which calls for a parasite dealing mechanism. Amino acids may be essential for the parasite growth. Though, the heme and iron may help in parasite's metabolic activities, both can also be toxic to the parasite.

Another explanation for hemoglobin hydrolysis is the space provided for the growth of the parasite once the hemoglobin is removed. To maintain the osmotic stability of the host cell

and to prevent the swelling and bursting of the host cell, the parasite degrades the hemoglobin [34, 215].

Free amino acids and globin-derived-peptides either diffuse or transported via multiple putative transport pathways [216] from the food vacuole to the parasite's cytosol. Excess amino acids are expelled from the infected cell via parasite derived permeation pathways [217, 218].

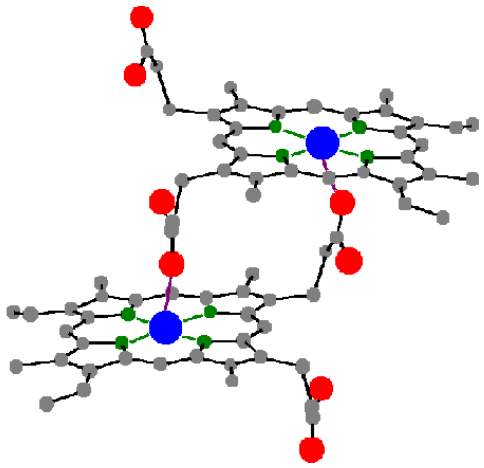

Figure 46 Ball and stick representation of β-hematin [223]

A great deal of heme is liberated during the hydrolysis of hemoglobin, some iron is released from this heme and utilized by the parasite [219]. Free heme lyses the parasite [220], the malarial parasite incorporates heme into hemozoin as a detoxification mechanism. Hemozoin consists of complexes of heme proteins, which are not associated with protein. The process of hemozoin formation is described as bio-mineralization in which rapid precipitation of amorphous hematin is followed by crystallization into hemozoin [221]. Its structure appears to be identical to β-hematin [222].

6.4 Diagnostic implication

According to a recent NIH report, blood smears are not conclusive of the malaria diagnosis [64], rather the person's condition and prior activities strongly suggest malaria. Micro-Raman spectroscopy has been suggested as a potential diagnostic marker to investigate changes in the vibrational band with hemozoin formation [223, 224]. Raman spectra show indeed clear differences between *Plasmodium falciparum* infected and uninfected cells in this region, and in the broadening of the peaks near 1210-1230 cm^{-1} (C-H methine deformation band) and 755 cm^{-1} (pyrrole ring breathing mode) [225-227]. As the hemoglobin is broken down by the parasite, the protein chain fragments are transported away for further digestion. The remaining toxic heme is then oxidized to a ferric state. The release of the heme from the protein is the first step in the formation of hemozoin. The changes in the spectra could be the result of this degradation and the changes in the vibrational modes of the now free heme. As the heme rings are no longer bound within the pocket of the protein the constraints on the various bonds will be much more random which accounts for the broadening of the bands [225]. In a comparative analysis, micro-Raman and micro-absorption were combined for healthy RBCs and RBCs invaded with the malaria parasite and it was seen that absorption is more sensitive to parasite invasion that Raman [225].

Both techniques are sensitive to heme degradation occurring during the multiplication cycle of the parasite. Though with micro-Raman the spectral changes associated with ring stage and schizont stage were hard to detect. Clear differences were present only between healthy and the trophozoite stage of the parasite cycle. However, the spectral changes observed in the micro-absorption spectra may enable a diagnostic probe at the single cell level as it showed clear differences among the healthy erythrocyte and various stages of parasite multiplication [228].

After investigating the effect of high pressure and malaria parasite on the cellular level, we move on to molecular level studies by investigating the functional building blocks of cells: proteins. Proteins are dynamic in nature and have several conformations which depend on elevated pressure. In the next chapter, I elucidate the effect of pressure on protein rebinding kinetics in heme proteins. Starting with the simplest heme protein, myoglobin, we conduct flash photolysis experiments at variable temperature and pressure and calculate the activation volume and the escape fraction of the ligand. The results show that the protein rebinding kinetics is a complex process in which the ligand has to overcome more than one barrier to rebind to the protein.

CHAPTER 7. LIGAND BINDING KINETICS TO MYOGLOBIN AT VARIABLE PRESSURE AND TEMPERATURE

The binding kinetics of ligands to heme proteins is a key marker to probe its function in situ, and it has been shown to be very sensitive to conformational changes [97-99, 101, 229]. The protein environment couples with the chromophore thereby inducing vibronic activity in numerous vibrational modes that serve to annihilate distinct vibronic structure [230].The spectral bands of the proteins displays inhomogeneous broadening [231]. The ligand binding kinetics to hemoglobin and myoglobin at ambient pressure has been studied extensively in protein solutions and various solvent environments [96, 98, 99, 232], but kinetic data over extended time range at variable pressure or inside the erythrocyte are scarce. In the following we present results on the pressure dependence of ligand binding to myoglobin, which is similar to one of the four subunits of hemoglobin.

7.1 Pressure effects on Soret absorption of hemoglobin

We investigate whether the ligand binding kinetics and structural relaxation in whole erythrocytes are similar to the one in hemoglobin in a test tube solution. The cooperative binding of ligands to the hemoglobin tetramer is accompanied by a transition of the structure of the protein from the unligated T to the ligand saturated R quaternary configuration [98]. Quaternary

structure changes are observed in the ligand binding kinetics of CO to hemoglobin [100]. The populations of R and T may be determined from the overall ligand recombination kinetics [233]. However, the 'crowded' cellular interior can significantly alter the equilibrium and rates of biochemical reactions relative to those in solution [234].

In initial experiments we measured the change of absorption with pressure in a suspension of red blood cells. The pressure dependence of the Soret absorption band in myoglobin has been reported previously [107, 235]. For the optical absorption experiments the erythrocyte stock solution was diluted with phosphate buffered saline (PBS, pH 7.2) by a factor of 2000. Initial spectra were measured in an optical cell with a sample volume of 20 µl. Two different pressurizing media were used; nitrogen gas and an inert liquid which gave consistent results. With increasing pressure the maximum of the Soret absorption band shifts to longer wavelengths. We attribute this shift to a conformational contribution. Pressure changes the local and the global arrangement of the atoms in the protein. However, the peakshift is about 0.8 nm (45 cm^{-1}) for a pressure difference of 200 MPa indicating that the hemoglobin stays oxygenated [236].

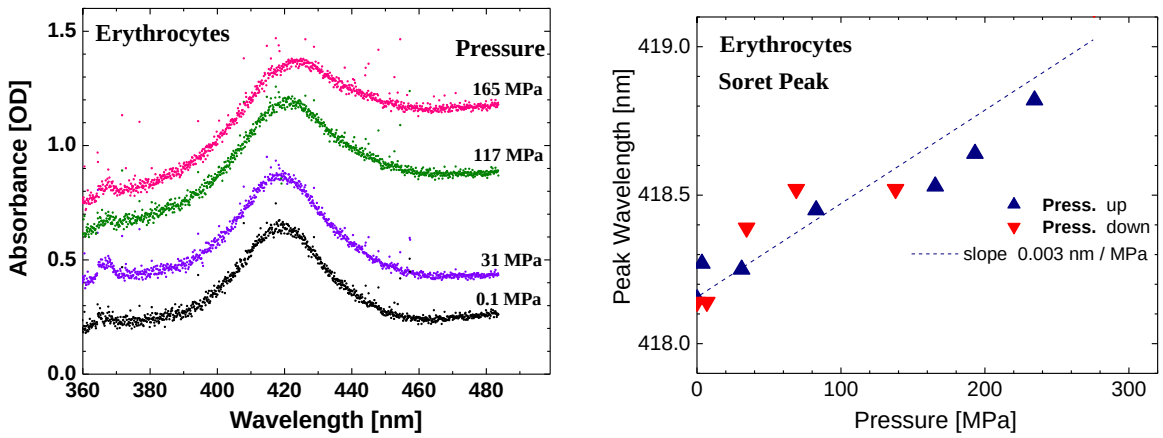

Figure 47 Pressure dependence of the Soret band of hemoglobin in erythrocytes: Absorption spectra (Left), peak position (Right)

A pressure induced red shift of chromophore absorption in proteins has been observed in heme proteins by various groups [107]. Fraunfelder et al measured the Soret band of sperm whale myoglobin in number of solvents and confirmed elastic shift in the conformations between P = 0.1 M Pa and P = 190 M Pa. This can be interpreted as change in substate populations with pressure. The shift was found to be independent of temperature which implies that pressure effects caused by thermal expansions are small. The comparison between high temperature and low temperature data shows that elastic compressibility alone is not enough to explain the shift and conformational rearrangements might occur.

7.2 Pressure effects on ligand binding kinetics

To unravel how pressure alters the individual processes of the complex ligand binding kinetics to heme proteins we have used transient absorption spectroscopy following flash photolysis. A 10 ns pulse from a frequency-doubled (532 nm) Nd:YAG laser is employed to break the bond between the ligand and the iron atom. The change in absorbance of the deligated myoglobin is monitored at 441 nm over more

than eight orders of magnitude in time with the help of a blue light source and a monochromator that is equipped with a photomultiplier tube and digitizing electronics.

Our general protocol was to measure transient absorption changes following a short laser flash over an extended time range at variable temperature and pressure. A pressure of approximately 200 MPa (where denaturation does not yet occur at pH 7) allowed us working at temperatures as low as 250 K without freezing the protein solution. We measured the intensity of transmitted beam through the sample after photolysis over several decades of time. N (t), the fraction of Mb molecules that have not rebound CO at the time t after the flash is determined from the absorption change ΔA. As a plot of log N (t) Vs t will either compress the fast or eliminates the slow part [23] , N (t) is plotted Vs t on log-log scale.

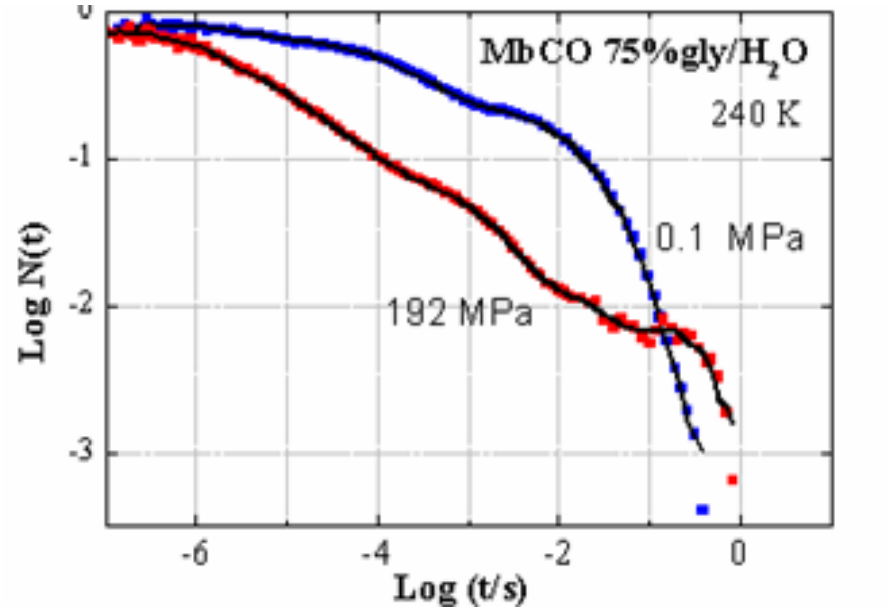

Figure 48 Rebinding of CO to Mb at 240 K and pressure of 0.1 MPa and 192 MPa

Figure 48 displays the rebinding kinetics of CO to horse Mb in 75% gly/water at 240 K at ambient and high pressure. Shown is on a double-logarithmic scale the number of unbound ligands N(t)

as a function of time t following photodissociation. The experimental curves demonstrate that the ligand rebinding to Mb is complex [236]. In their pioneering flash photolysis experiments Austin et al already showed that rebinding of CO to heme proteins contain at least three different processes in the temperature range between 40K and 300K [23]. Our work presents the effect of temperature and pressure on the component processes over wide time range.

The data clearly shows that the properties of ligand binding to the model system myoglobin depend on pressure. Kinetic data over a limited time range (50 ms) by Hasinoff show that for the 'slow' process ligand binding to hemoglobin speeds up with pressure [108]. Overall, rebinding process speeds up with increasing pressure including the previously unexplored intermediate time regime. The amplitude of the geminate process increases with pressure corresponding to a smaller escape fraction of ligands into the solvent and a smaller inner barrier. Therefore a simple extrapolation of the fastest process as proposed by Adachi and Morishima [105] to longer times is inadequate to model the pressure dependence of the binding. The plot shows that the pressure significantly affects the amplitudes and not just the rates of the component processes.

The shape of N (t) curve suggests three component processes. In a log-log plot a power law corresponds to a straight line [131]. The two fastest processes deviate remarkably from exponential curves and are much closer to the power law. The third process resembles an exponential curve.

The non-exponential behavior suggests a distribution of barrier heights. Thus, the rate process may be described with a spectrum of rate coefficients,

$$N(t) = \int d\lambda h(\lambda) e^{-\lambda t} \tag{24}$$

Here, N (t) is the fraction of proteins without a ligand at time t after photo dissociation

t is the time

and λ is the binding rate

$h(\lambda)d\lambda$ is the probability that the process occurs with the rate coefficients between λ and $\lambda+d\lambda$.

The rate distribution can be extracted from the above expression using Inverse Laplace transformation. However, this is an ill-posed mathematical problem. Various techniques have been developed to obtain reasonable distributions $f(\lambda)$ [131]. In our present work, to reveal the complex kinetics and to derive the rate distributions, the derivative approximation was used for numerical inversion.

The derivative approximation is derived as follows:

We set
$$h(\lambda)d\lambda = f(\lambda)d\log\lambda \tag{25}$$

and thus obtain

$$N(t) = \int d\log\lambda\, f(\lambda)e^{-\lambda t} \tag{26}$$

For broad rate distributions that extend smoothly over several decades, there is a simple way of getting a rough idea of $f(\lambda)$ by using the derivative approximation

$$-N(t)\frac{d\log N(t)}{d\log t} = -\frac{dN(t)}{\ln 10\, d\log t} = \int d\log\lambda\, f(\lambda)R(\lambda,T) \tag{27}$$

Where

$$R(\lambda,T) = \lambda t e^{-\lambda t} \tag{28}$$

Thus, we get the rate distribution as:

$$f(\lambda) \approx -N(t)\frac{d\log N(t)}{d\log t} \tag{29}$$

Using the above approximation, the spectrum of rebinding rates is obtained. The rate distribution at ambient pressure shows three peaks corresponding to the three component processes.

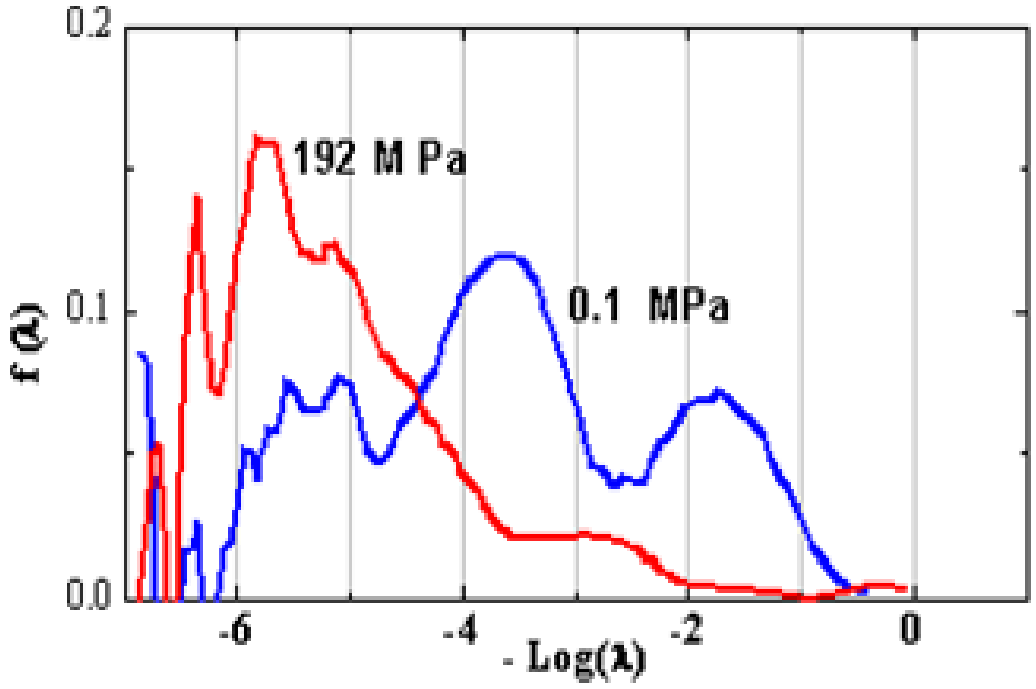

Figure 49 Distribution of rebinding rates of CO to Mb at pressure of 0.1 MPa and 192MPa

As pressure is increased from 0.1 MPa to 192 MPa, the overall kinetics speeds up. The rate distribution peaks shift to the left which further suggests faster rebinding. The results at 0.1 MPa shows three processes in rebinding of ligands to Mb after photo dissociation. Processes I and M are ligand concentration independent and non exponential in nature while the solvent process S depends on the ligand concentration and the protein- solvent interaction. The rates of all these processes are governed by the barriers heights [23, 237]. The peaks at higher pressure are more complex and its hard to deconvolute

them and separate the component processes. The protein ligand binding reaction is a prototype reaction for protein functions. It involves changes along the reaction as well as conformational coordinates [86].

Protein molecules are complex systems that can assume a myriad of conformational states, which vary slightly in their 3-D structures and function with different rates [23]. The energy surface is highly degenerate. They are dynamic systems which fluctuate between its equilibrium conformations in its native state. Thus, the rate coefficients for the processes are not single valued but are characterized by a distribution [131, 238]. As described by some authors, Process I, the non-exponential rebinding at low temperatures suggests a distribution of barrier heights which implies that a protein can be found in various conformational states. This distribution of various confirmation states brings in the concept of energy landscape [85, 86]. It can be assumed that a given primary sequence can fold into a large number of different conformational substates, which are separated by free energy barriers [87]. The existence of substates has already been demonstrated by various experiments [89] and by computer simulations [90, 91]. During this process, Rebinding is governed by thermally activated hopping over the barrier. It is independent of ligand molecule concentration [88].

The understanding of the component processes is important for understanding the dynamics and functions of the protein. Several models have been discussed in the literature [26, 107]. According to Kleinart et al., the following kinetic model is motivated by kinetic and X-ray structural experiments at ambient pressure to reveal component processes.

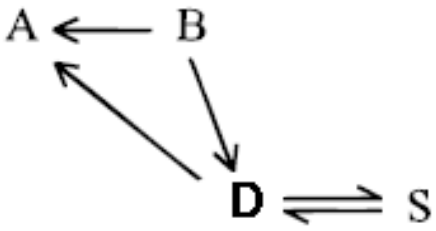

Figure 50 Kinetic Scheme according to ref [26].

The ligand initially occupies state A. During flash photolysis a photon breaks the covalent bond between the iron atom and the ligand molecule and the ligand moves to the state B. At this instant the Mb is said to be in the photolysed state with the ligand still in the heme pocket. Process I, can take place immediately after photo dissociation resulting from the binding of the ligand to Mb from the state B to A. If ligand has enough thermal energy it may also jump the second barrier to the state D. From state D, it rebinds to state A. This constitutes the process M. At higher temperatures and after longer elapsed time, the ligand may jump the third barrier and diffuses to the solvent. All the ligand molecules in the solvent now compete for the vacant site and in process S the rebinding occurs through jumping over the three barriers vis S to D to B to A. In this interpretation, Process I and M are independent of the ligand concentration and process S is proportional to it.

Raman measurements on a pico-second time scale have shown that within picoseconds of photo dissociation the iron moves out of the heme plane [239]. The CO moves to its docking site. X ray structures suggested penetration of water molecules into the CO binding site which further inhibits CO rebinding [119]. During the process M the ligand escapes the heme pocket and explores the protein structure. Its a slower process in which the ligand reaches back its binding site with the help of the protein

relaxations and fluctuations [85, 86], and rebinds to the iron atom. The process has non-exponential time dependence.

7.3 Analysis of pressure dependence of ligand binding kinetics for 180-320K

We first analyze the kinetics in the range close to physiological temperature. Figure 48 depict rebinding of CO to horse Mb in H_2O and 75% gly/H_2O at 124MPa (left) and 190MPa (right) over the temperature range 274K-320K on a double logarithmic scale. Distributions of rebinding rates f(λ) determined with the derivative approximation are shown in the bottom panels.

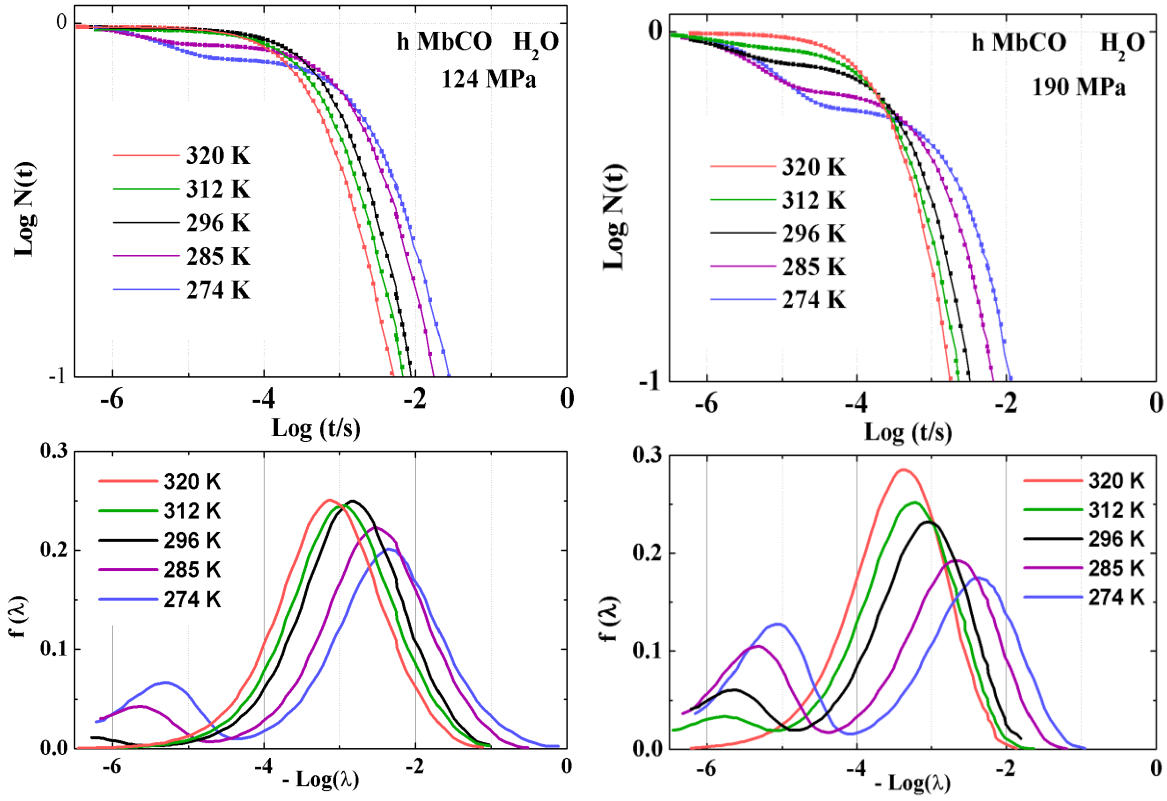

Figure 51 Distribution of rate kinetics for a temperature range from 274K-320K with H_2O as a solvent

The data displayed in Figure 51 shows the rebinding kinetics of CO to horse myoglobin with water as a solvent. The shape of log N (t) Vs log t does not depend on the rate. The rate determines the position along the λ axis. The graph indicates that at higher temperatures the rebinding is dominated by solvent process S. At higher temperatures a larger number of ligand are able to escape to the solvent due to higher thermal energy [107] causing higher amplitudes of solvent process at higher temperatures. As, the temperature is decreased the internal process becomes visible and the amplitude of geminate process further increases as the temperature goes down.

The rates as well as amplitudes of the component processes are affected by altering the pressure as shown in Figure 48. Its apparent that kinetic peaks are smoother and well defined at lower pressure. As pressure increases the protein solvent interface becomes rigid and the ligand can not escape to the solvent. The altered solvent dynamics may introduce conformational changes in the heme environment and thus affects binding kinetics [26]. With increase in pressure, the heme assumes a more planar form, thus lowering the barrier for rebinding and increasing the rebinding rate [102]. The amplitude of Process I increases with pressure corresponding to smaller escape fraction of ligands into the solvent and a smaller inner barrier height. It was noted that the amplitude of slow reaction was more affected by pressure than fast reaction.

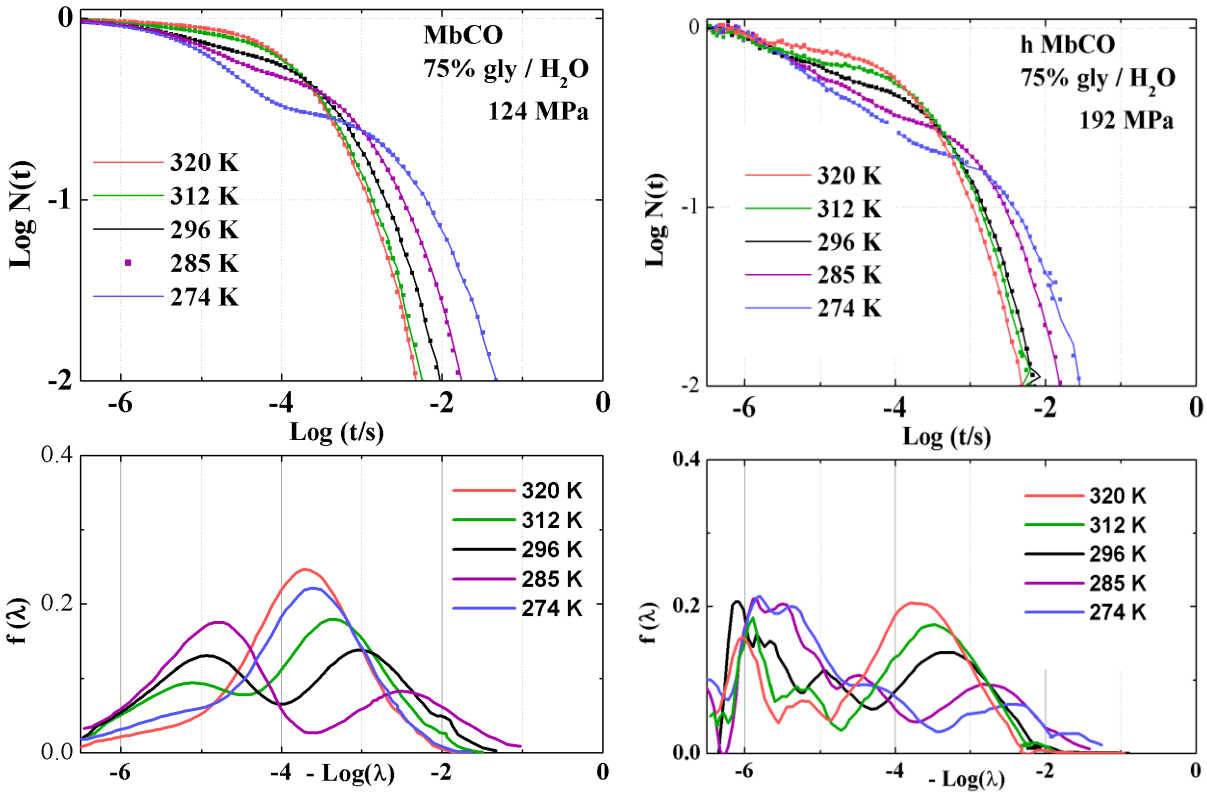

Figure 52 Distribution of rate kinetics for a temperature range from 274K-320K with 75% gly/H_2O as a solvent

The graph in Figure 52 displays rebinding of CO to horse myoglobin with 75% glycerol/water as a solvent. The effect of solvent on rebinding kinetics is apparent. When water is used as a solvent, the peaks are smoother and well defined suggesting the significance of viscosity and protein solvent interaction [25, 26]. The amplitude of the solvent process S is less when glycerol/water is used as a solvent. Beece suggested that the solvent composition mainly affect the rate as well as the amplitude of the slower process S in which the Mb has lost its ligand to the solvent [26]. The amplitude and rate of the process S decreases with the increase in viscosity. The effect on process I is too small to be viscosity related and reflects structural adjustments in response to the solvent [26]. The viscosity also affects the

structural relaxation of the protein affecting the rates for the process M. The escape rates also decrease with the increase in the viscosity resulting in faster rebinding.

7.4 Gibbs free energy and Activation Volume using a Three well model

The experimental data shows at least three component processes. To connect these macroscopic rates with the microscopic steps of the binding reaction we employ a simplified model consisting of three sequential wells (Figure 53). In the three well model, the relaxation is neglected [145]. It gives us the advantage that it can be solved analytically and provides volume changes for microscopic rates. On its path from the solvent to the binding at the heme atom the ligand has to overcome at least three barriers [23]. Since at high temperature ligand has enough thermal energy that it stays in the intermediate state for negligible amount of time, a three well model is a good approximation and the rate equations can be solved analytically. From the kinetic data we have determined the distribution of rebinding rates. Distributions yield average rates, which yield enthalpies as a function of temperature and pressure from an Arrhenius plot and a volume profile of the reaction.

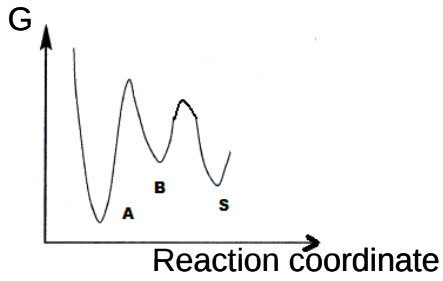

Figure 53 Three-well model

The kinetic scheme of the 3-Well model can be described by the following equation.

$$A \xleftarrow{k_{BA}} B \underset{k_{SB}}{\overset{k_{BS}}{\rightleftharpoons}} S \tag{30}$$

where thermal dissociation rate $k_{AB} \approx 0$

Here A is the protein state with ligand covalently bound to the iron, B is the state with ligand in the heme pocket and S with the ligand escaped to the solvent. After photo dissociation the protein is in state B. From B depending on the inner and outer kinetic barrier height which is different for CO and same for O_2 [237] ligand can either bind to the iron or escape to the solvent. Three well sequential model can be solved analytically and gives an insight into the relation between the measured λ and the microscopics rates k.

Assuming that flash photolysis experiment yields

$$N(t) = 1 - N_A(t) = N_B(t) + N_S(t) \tag{31}$$

and the thermal dissociation rate to be negligible allows us to eliminate the third eigen value.

Solving the set of differential equation $\dot{N}(t) = kN(t)$ (32)

where $N(t) = \begin{pmatrix} N_A \\ N_B \\ N_S \end{pmatrix}$ and $k = \begin{pmatrix} 0 & k_{BA} & 0 \\ 0 & -k_{BA} - k_{BS} & k_{SB} \\ 0 & k_{BS} & -k_{SB} \end{pmatrix}$ (33)

we get

$$N_1 = \frac{k_{BA}}{k_{BA} + k_{BS}} \tag{34}$$

$$N_S = \frac{k_{BS}}{k_{BA} + k_{BS}} \tag{35}$$

$$\lambda_1 = k_{BA} + k_{BS} \tag{36}$$

$$\lambda_S = \frac{k_{BA}k_{SB}}{k_{BA} + k_{BS}} \tag{37}$$

The above set of equations can be solved to extract the microscopic rate constants as:

$$k_{BA} = \lambda_1 N_1 \tag{38}$$

$$k_{BS} = \lambda_1 N_S \tag{39}$$

$$k_{SB} = \lambda_S \frac{N_1 + N_S}{N_1} \tag{40}$$

The fit to the experimental data allows us to determine the recombination rate coefficients λ_1, λ_S which are the eigen values of the transition rate matrix; N_1 and N_S. Using these values, we determine the microscopic rate constants k_{BA}, k_{BS} and k_{SB} of rebinding kinetics.

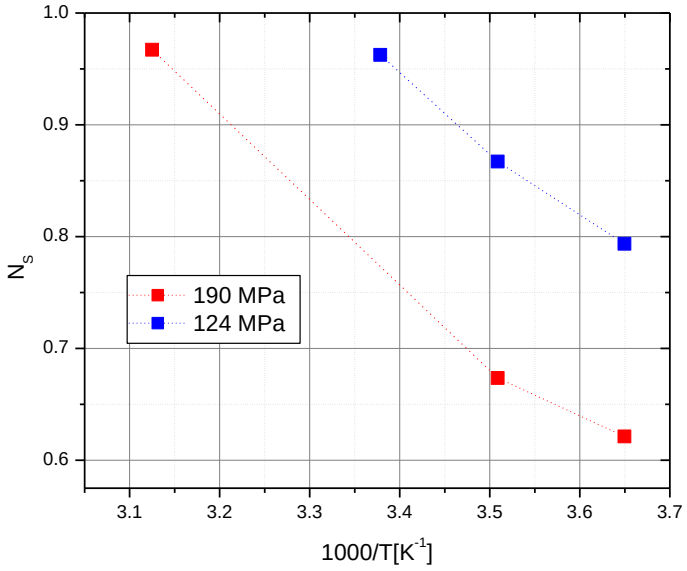

Figure 54 Escape Fraction versus 1000/T at 124 MPa and 190 MPa

Figure 54 displays the number N_S of ligands escaping to the solvent versus 1000/T. With increasing pressure a smaller fraction of ligands escapes to the solvent. The significant decrease of ligand escape may be attributed to the slowing down of solvent relaxation with pressure.

Figure 55 shows the dependence of the rate constant with inverse of temperature for the range 274K-320K with pressure as a fixed parameter. The peak positions of the microscopic rebinding rates are plotted versus inverse of temperature using the data in figure.51.

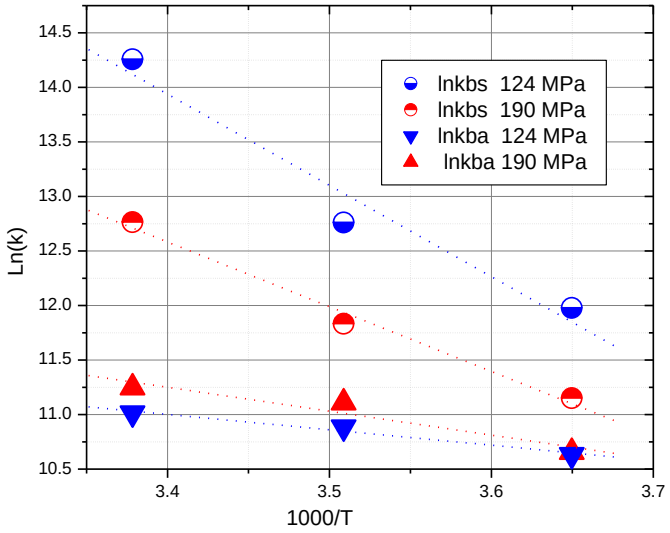

Figure 55 Rate constant versus 1000/T with Pressure as fixed parameter

As the temperature increases more number of ligands escape to the solvent due to higher thermal energy and simultaneously rebinding rate from solvent increases.

To determine enthalpy and volume chnages, it was assumed that all rates obey Arrhenius equation. Taking ***G"*** and ν to be temperature independent [23], the ratio of transition rates between B to A and B to

D becomes lower at higher temperatures, suggesting that at low temperatures rebinding occurs directly from B while at higher temperatures, ligand explores the well D before rebinding.

Taking the ln on both sides of the arrhenius equation, we get:

$$\ln k = \ln \upsilon - \left(\frac{G''}{R}\right)\frac{1}{T} \tag{41}$$

Thus plotting the curve between Ln k and inverse of temperature the frequency factor and the activation energy deduced using the straight line fit are given in the table below.

Table 2 Activation energies as calculated from Arrhenius equation

Pressure	**ln υ_I**	**Log υ_I**	**G_I'' (KJ/mol)**	**ln υ_S**	**Log υ_S**	**G_S'' (KJ/mol)**
124 MPa	**15.8**	**6.9**	**11.7**	**42.4**	**18.4**	**69.6**
190MPa	**18.7**	**8.1**	**18.2**	**32.7**	**14.2**	**49.4**

As suggested by the model, at higher temperatures more number of ligands escapes the protein and diffuses into the solvent [240]. The rebinding then occur from the solvent and thus its a slower process.

The activation volume is calculated using transition state theory. The pressure dependence of the rate coefficient is given by

$$k(P) = k(P_0) * e^{-PV/RT} \tag{42}$$

and the activation volume can be calculated as the ratio of ***k(P)/k(P')***

Thus we get

$$\frac{\partial \ln k}{\partial P} = \frac{-V''}{RT} \tag{43}$$

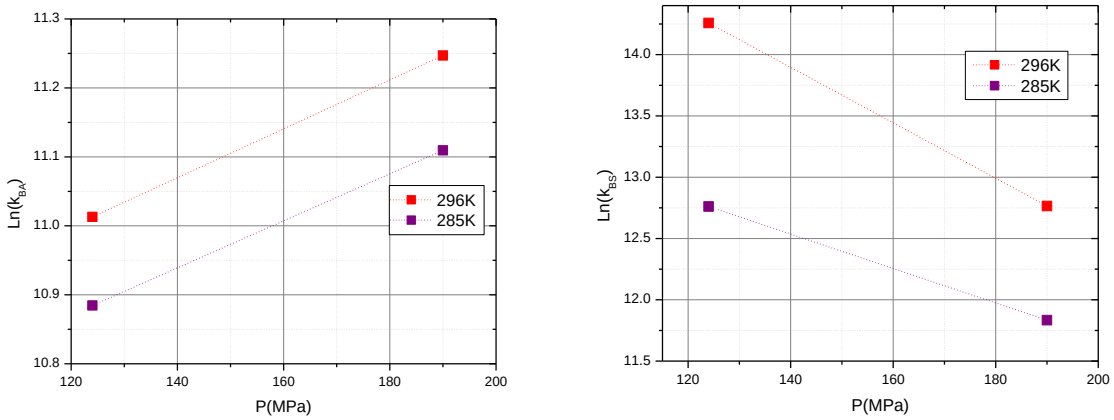

Figure 56 Kinetics rate coefficient versus pressure for a temperature range from 285K-296K

Using the above plotted graphs we can derive the activation volumes using the respective microscopic rates. The calculated values of activation volumes are tabulated below:

Table 3 Activation volumes associated with rebinding kinetics

Temp	**285 K**	**296 K**
V_{BA} (ml/mol)	**-8.1**	**-8.7**
V_{BS} (ml/mol)	**33.3**	**55.7**

As k_{BS} decreases with increase in pressure, the activation volume V_{BS} is positive. The effect of pressure on the reaction rate is measured by the activation volume V_{BA}, the volume difference between initial and the transition state. A molecular interpretation of kinetic and thermodynamic data is usually based on data from low molecular weight model systems [7, 110, 241]. This is done in terms of intrinsic

volume and solvent effects. For proteins and other biopolymers the conformational arrangement of the atoms has to be taken into account. The partial molar volume V_i of a protein in solution is considered as being composed of three contributions: the atoms, the cavities and the hydration. $V_i = V_{atoms} + V_{cavities} + \Delta V_{hydration}$. These can be due to residues participating in hydrogen bonding and increased or decreased binding of water [242].

The absolute value of the activation volume V_{BA} for the geminate barrier obtained is comparable with values for covalent bond formation or breaking. The values obtained are very small compared to the total molar volume of myoglobin ($V_{Mb} = 3.2 \times 10^4$ Å^3, $V_{mol,Mb} = 19.2 l / mol$). Literature suggests that a small decrease in volume may occur when the Fe atom becomes planar on bond formation [108]. The pioneering work of Kauzmann pointed out that the partial molal volume of a protein in solution is determined by constitutive volume, conformational volume and salvation volume [243]. The activation volume for ligand-rebinding reaction may be affected by changes in these above mentioned volumes along with bond making and breaking process [108]. Our data clearly show that the properties of ligand binding to Mb depend on pressure. The effect of pressure on the binding CO to Mb after photo-dissociation points to the strong influence of conformational substates on protein reactions. Pressure controls the rate of rebinding through the activation volume and through redistribution of substate populations.

CHAPTER 8. CONCLUSIONS AND OUTLOOK

The research in this dissertation has provided new results on volume changes in single red blood cells and change of hemoglobin absorption in cells affected by malaria parasite. First, a new method for confocal absorption at single cell level is introduced. Single cell absorption spectroscopy reveals that the intra-erythrocytic parasite growth and resultant heme degradation can be correlated to change in the electronic spectra of the red blood cell. Second, pressure induced volume changes and compressibility of the healthy and malaria infected red blood cell is measured and the results show that the elastic properties are affected by infection. In addition, the pressure dependence of ligand binding to the model protein myoglobin was investigated. The pressure dependence of ligand binding kinetics over eight orders of magnitude in time is measured and the volume changes, using a simple three well model, are determined.

8.1 Summary

A novel approach to confocal absorption microscopy (CAM) by combining confocal detection and broadband illumination in a transmission geometry is demonstrated. The attenuation of the light beam in the axial direction due to absorption provides a mechanism for contrast. The method has been used to study cells in their native environment and other biological assemblies. This is illustrated through

confocal absorption measurements of single live erythrocytes and of nanoliter solutions in micro-capillaries.

The technique is used to investigate the effect of malaria parasite on the host red blood cell. Understanding the structural changes in the degradation of hemoglobin may open new targets for anti-malarial drug treatments. Observing the cells in a native-like environment facilitates the transfer of new diagnostics for faster detection of the parasite's presence in the human body. The technique is sensitive to heme degradation occurring during the multiplication cycle of the parasite. The spectral changes observed in the micro-absorption spectra may enable a diagnostic probe at the single cell level. This may lead to methods for detecting the parasite before it is even visible to the laboratory technician under stain leading to almost instantaneous detection of infections.

The use of micro-capillary high pressure chamber was extended to investigate the volume and morphological changes in red blood cells with pressure. The results show that the cells are soft bodies elastic medium and can undergo large reversible changes when under external stress. Parasite invasion and multiplication showed remarkable effect on the membrane permeability and deformability of the host red blood cell. The stiffness of the red blood cell was found to increase with the parasite invasion. The approach developed here has application beyond the erythrocyte parasite system. It can be applied to study a wide range of live cellular systems under varying pressures.

The last part of the research in this dissertation leads to a deeper understanding of pressure effects in proteins and how their conformational dynamics determines biological function. In the interpretation of the results, structural and dynamic data is combined with

models of protein reactions and results from molecular dynamics. The associated volume changes is determined and related to possible mechanisms such as hydrophobic interaction, free volume, and solvation effects.

8.2 Future work

The research presented in this dissertation opens up new avenues to study. In this section we briefly describe further investigations that can be implemented based on the methods and results of the dissertation.

Expanding Confocal Absorption Microscopy, variations in composition of inhomogeneous samples (e. g. thin films) may be determined from spatially resolved absorption spectra. The method presented can be extended to the ultraviolet and infrared regions of the spectrum. Potential applications are in micro-fluidics and nano-materials characterization. The number of molecules in the beam (currently 10^7) may be reduced (preliminary experiments conducted shows 10^3) and thus sensitivity of the technique may be increased towards single molecule detection. The micro-absorption spectroscopy technique may be used to study pressure and temperature dependence of ligand binding kinetics inside a living cell.

To elucidate the effect of phospholipid composition on pathogenesis with malaria parasite, model membranes which mimic the lipid composition of healthy and infected red blood cells can be assembled into vesicles and their deformability with high pressure be investigated.

LIST OF REFERENCES

[1] E. Schrödinger, *What is life?*: Cambridge University Press, 1944.

[2] H. Frauenfelder, P. G. Wolynes, and R. H. Austin, "Biological physics," *Reviews of Modern Physics*, vol. 71, pp. 419-430, 1999.

[3] D. A. Fletcher and R. D. Mullins, "Cell mechanics and the cytoskeleton," *Nature*, vol. 463, pp. 485-492.

[4] A. P. Minton, "How can biochemical reactions within cells differ from those in test tubes?," *Journal of cell science*, vol. 119, p. 2863, 2006.

[5] M. B. Jackson, *Molecular and cellular biophysics*: Cambridge Univ Pr, 2006.

[6] K. Akasaka, "Highly fluctuating protein structures revealed by variable-pressure nuclear magnetic resonance," *Biochemistry*, vol. 42, pp. 10875-10885, 2003.

[7] C. Balny, P. Masson, and K. Heremans, "High pressure effects on biological macromolecules: from structural changes to alteration of cellular processes," *Biochimica et Biophysica Acta (BBA) - Protein Structure and Molecular Enzymology*, vol. 1595, pp. 3-10, 2002.

[8] R. Winter and J. Jonas, *High pressure chemistry, biochemistry, and materials science*: Kluwer Academic, Dordrecht, 1993.

[9] T. G. Spiro and X. Y. Li, *Biological applications of Raman spectroscopy*: Wiley New York, 1988.

[10] A. Fersht and G. Winter, "Protein engineering," *Trends in Biochemical Sciences*, vol. 17, pp. 292-294, 1992.

[11] J. R. Lakowicz, "Principles of Fluorescence spectroscopy. 1999," *Kluwer Academic/Plenum Publisher, New York, Kap*, vol. 9.

[12] A. M. Armani, R. P. Kulkarni, S. E. Fraser, R. C. Flagan, and K. J. Vahala, "Label-free, single-molecule detection with optical microcavities," *science*, vol. 317, p. 783, 2007.

[13] R. P. Kulkarni, K. Castelino, A. Majumdar, and S. E. Fraser, "Intracellular Transport Dynamics of Endosomes Containing DNA Polyplexes along the Microtubule Network," *Biophysical journal*, vol. 90, pp. L42-L44, 2006.

[14] B. D. Moore, L. Stevenson, A. Watt, S. Flitsch, N. J. Turner, C. Cassidy, and D. Graham, "Rapid and ultra-sensitive determination of enzyme activities using surface-enhanced resonance Raman scattering," *Nat Biotech*, vol. 22, pp. 1133-1138, 2004.

[15] J. R. Lakowicz, *Principles of fluorescence spectroscopy*, Third ed.: Springer, 2006.

[16] S. Arora, J. Mauser, D. Chakrabarti, and A. Schulte, "Spatially resolved micro-absorption spectroscopy with a broadband source and confocal detection," 2011 submitted.

[17] H. Frauenfelder, *The Physics of Proteins*: Springer, 2010.

[18] G. Weber and H. G. Drickamer, "The effect of high pressure upon proteins and other biomolecules," *Quarterly Reviews of Biophysics*, vol. 16, pp. 89-112, 1983.

[19] D. H. Bartlett, "Pressure effects on in vivo microbial processes," *Biochimica et Biophysica Acta (BBA)-Protein Structure and Molecular Enzymology*, vol. 1595, pp. 367-381, 2002.
[20] N. Borghi and F. Brochard-Wyart, "Tether extrusion from red blood cells: integral proteins unbinding from cytoskeleton," *Biophysical journal*, vol. 93, pp. 1369-1379, 2007.
[21] J. Mauritz, A. Esposito, T. Tiffert, J. N. Skepper, A. Warley, Y. Z. Yoon, P. Cicuta, V. L. Lew, J. R. Guck, and C. F. Kaminski, "Biophotonic techniques for the study of malaria-infected red blood cells," *Medical & biological engineering & computing*, vol. 48, pp. 1055-1063.
[22] B. Alberts, "The cell as a collection overview of protein machines: Preparing the next generation of molecular biologists," *Cell*, vol. 92, pp. 291-294, 1998.
[23] R. H. Austin, K. W. Beeson, L. Eisenstein, H. Frauenfelder, and I. C. Gunsalus, "Dynamics of ligand binding to myoglobin," *Biochemistry*, vol. 14, pp. 5355-5373, 1975.
[24] M. Sassaroli, S. Dasgupta, and D. L. Rousseau, "Cryogenic stabilization of myoglobin photoproducts," *Journal of Biological Chemistry*, vol. 261, p. 13704, 1986.
[25] D. Beece, L. Eisenstein, H. Frauenfelder, D. Good, M. C. Marden, L. Reinisch, A. H. Reynolds, L. B. Sorensen, and K. T. Yue, "Solvent viscosity and protein dynamics," *Biochemistry*, vol. 19, pp. 5147-5157, 1980.
[26] T. Kleinert, W. Doster, H. Leyser, W. Petry, V. Schwarz, and M. Settless, "Solvent Composition and Viscosity Effects on the Kinetics of CO Binding to Horse Myoglobin†," *Biochemistry*, vol. 37, pp. 717-733, 1998.
[27] B. Alberts, D. Bray, A. Johnson, J. Lewis, M. Raff, K. Roberts, P. Walter, and A. M. Campbell, *Essential cell biology*: Garland Science New York, 2004.
[28] X. An, M. C. Lecomte, J. A. Chasis, N. Mohandas, and W. Gratzer, "Shear-response of the spectrin dimer-tetramer equilibrium in the red blood cell membrane," *Journal of Biological Chemistry*, vol. 277, p. 31796, 2002.
[29] P. Nelson, M. Radosavljevic, and S. Bromberg, *Biological physics*: WH Freeman and Co., 2004.
[30] J. B. Wittenberg and B. A. Wittenberg, "Mechanisms of cytoplasmic hemoglobin and myoglobin function," *Annual review of biophysics and biophysical chemistry*, vol. 19, pp. 217-241, 1990.
[31] M. F. Perutz, "Nature of haem-haem interaction," *Nature*, vol. 237, pp. 495-499, 1972.
[32] D. Halle and S. Yedgar, "Mild pressure induces resistance of erythrocytes to hemolysis by snake venom phospholipase A2," *Biophysical journal*, vol. 54, pp. 393-396, 1988.
[33] K. Haldar, B. U. Samuel, N. Mohandas, T. Harrison, and N. L. Hiller, "Transport mechanisms in Plasmodium-infected erythrocytes: lipid rafts and a tubovesicular network," *International journal for parasitology*, vol. 31, pp. 1393-1401, 2001.
[34] V. L. Lew, T. Tiffert, and H. Ginsburg, "Excess hemoglobin digestion and the osmotic stability ofPlasmodium falciparum–infected red blood cells," *Blood*, vol. 101, p. 4189, 2003.
[35] Y. Yawata, *Cell membrane: the red blood cell as a model*: Vch Verlagsgesellschaft Mbh, 2003.
[36] N. Mohandas and E. Evans, "Mechanical properties of the red cell membrane in relation to molecular structure and genetic defects," *Annual review of biophysics and biomolecular structure*, vol. 23, pp. 787-818, 1994.
[37] S. Chien, "Red cell deformability and its relevance to blood flow," *Annual review of physiology*, vol. 49, pp. 177-192, 1987.
[38] G. Barshtein, L. Bergelson, A. Dagan, E. Gratton, and S. Yedgar, "Membrane lipid order of human red blood cells is altered by physiological levels of hydrostatic pressure," *American Journal of Physiology-Heart and Circulatory Physiology*, vol. 272, p. H538, 1997.

[39] J. F. Hoffman and S. Inoué, "Directly observed reversible shape changes and hemoglobin stratification during centrifugation of human and Amphiuma red blood cells," *Proceedings of the National Academy of Sciences of the United States of America,* vol. 103, p. 2971, 2006.
[40] M. M. Gedde, E. Yang, and W. H. Huestis, "Shape response of human erythrocytes to altered cell pH," *Blood,* vol. 86, p. 1595, 1995.
[41] M. M. Gedde and W. H. Huestis, "Membrane potential and human erythrocyte shape," *Biophysical journal,* vol. 72, pp. 1220-1233, 1997.
[42] R. Glaser, "The shape of red blood cells as a function of membrane potential and temperature," *Journal of Membrane Biology,* vol. 51, pp. 217-228, 1979.
[43] M. M. Gedde, D. K. Davis, and W. H. Huestis, "Cytoplasmic pH and human erythrocyte shape," *Biophysical journal,* vol. 72, pp. 1234-1246, 1997.
[44] J. Li, G. Lykotrafitis, M. Dao, and S. Suresh, "Cytoskeletal dynamics of human erythrocyte," *Proceedings of the National Academy of Sciences,* vol. 104, p. 4937, 2007.
[45] C. Ceylan, M. Severcan, F. Bozoglu, and F. Severcan, "Evaluation of high hydrostatic pressure effects on bovine red blood cells and platelets," *High Pressure Research,* vol. 29, pp. 358-368, 2009.
[46] E. M. Bevers, P. Comfurius, D. W. C. Dekkers, and R. F. A. Zwaal, "Lipid translocation across the plasma membrane of mammalian cells," *Biochimica et Biophysica Acta (BBA)-Molecular and Cell Biology of Lipids,* vol. 1439, pp. 317-330, 1999.
[47] D. Dolis, C. Moreau, A. Zachowski, and P. F. Devaux, "Aminophospholipid translocase and proteins involved in transmembrane phospholipid traffic," *Biophysical chemistry,* vol. 68, pp. 221-231, 1997.
[48] D. J. Hanahan, *A guide to phospholipid chemistry*: Oxford University Press, USA, 1997.
[49] T. L. Steck, "The organization of proteins in the human red blood cell membrane," *The Journal of Cell Biology,* vol. 62, p. 1, 1974.
[50] V. Bennett, "The membrane skeleton of human erythrocytes and its implications for more complex cells," *Annual review of biochemistry,* vol. 54, pp. 273-304, 1985.
[51] H. Engelhardt and E. Sackmann, "On the measurement of shear elastic moduli and viscosities of erythrocyte plasma membranes by transient deformation in high frequency electric fields," *Biophysical journal,* vol. 54, pp. 495-508, 1988.
[52] S. Svetina and B. Žekš, "Membrane bending energy and shape determination of phospholipid vesicles and red blood cells," *European Biophysics Journal,* vol. 17, pp. 101-111, 1989.
[53] E. Ponder and W. G. Millar, "The measurement of the diameters of erythrocytes. I. The mean diameter of the red cells in man," *Experimental Physiology,* vol. 14, pp. 67-82, April 1, 1924 1924.
[54] P. Teitel, "Basic principles of the" filterability test"(FT) and analysis of erythrocyte flow behavior," *Blood cells,* vol. 3, pp. 55-70, 1977.
[55] P. J. Bronkhorst, G. J. Streekstra, J. Grimbergen, E. J. Nijhof, J. J. Sixma, and G. J. Brakenhoff, "A new method to study shape recovery of red blood cells using multiple optical trapping," *Biophysical journal,* vol. 69, pp. 1666-1673, 1995.
[56] E. A. Evans, "New membrane concept applied to the analysis of fluid shear-and micropipette-deformed red blood cells," *Biophysical journal,* vol. 13, pp. 941-954, 1973.
[57] E. A. Evans, "Bending elastic modulus of red blood cell membrane derived from buckling instability in micropipet aspiration tests," *Biophysical journal,* vol. 43, pp. 27-30, 1983.

[58] E. A. Evans, "Structure and deformation properties of red blood cells: Concepts and quantitative methods," *Methods in enzymology*, vol. 173, pp. 3-35, 1989.
[59] O. Linderkamp and H. J. Meiselman, "Geometric, osmotic, and membrane mechanical properties of density-separated human red cells," *Blood*, vol. 59, p. 1121, 1982.
[60] E. Ponder and W. G. Millar, "The measurement of the diameters of erythrocytes. II. The effect of drying on the diameter of the red cells in man," *Experimental Physiology*, vol. 14, pp. 319-326, 1924.
[61] S. Arora, S. Hoon Park, J. Mauser, D. Chakrabarti, and A. Schulte, "Volume and Morphological Changes in Red Blood Cells with Pressure Probed by Optical Imaging In-Situ," *Biophysical journal*, vol. 100, p. 143.
[62] S. Rao, S. Bálint, B. Cossins, V. Guallar, and D. Petrov, "Raman study of mechanically induced oxygenation state transition of red blood cells using optical tweezers," *Biophysical journal*, vol. 96, pp. 209-216, 2009.
[63] "US Department of Health and Human Services National Institutes of Health National Institute of Allergy and Infectious Diseases NIH Publication No. 02-139," 2002.
[64] "US Department of Health and Human Services National Institutes of Health National Institute of Allergy and Infectious Diseases NIH Publication No. 07-139," 2007.
[65] M. Aregawi, R. Cibulskis, M. Otten, R. Williams, and C. Dye, "World Malaria Report," 2008.
[66] I. W. Sherman, *Molecular approaches to malaria*: Amer Society for Microbiology, 2005.
[67] C. Doerig, J. Endicott, and D. Chakrabarti, "Cyclin-dependent kinase homologues of Plasmodium falciparum," *International journal for parasitology*, vol. 32, pp. 1575-1585, 2002.
[68] C. Doerig, D. Chakrabarti, B. Kappes, and K. Matthews, "The cell cycle in protozoan parasites," *Progress in cell cycle research*, vol. 4, pp. 163-184, 1998.
[69] Y. K. Park, M. Diez-Silva, G. Popescu, G. Lykotrafitis, W. Choi, M. S. Feld, and S. Suresh, "Refractive index maps and membrane dynamics of human red blood cells parasitized by Plasmodium falciparum," *Proceedings of the National Academy of Sciences*, vol. 105, p. 13730, 2008.
[70] S. Suresh, "Mechanical response of human red blood cells in health and disease: some structure-property-function relationships," *J. Mater. Res*, vol. 21, pp. 1871-1877, 2006.
[71] C. T. Lim, J. C. H. Goh, F. Demeke, and V. K. Katiyar, "Analysis of Mechanical Behavior of Red Blood Cell Membrane in Pathological Condition," in *6th World Congress of Biomechanics (WCB 2010). August 1-6, 2010 Singapore*. vol. 31, R. Magjarevic, Ed.: Springer Berlin Heidelberg, pp. 1114-1116.
[72] Qiagen, "Structure of Plasmodium Merozoite," 2003.
[73] I. W. Sherman, "Biochemistry of Plasmodium (malarial parasites)," *Microbiology and Molecular Biology Reviews*, vol. 43, p. 453, 1979.
[74] D. A. Warrell, *Oxford textbook of medicine* vol. 2: Oxford University Press, 2003.
[75] L. H. Miller, S. J. Mason, J. A. Dvorak, M. H. McGinniss, and I. K. Rothman, "Erythrocyte receptors for (Plasmodium knowlesi) malaria: Duffy blood group determinants," *science*, vol. 189, p. 561, 1975.
[76] M. Aikawa, L. H. Miller, J. Johnson, and J. Rabbege, "Erythrocyte entry by malarial parasites. A moving junction between erythrocyte and parasite," *The Journal of Cell Biology*, vol. 77, p. 72, 1978.

[77] K. W. Deitsch and T. E. Wellems, "Membrane modifications in erythrocytes parasitized by Plasmodium falciparum," *Molecular and biochemical parasitology,* vol. 76, pp. 1-10, 1996.
[78] M. Lanzer, H. Wickert, G. Krohne, L. Vincensini, and C. Braun Breton, "Maurer's clefts: a novel multi-functional organelle in the cytoplasm of Plasmodium falciparum-infected erythrocytes," *International journal for parasitology,* vol. 36, pp. 23-36, 2006.
[79] C. Spycher, M. Rug, N. Klonis, D. J. P. Ferguson, A. F. Cowman, H. P. Beck, and L. Tilley, "Genesis of and trafficking to the Maurer's clefts of Plasmodium falciparum-infected erythrocytes," *Molecular and cellular biology,* vol. 26, p. 4074, 2006.
[80] H. Wickert, W. Göttler, G. Krohne, and M. Lanzer, "Maurer's cleft organization in the cytoplasm of Plasmodium falciparum-infected erythrocytes: new insights from three-dimensional reconstruction of serial ultrathin sections," *European journal of cell biology,* vol. 83, pp. 567-582, 2004.
[81] B. R. Wood, S. J. Langford, B. M. Cooke, F. K. Glenister, J. Lim, and D. McNaughton, "Raman imaging of hemozoin within the food vacuole of Plasmodium falciparum trophozoites," *FEBS letters,* vol. 554, pp. 247-252, 2003.
[82] D. J. Sullivan, I. Y. Gluzman, and D. E. Goldberg, "Plasmodium hemozoin formation mediated by histidine-rich proteins," *science,* vol. 271, p. 219, 1996.
[83] A. U. Orjih and C. D. Fitch, "Hemozoin production by Plasmodium falciparum: variation with strain and exposure to chloroquine," *Biochimica et Biophysica Acta (BBA)-General Subjects,* vol. 1157, pp. 270-274, 1993.
[84] L. Stryer, *Biochemistry*: W.H.Freeman&Company, 1995.
[85] H. Frauenfelder, B. H. McMahon, R. H. Austin, K. Chu, and J. T. Groves, "The role of structure, energy landscape, dynamics, and allostery in the enzymatic function of myoglobin," *Proceedings of the National Academy of Sciences of the United States of America,* vol. 98, p. 2370, 2001.
[86] H. Frauenfelder and B. H. McMahon, "Relaxations and fluctuations in myoglobin," *Biosystems,* vol. 62, pp. 3-8, 2001.
[87] G. Ulrich Nienhaus, J. D. Müller, B. H. McMahon, and H. Frauenfelder, "Exploring the conformational energy landscape of proteins," *Physica D: Nonlinear Phenomena,* vol. 107, pp. 297-311, 1997.
[88] B. H. McMahon, B. P. Stojkovi, P. J. Hay, R. L. Martin, and A. E. García, "Microscopic model of carbon monoxide binding to myoglobin," *The Journal of Chemical Physics,* vol. 113, 2000.
[89] H. Frauenfelder, F. Parak, and R. D. Young, "Conformational substates in proteins," *Annual review of biophysics and biophysical chemistry,* vol. 17, pp. 451-479, 1988.
[90] D. Sherrington, "Landscape paradigms in physics and biology: Introduction and overview," *Physica D: Nonlinear Phenomena,* vol. 107, pp. 117-121, 1997.
[91] D. R. Nutt and M. Meuwly, "Theoretical investigation of infrared spectra and pocket dynamics of photodissociated carbonmonoxy myoglobin," *Biophysical journal,* vol. 85, pp. 3612-3623, 2003.
[92] E. Antonini and M. Brunori, *Hemoglobin and Myoglobin in their Reactions with Ligands*: North-Holland Pub. Co., 1971.
[93] R. E. Dickerson and I. Geis, "Hemoglobin: structure, function, evolution, and pathology," 1983.
[94] J. Kuriyan, S. Wilz, M. Karplus, and G. A. Petsko, "X-ray structure and refinement of carbon-monoxy (Fe II)-myoglobin at 1.5 Å resolution," *Journal of molecular biology,* vol. 192, pp. 133-154, 1986.

[95] I. Schlichting, J. Berendzen, G. N. Phillips, and R. M. Sweet, "Crystal structure of photolysed carbonmonoxy-myoglobin," 1994.
[96] E. R. Henry, C. M. Jones, J. Hofrichter, and W. A. Eaton, "Can a two-state MWC allosteric model explain hemoglobin kinetics?," *Biochemistry,* vol. 36, pp. 6511-6528, 1997.
[97] Q. H. Gibson, "The photochemical formation of a quickly reacting form of haemoglobin," *Biochemical Journal,* vol. 71, p. 293, 1959.
[98] W. A. Eaton, E. R. Henry, J. Hofrichter, and A. Mozzarelli, "Is cooperative oxygen binding by hemoglobin really understood?," *Nature Structural Biology,* vol. 6, p. 351, 1999.
[99] W. G. Cobau, J. D. LeGrange, and R. H. Austin, "Kinetic differences at low temperatures between R and T state carbon monoxide-carp hemoglobin," *Biophysical journal,* vol. 47, pp. 781-786, 1985.
[100] J. Hofrichter, J. H. Sommer, E. R. Henry, and W. A. Eaton, "Nanosecond absorption spectroscopy of hemoglobin: elementary processes in kinetic cooperativity," *Proceedings of the National Academy of Sciences of the United States of America,* vol. 80, p. 2235, 1983.
[101] U. Samuni, C. J. Roche, D. Dantsker, and J. M. Friedman, "Conformational dependence of hemoglobin reactivity under high viscosity conditions: the role of solvent slaved dynamics," *J. Am. Chem. Soc,* vol. 129, pp. 12756-12764, 2007.
[102] O. Galkin, S. Buchter, A. Tabirian, and A. Schulte, "Pressure effects on the proximal heme pocket in myoglobin probed by Raman and near-infrared absorption spectroscopy," *Biophysical journal,* vol. 73, pp. 2752-2763, 1997.
[103] F. Abe, C. Kato, and K. Horikoshi, "Pressure-regulated metabolism in microorganisms," *Trends in Microbiology,* vol. 7, pp. 447-453, 1999.
[104] T. J. Welch, A. Farewell, F. C. Neidhardt, and D. H. Bartlett, "Stress response of Escherichia coli to elevated hydrostatic pressure," *Journal of bacteriology,* vol. 175, p. 7170, 1993.
[105] S. Adachi and I. Morishima, "The effects of pressure on oxygen and carbon monoxide binding kinetics for myoglobin. A high pressure laser flash photolysis study," *Journal of Biological Chemistry,* vol. 264, p. 18896, 1989.
[106] B. Gavish, E. Gratton, and C. J. Hardy, "Adiabatic compressibility of globular proteins," *Proceedings of the National Academy of Sciences of the United States of America,* vol. 80, p. 750, 1983.
[107] H. Frauenfelder, N. A. Alberding, A. Ansari, D. Braunstein, B. R.. Cowen, M.. K.. Hong, I. E. T. Iben, J. B. Johnson, and S. Luck, M.. C. Marden, J. .R. Mourant, P. Ormos, L. Reinisch, R. Scholl, A. Schulte, E. Shyamsunder, L. .B. Sorensen, P. J. Steinbach, A. Xie, R. .D. Young, K. T. Yue "Proteins and pressure," *Journal of Physical Chemistry,* vol. 94, pp. 1024-1037, 1990.
[108] B. B. Hasinoff, "Kinetic activation volumes of the binding of oxygen and carbon monoxide to hemoglobin and myoglobin studied on a high-pressure laser flash photolysis apparatus," *Biochemistry,* vol. 13, pp. 3111-3117, 1974.
[109] D. P. Kharakoz, "Partial volumes and compressibilities of extended polypeptide chains in aqueous solution: additivity scheme and implication of protein unfolding at normal and high pressure," *Biochemistry,* vol. 36, pp. 10276-10285, 1997.
[110] C. A. Royer, "Revisiting volume changes in pressure-induced protein unfolding," *Biochimica et Biophysica Acta (BBA)-Protein Structure and Molecular Enzymology,* vol. 1595, pp. 201-209, 2002.

[111] P. Tauc, C. R. Mateo, and J. C. Brochon, "Investigation of the effect of high hydrostatic pressure on proteins and lipidic membranes by dynamic fluorescence spectroscopy," *Biochimica et Biophysica Acta (BBA)-Protein Structure and Molecular Enzymology,* vol. 1595, pp. 103-115, 2002.
[112] C. Nicolini, A. Celli, E. Gratton, and R. Winter, "Pressure tuning of the morphology of heterogeneous lipid vesicles: a two-photon-excitation fluorescence microscopy study," *Biophysical journal,* vol. 91, pp. 2936-2942, 2006.
[113] A. Ishii, T. Sato, M. Wachi, K. Nagai, and C. Kato, "Effects of high hydrostatic pressure on bacterial cytoskeleton FtsZ polymers in vivo and in vitro," *Microbiology,* vol. 150, p. 1965, 2004.
[114] K. W. Ranatunga, N. S. Fortune, and M. A. Geeves, "Hydrostatic compression in glycerinated rabbit muscle fibers," *Biophysical journal,* vol. 58, pp. 1401-1410, 1990.
[115] N. S. Fortune, M. A. Geeves, and K. W. Ranatunga, "Tension responses to rapid pressure release in glycerinated rabbit muscle fibers," *Proceedings of the National Academy of Sciences,* vol. 88, p. 7323, 1991.
[116] M. Nishiyama, Y. Kimura, Y. Nishiyama, and M. Terazima, "Pressure-induced changes in the structure and function of the kinesin-microtubule complex," *Biophysical journal,* vol. 96, pp. 1142-1150, 2009.
[117] N. Alberding, S. S. Chan, L. Eisenstein, H. Frauenfelder, D. Good, I. C. Gunsalus, T. M. Nordlund, M. F. Perutz, A. H. Reynolds, and L. B. Sorensen, "Binding of carbon monoxide to isolated hemoglobin chains," *Biochemistry,* vol. 17, pp. 43-51, 1978.
[118] S. E. V. Phillips, "Structure and refinement of oxymyoglobin at 1· 6 Å resolution," *Journal of molecular biology,* vol. 142, pp. 531-554, 1980.
[119] K. Chu, J. Vojtchovsky, B. H. McMahon, R. M. Sweet, J. Berendzen, and I. Schlichting, "Structure of a ligand-binding intermediate in wild-type carbonmonoxy myoglobin," *Nature,* vol. 403, pp. 921-923, 2000.
[120] E.E.Scott and Q.H.Gibson, "Ligand migration in sperm whale myoglobin," *Biochemistry,* vol. 14, pp. 5355-5373, 1997.
[121] M. Brunori, B. Vallone, F. Cutruzzolà, C. Travaglini-Allocatelli, J. Berendzen, K. Chu, R. M. Sweet, and I. Schlichting, "The role of cavities in protein dynamics: crystal structure of a photolytic intermediate of a mutant myoglobin," *Proceedings of the National Academy of Sciences of the United States of America,* vol. 97, p. 2058, 2000.
[122] K. Nienhaus, P. Deng, J. M. Kriegl, and G. U. Nienhaus, "Structural dynamics of myoglobin: Effect of internal cavities on ligand migration and binding," *Biochemistry,* vol. 42, pp. 9647-9658, 2003.
[123] C. Tetreau, Y. Blouquit, E. Novikov, E. Quiniou, and D. Lavalette, "Competition with xenon elicits ligand migration and escape pathways in myoglobin," *Biophysical journal,* vol. 86, pp. 435-447, 2004.
[124] V. Šrajer, T. Teng, T. Ursby, C. Pradervand, Z. Ren, S. Adachi, W. Schildkamp, D. Bourgeois, M. Wulff, and K. Moffat, "Photolysis of the carbon monoxide complex of myoglobin: nanosecond time-resolved crystallography," *science,* vol. 274, p. 1726, 1996.
[125] N. Agmon and G.M.Sastry, "A temperature-dependent effective potential can explain CO binding to myoglobin," *Chemical Physics,* vol. 212, 1996.
[126] J. Cohen, A. Arkhipov, R. Braun, and K. Schulten, "Imaging the migration pathways for O2, CO, NO, and Xe inside myoglobin," *Biophysical journal,* vol. 91, pp. 1844-1857, 2006.

[127] A. Ansari, B. R. Cowen, H. Frauenfelder, P. Ormos, T. B. Sauke, A. Schulte, and R. D. Young, "Kinetic hole-burning and comformational relaxation in myoglobin," *Biophysical Journal,* vol. 51, 1988.
[128] P. Urayama and G. N. Phillips, "Probing substates in sperm whale myoglobin using high-pressure crystallography," *Structure,* vol. 10, pp. 51-60, 2002.
[129] R. F. Tilton Jr and G. A. Petsko, "A structure of sperm whale myoglobin at a nitrogen gas pressure of 145 atmospheres," *Biochemistry,* vol. 27, pp. 6574-6582, 1988.
[130] G. U. Nienhaus, *Protein-ligand interactions: methods and applications*: Humana Pr Inc, 2005.
[131] P. J. Steinbach, K. Chu, H. Frauenfelder, J. B. Johnson, D. C. Lamb, G. U. Nienhaus, T. B. Sauke, and R. D. Young, "Determination of rate distributions from kinetic experiments," *Biophysical journal,* vol. 61, pp. 235-245, 1992.
[132] J. D. Müller and E. Gratton, "High-pressure fluorescence correlation spectroscopy," *Biophysical journal,* vol. 85, pp. 2711-2719, 2003.
[133] L. Erijman and R. M. Clegg, "High pressure electrophoresis in narrow bore glass tubes: One and two dimensional separations of protein subunits," *Review of Scientific Instruments,* vol. 67, pp. 813-817, 1996.
[134] M. Hartmann, F. Pfeifer, G. Dornheim, and K. Sommer, "HPDS Hochdruckzelle zur Beobachtung mikroskopischer Phänomene unter Hochdruck," *Chemie Ingenieur Technik,* vol. 75, pp. 1763-1767, 2003.
[135] J. Xu and H. Mao, "Moissanite: a window for high-pressure experiments," *science,* vol. 290, p. 783, 2000.
[136] M. Hartmann, M. Kreuss, and K. Sommer, "High pressure microscopy--a powerful tool for monitoring cells and macromolecules under high hydrostatic pressure," *Cellular and molecular biology (Noisy-le-Grand, France),* vol. 50, p. 479, 2004.
[137] O. Friedrich, F. V. Wegner, M. Hartmann, B. Frey, K. Sommer, H. Ludwig, and R. H. Fink, "'In situ'high pressure confocal Ca (2+)-fluorescence microscopy in skeletal muscle: a new method to study pressure limits in mammalian cells," *Undersea Hyperb Med,* vol. 33, pp. 181-95, 2006.
[138] B. Frey, M. Hartmann, M. Herrmann, R. Meyer Pittroff, K. Sommer, and G. Bluemelhuber, "Microscopy under pressure—an optical chamber system for fluorescence microscopic analysis of living cells under high hydrostatic pressure," *Microscopy research and technique,* vol. 69, pp. 65-72, 2006.
[139] E. D. Salmon and G. W. Ellis, "A new miniature hydrostatic pressure chamber for microscopy. Strain-free optical glass windows facilitate phase-contrast and polarized-light microscopy of living cells. Optional fixture permits simultaneous control of pressure and temperature," *The Journal of Cell Biology,* vol. 65, p. 587, 1975.
[140] S. H. Park, S. Arora, and A. Schulte, "Micro-Spectroscopy of Biomolecules and Cells at Variable Pressure in a Micro-Capillary," *Biophysical journal,* vol. 98, p. 742.
[141] S. H. Park, S. Arora, and A. Schulte, "Micro-Spectroscopy of Proteins and Cells at Variable Pressure in a Micro-Capillary," *Bulletin of the American Physical Society,* vol. 54, 2009.
[142] T. Oakeson, "Development of a novel setup for high pressure Raman spectroscopy using a micro-capillary," in *Department of Physics*: University of Central Florida, 2007.
[143] A. Schulte, "High-pressure near-infrared Raman spectroscopy of bacteriorhodopsin light to dark adaptation," *Biophysical journal,* vol. 69, pp. 1554-1562, 1995.
[144] "National semiconductor corporation," in *www.national.com/ds/CL/CLC425.pdf,* 2009.

[145] N. Alberding, R. H. Austin, S. S. Chan, L. Eisenstein, H. Frauenfelder, I. C. Gunsalus, and T. M. Nordlund, "Dynamics of carbon monoxide binding to protoheme," *The Journal of Chemical Physics*, vol. 65, p. 4701, 1976.
[146] P. J. Steinbach, A. Ansari, J. Berendzen, D. Braunstein, K. Chu, B. R. Cowen, D. Ehrenstein, H. Frauenfelder, and J. B. Johnson, "Ligand binding to heme proteins: connection between dynamics and function," *Biochemistry*, vol. 30, pp. 3988-4001, 1991.
[147] W. Trager and J. B. Jensen, "Human malaria parasites in continuous culture," *science*, vol. 193, p. 673, 1976.
[148] K. Haldar, M. A. Ferguson, and G. A. Cross, "Acylation of a Plasmodium falciparum merozoite surface antigen via sn-1, 2-diacyl glycerol," *Journal of Biological Chemistry*, vol. 260, p. 4969, 1985.
[149] I. D. Campbell and A. D. Raymond, *Biological Spectroscopy*: The Benjamin/Cummings Publishing Co., 1984.
[150] K. E. Van Holde, W. C. Johnson, and P. S. Ho, *Principles of physical biochemistry* vol. 646: Prentice Hall Upper Saddle River, NJ, 1998.
[151] W. C. Johnson Jr, *Circular dichroism and its empirical application to biopolymers*, 1985.
[152] j. b. pawley, "handbook of biological confocal microscopy," 1995.
[153] K. Sasaki, M. Koshioka, and H. Masuhara, "Confocal laser-induced absorption microscope," *Journal of the Optical Society of America A*, vol. 9, pp. 932-936, 1992.
[154] J. S. Park, C. K. Choi, and K. D. Kihm, "Optically sliced micro-PIV using confocal laser scanning microscopy (CLSM)," *Experiments in Fluids*, vol. 37, pp. 105-119, 2004.
[155] C. Yang, W. Kuang, and H. Li, "Study of the imaging property of a fluorescent confocal microscopy with a phase-only filter in an extended source," *Optoelectronics Letters*, vol. 3, pp. 299-302, 2007.
[156] I. Itzkan, L. Qiu, H. Fang, M. M. Zaman, E. Vitkin, I. C. Ghiran, S. Salahuddin, M. Modell, C. Andersson, and L. M. Kimerer, "Confocal light absorption and scattering spectroscopic microscopy monitors organelles in live cells with no exogenous labels," *Proceedings of the National Academy of Sciences*, vol. 104, p. 17255, 2007.
[157] P. Kukura, M. Celebrano, A. Renn, and V. Sandoghdar, "Single-Molecule Sensitivity in Optical Absorption at Room Temperature," *The Journal of Physical Chemistry Letters*, vol. 1, pp. 3323-3327, 2010.
[158] T. Wilson and C. Sheppard, "Theory and practice of scanning optical microscopy," *London: Academic Press,| c1984*, vol. 1, 1984.
[159] G. H. Patterson and D. W. Piston, "Photobleaching in two-photon excitation microscopy," *Biophysical journal*, vol. 78, pp. 2159-2162, 2000.
[160] A. R. Pearson, A. Mozzarelli, and G. L. Rossi, "Microspectrophotometry for structural enzymology," *Current Opinion in Structural Biology*, vol. 14, pp. 656-662, 2004.
[161] M. B. Cannell, A. McMorland, and C. Soeller, "Image enhancement by deconvolution," *Handbook of biological confocal microscopy*, pp. 488-500, 2006.
[162] N. Streibl, "Depth transfer by an imaging system," *Journal of Modern Optics*, vol. 31, pp. 1233-1241, 1984.
[163] N. Streibl, "Three-dimensional imaging by a microscope," *JOSA A*, vol. 2, pp. 121-127, 1985.
[164] T. Wilson, *Confocal Microscopy*: Academic Press, 1990.
[165] M. Born and E. Wolf, *Principles of Optics, 7-th ed*, 1999.

[166] R. Juškaitis, "Measuring the real point spread function of high numerical aperture microscope objective lenses," *Handbook of biological confocal microscopy*, pp. 239-250, 2006.
[167] T. Wilson and A. R. Carlini, "Size of the detector in confocal imaging systems," *Optics Letters*, vol. 12, pp. 227-229, 1987.
[168] H. H. Hopkins, "The Frequency Response of a Defocused Optical System," *Proceedings of the Royal Society of London. Series A. Mathematical and Physical Sciences*, vol. 231, pp. 91-103, 1955.
[169] C. J. R. Sheppard, "The spatial frequency cut-off in three-dimensional imaging II," *Optik*, vol. 74, pp. 128-129, 1986.
[170] A. Egner and S. W. Hell, "Aberrations in confocal and multi-photon fluorescence microscopy induced by refractive index mismatch," *Handbook of biological confocal microscopy*, pp. 404-413, 2006.
[171] M. Schrader, M. Kozubek, S. W. Hell, and T. Wilson, "Optical transfer functions of 4Pi confocal microscopes: theory and experiment," *Optics Letters*, vol. 22, pp. 436-438, 1997.
[172] C. J. R. Sheppard and X. Q. Mao, "Three-dimensional imaging in a microscope," *JOSA A*, vol. 6, pp. 1260-1269, 1989.
[173] S. Arora, S. H. Park, L. Ayong, D. Chakrabarti, and A. Schulte, "Spectroscopic Studies of High Pressure Effects on Single Erythrocytes," *Bulletin of the American Physical Society*, vol. 55.
[174] D. R. Gaskell, *Introduction to the Thermodynamics of Materials*: Hemisphere Pub, 2003.
[175] G. Careri, P. Fasella, and E. Gratton, "Enzyme Dynamics: The Statistical Physics Approach," *Annual Review of Biophysics and Bioengineering*, vol. 8, pp. 69-97, 1979.
[176] R. A. Fine and F. J. Millero, "Compressibility of water as a function of temperature and pressure," *The Journal of Chemical Physics*, vol. 59, p. 5529, 1973.
[177] E. W. Washburn and C. J. West, *International critical tables of numerical data, physics, chemistry and technology*: National Academies, 1926.
[178] D. Eden, J. B. Matthew, J. J. Rosa, and F. M. Richards, "Increase in apparent compressibility of cytochrome c upon oxidation," *Proceedings of the National Academy of Sciences*, vol. 79, pp. 815-819, February 1, 1982 1982.
[179] A. P. Sarvazyan and P. Hemmes, "Relaxational contributions to protein compressibility from ultrasonic data," *Biopolymers*, vol. 18, pp. 3015-3024, 1979.
[180] D. H. Boal, U. Seifert, and A. Zilker, "Dual network model for red blood cell membranes," *Physical Review Letters*, vol. 69, pp. 3405-3408, 1992.
[181] J. C. Hansen, R. Skalak, S. Chien, and A. Hoger, "Influence of network topology on the elasticity of the red blood cell membrane skeleton," *Biophysical journal*, vol. 72, pp. 2369-2381, 1997.
[182] J. S. Morrow and V. T. Marchesi, "Self-assembly of spectrin oligomers in vitro: a basis for a dynamic cytoskeleton," *The Journal of Cell Biology*, vol. 88, p. 463, 1981.
[183] J. A. Chasis and N. Mohandas, "Erythrocyte membrane deformability and stability: two distinct membrane properties that are independently regulated by skeletal protein associations," *The Journal of Cell Biology*, vol. 103, p. 343, 1986.
[184] J. Hofrichter, P. D. Ross, and W. A. Eaton, "Kinetics and mechanism of deoxyhemoglobin S gelation: a new approach to understanding sickle cell disease," *Proceedings of the National Academy of Sciences*, vol. 71, p. 4864, 1974.
[185] R. J. W. Allen and K. Kirk, "Cell volume control in the Plasmodium-infected erythrocyte," *Trends in parasitology*, vol. 20, pp. 7-10, 2004.

[186] S. Külzer, M. Rug, K. Brinkmann, P. Cannon, A. Cowman, K. Lingelbach, G. L. Blatch, A. G. Maier, and J. M. Przyborski, "Parasite encoded Hsp40 proteins define novel mobile structures in the cytosol of the P. falciparum infected erythrocyte," *Cellular Microbiology,* vol. 12, pp. 1398-1420, 2010.
[187] A. Esposito, J. B. Choimet, J. N. Skepper, J. Mauritz, V. L. Lew, C. F. Kaminski, and T. Tiffert, "Quantitative imaging of human red blood cells infected with Plasmodium falciparum," *Biophysical journal,* vol. 99, pp. 953-960.
[188] V. L. Lew and A. R. Hockaday, *The effects of transport and the consequent influx perturbations on the homeostasis of erythrocytes. In Transport and Trafficking in the Malaria-Infected Erythrocyte*: Wiley, 1999.
[189] D. E. Goldberg, A. F. Slater, A. Cerami, and G. B. Henderson, "Hemoglobin degradation in the malaria parasite Plasmodium falciparum: an ordered process in a unique organelle," *Proceedings of the National Academy of Sciences,* vol. 87, p. 2931, 1990.
[190] K. G. Le Roch, Y. Zhou, P. L. Blair, M. Grainger, J. K. Moch, J. D. Haynes, P. De la Vega, A. A. Holder, S. Batalov, and D. J. Carucci, "Discovery of gene function by expression profiling of the malaria parasite life cycle," *science,* vol. 301, p. 1503, 2003.
[191] Z. Bozdech, M. Llinás, B. L. Pulliam, E. D. Wong, J. Zhu, and J. L. DeRisi, "The transcriptome of the intraerythrocytic developmental cycle of Plasmodium falciparum," *PLoS Biology,* vol. 1, p. e5, 2003.
[192] G. G. Holz, "Lipids and the malarial parasite," *Bull. World Health Organization,* vol. 55, pp. 237-248, 1977.
[193] H. J. Vial, M. L. Ancelin, J. L. Avila, and J. R. Harris, "Malarial lipids: an overview," *Subcellular biochemistry, volume 18: Intracellular parasites.*, pp. 259-306, 1992.
[194] H. J. Vial, M. L. Ancelin, J. R. Philippot, and M. J. Thuet, "Biosynthesis and dynamics of lipids in Plasmodium-infected mature mammalian erythrocytes," *Blood cells,* vol. 16, pp. 531-555, 1990.
[195] P. Nawabi, A. Lykidis, D. Ji, and K. Haldar, "Neutral-lipid analysis reveals elevation of acylglycerols and lack of cholesterol esters in Plasmodium falciparum-infected erythrocytes," *Eukaryotic Cell,* vol. 2, p. 1128, 2003.
[196] N. M. Q. Palacpac, Y. Hiramine, F. Mi-ichi, M. Torii, K. Kita, R. Hiramatsu, T. Horii, and T. Mitamura, "Developmental-stage-specific triacylglycerol biosynthesis, degradation and trafficking as lipid bodies in Plasmodium falciparum-infected erythrocytes," *Journal of cell science,* vol. 117, p. 1469, 2004.
[197] F. Omodeo-Salè, A. Motti, N. Basilico, S. Parapini, P. Olliaro, and D. Taramelli, "Accelerated senescence of human erythrocytes cultured with Plasmodium falciparum," *Blood,* vol. 102, p. 705, 2003.
[198] D. Taramelli, M. F. Omodeo-Sale, A. Motti, N. Basilico, S. Parapini, and P. Olliaro, "Accelerated senescence of human erythrocytes cultured with."
[199] V. B. Brand, C. D. Sandu, C. Duranton, V. Tanneur, K. S. Lang, S. M. Huber, and F. Lang, "Dependence of Plasmodium falciparum In Vitro Growth on the Cation Permeability of the Human Host Erythrocyte," *Cellular Physiology and Biochemistry,* vol. 13, pp. 347-356, 2000.
[200] F. Lang, P. A. Lang, K. S. Lang, V. Brand, V. Tanneur, C. Duranton, T. Wieder, and S. M. Huber, "Channel-induced apoptosis of infected host cells—the case of malaria," *Pflügers Archiv European Journal of Physiology,* vol. 448, pp. 319-324, 2004.

[201] S. Eda and I. W. Sherman, "Cytoadherence of malaria-infected red blood cells involves exposure of phosphatidylserine," *Cellular Physiology and Biochemistry,* vol. 12, pp. 373-384, 2000.
[202] M. L. Ancelin, M. Parant, M. J. Thuet, J. R. Philippot, and H. J. Vial, "Increased permeability to choline in simian erythrocytes after Plasmodium knowlesi infection," *Biochemical Journal,* vol. 273, p. 701, 1991.
[203] C. A. Homewood and K. D. Neame, "Malaria and the permeability of the host erythrocyte," *Nature,* vol. 252, pp. 718-719, 1974.
[204] M. Nakao, T. Nakao, and S. Yamazoe, "Adenosine Triphosphate and Maintenance of Shape of the Human Red Cells," *Nature,* vol. 187, pp. 945-946, 1960.
[205] M. W. Makinen, A. K. Churg, A. B. P. Lever, and M. B. Gray, "Iron Porphyrins Part 1," Addison-Wesley Publishing Co., Mass, 1983.
[206] P. L. Olliaro and D. E. Goldberg, "The Plasmodium digestive vacuole: metabolic headquarters and choice drug target," *Parasitology Today,* vol. 11, pp. 294-297, 1995.
[207] C. Slomianny, "Three-dimensional reconstruction of the feeding process of the malaria parasite," *Blood cells,* vol. 16, p. 369, 1990.
[208] S. G. Langreth, J. B. Jensen, R. T. Reese, and W. Trager, "Fine Structure of Human Malaria In Vitro*†," *Journal of Eukaryotic Microbiology,* vol. 25, pp. 443-452, 1978.
[209] B. R. Shenai and P. J. Rosenthal, "Reducing requirements for hemoglobin hydrolysis by Plasmodium falciparum cysteine proteases," *Molecular and biochemical parasitology,* vol. 122, p. 99, 2002.
[210] T. Gabay and H. Ginsburg, "Hemoglobin denaturation and iron release in acidified red blood cell lysate-A possible source of iron for intraerythrocytic malaria parasites," *Experimental Parasitology,* vol. 77, pp. 261-272, 1993.
[211] N. D. Gamboa de Dominguez and P. J. Rosenthal, "Cysteine proteinase inhibitors block early steps in hemoglobin degradation by cultured malaria parasites," *Blood,* vol. 87, p. 4448, 1996.
[212] K. J. Saliba, R. J. W. Allen, S. Zissis, P. G. Bray, S. A. Ward, and K. Kirk, "Acidification of the malaria parasite's digestive vacuole by a H+-ATPase and a H+-pyrophosphatase," *Journal of Biological Chemistry,* vol. 278, p. 5605, 2003.
[213] J. H. McKerrow, E. Sun, P. J. Rosenthal, and J. Bouvier, "The proteases and pathogenicity of parasitic protozoa," *Annual Reviews in Microbiology,* vol. 47, pp. 821-853, 1993.
[214] W. Asawamahasakda and Y. Yuthavong, "The methionine synthesis cycle and salvage of methyltetrahydrofolate from host red cells in the malaria parasite *Plasmodium falciparum*," *Parasitology,* vol. 107, pp. 1-10, 1993.
[215] V. L. Lew, L. Macdonald, H. Ginsburg, M. Krugliak, and T. Tiffert, "Excess haemoglobin digestion by malaria parasites: a strategy to prevent premature host cell lysis," *Blood Cells, Molecules, and Diseases,* vol. 32, pp. 353-359, 2004.
[216] J. Mu, M. T. Ferdig, X. Feng, D. A. Joy, J. Duan, T. Furuya, G. Subramanian, L. Aravind, R. A. Cooper, and J. C. Wootton, "Multiple transporters associated with malaria parasite responses to chloroquine and quinine," *Molecular microbiology,* vol. 49, pp. 977-989, 2003.
[217] K. Kirk, "Membrane transport in the malaria-infected erythrocyte," *Physiological reviews,* vol. 81, p. 495, 2001.
[218] S. Zarchin, M. Krugliak, and H. Ginsburg, "Digestion of the host erythrocyte by malaria parasites is the primary target for quinolinecontaining antimalarials," *Biochemical pharmacology,* vol. 35, pp. 2435-2442, 1986.

[219] G. F. Mabeza, M. Loyevsky, V. R. Gordeuk, and G. Weiss, "Iron Chelation Therapy for Malaria:: A Review," *Pharmacology & therapeutics*, vol. 81, pp. 53-75, 1999.
[220] A. U. Orjih, H. S. Banyal, R. Chevli, and C. D. Fitch, "Hemin lyses malaria parasites," *science*, vol. 214, p. 667, 1981.
[221] N. T. Huy, A. Maeda, D. T. Uyen, D. T. X. Trang, M. Sasai, T. Shiono, T. Oida, S. Harada, and K. Kamei, "Alcohols induce beta-hematin formation via the dissociation of aggregated heme and reduction in interfacial tension of the solution," *Acta Tropica*, vol. 101, pp. 130-138, 2007.
[222] D. S. Bohle, R. E. Dinnebier, S. K. Madsen, and P. W. Stephens, "Characterization of the products of the heme detoxification pathway in malarial late trophozoites by X-ray diffraction," *Journal of Biological Chemistry*, vol. 272, p. 713, 1997.
[223] B. R. Wood, B. Tait, and D. McNaughton, "Micro-Raman characterisation of the R to T state transition of haemoglobin within a single living erythrocyte," *Biochimica et Biophysica Acta (BBA) - Molecular Cell Research*, vol. 1539, pp. 58-70, 2001.
[224] B. R. Wood and D. McNaughton, "Raman excitation wavelength investigation of single red blood cells in vivo," *Journal of Raman Spectroscopy*, vol. 33, pp. 517-523, 2002.
[225] S. Arora, S. H. Park, J. Mauser, D. Chakrabarti, and A. Schulte, "Micro-Spectroscopy of Single Erythrocytes Infected with the Malaria Parasite " Invited paper, *Proceedings of ICNBME*, 2011.
[226] W. D. Carter, "Raman spectroscopic study of single red blood cells infected by the malaria parasite plasmodium falciparum," in *Department of Physics*: University of Central Florida, 2007.
[227] B. R. Wood, S. J. Langford, B. M. Cooke, J. Lim, F. K. Glenister, M. Duriska, J. K. Unthank, and D. McNaughton, "Resonance Raman spectroscopy reveals new insight into the electronic structure of -hematin and malaria pigment," *Journal of the American Chemical Society*, vol. 126, pp. 9233-9239, 2004.
[228] S. Arora, J. Mauser, D. Chakrabarti, and A. Schulte, "Spatially resolved absorption spectroscopy of bio-assemblies on a micron scale," *Bulletin of the American Physical Society*, vol. 56.
[229] J. Hofrichter, J. H. Sommer, E. R. Henry, and W. A. Eaton, "Nanosecond absorption spectroscopy of hemoglobin: elementary processes in kinetic cooperativity," *Proceedings of the National Academy of Sciences*, vol. 80, p. 2235, 1983.
[230] R. R. Birge, D. F. Bocian, and L. M. Hubbard, "Origins of inhomogeneous broadening in the vibronic spectra of visual chromophores and visual pigments," *Journal of the American Chemical Society*, vol. 104, pp. 1196-1207, 1982.
[231] J. Friedrich, J. Gafert, J. Zollfrank, J. Vanderkooi, and J. Fidy, "Spectral hole burning and selection of conformational substates in chromoproteins," *Proceedings of the National Academy of Sciences of the United States of America*, vol. 91, p. 1029, 1994.
[232] U. Samuni, D. Dantsker, L. J. Juszczak, S. Bettati, L. Ronda, A. Mozzarelli, and J. M. Friedman, "Spectroscopic and Functional Characterization of T State Hemoglobin Conformations Encapsulated in Silica Gels†," *Biochemistry*, vol. 43, pp. 13674-13682, 2004.
[233] M. C. Marden, E. S. Hazard, C. Kimble, and Q. H. Gibson, "Geminate ligand recombination as a probe of the R, T equilibrium in hemoglobin," *European Journal of Biochemistry*, vol. 169, pp. 611-615, 1987.
[234] W. Doster and S. Longeville, "Microscopic diffusion and hydrodynamic interactions of hemoglobin in red blood cells," *Biophysical journal*, vol. 93, pp. 1360-1368, 2007.
[235] A. Zipp and W. Kauzmann, "Pressure denaturation of metmyoglobin," *Biochemistry*, vol. 12, pp. 4217-4228, 1973.

[236] A. Schulte, S. Arora, and S. H. Park, "Ligand Binding Kinetics in Myoglobin and Solvent Relaxation at High Pressure," *Bulletin of the American Physical Society*, vol. 53, 2008.
[237] W. Doster, D. Beece, S. F. Bowne, E. E. DiIorio, L. Eisenstein, H. Frauenfelder, L. Reinisch, E. Shyamsunder, K. H. Winterhalter, and K. T. Yue, "Control and pH dependence of ligand binding to heme proteins," *Biochemistry*, vol. 21, pp. 4831-4839, 1982.
[238] R. D. Young and S. F. Bowne, "Conformational substates and barrier height distributions in ligand binding to heme proteins," *The Journal of Chemical Physics*, vol. 81, p. 3730, 1984.
[239] J. M. Friedman, T. W. Scott, and G. J. Fisanick, "Localized control of ligand binding in hemoglobin: effect of tertiary structure on picosecond geminate recombination," *science*, vol. 229, p. 187, 1985.
[240] W. Doster and M. Settles, "Protein-water displacement distributions," *Biochimica et Biophysica Acta (BBA)-Proteins & Proteomics*, vol. 1749, pp. 173-186, 2005.
[241] D. P. Kharakoz, "Partial molar volumes of molecules of arbitrary shape and the effect of hydrogen bonding with water," *Journal of solution chemistry*, vol. 21, pp. 569-595, 1992.
[242] D. P. Kharakoz, "Protein compressibility, dynamics, and pressure," *Biophysical journal*, vol. 79, pp. 511-525, 2000.
[243] W. Kauzmann, "Some factors in the interpretation of protein denaturation," *Adv Protein Chem*, vol. 14, pp. 1-63, 1959.